

https://dspace.org/

Assessment of the anti-cancer potential of mushroom extracts in A549 lung cancer cells and the efficacy of doxorubicin

Patel, Yaseera

2025

University of the Witwatersrand, Johannesburg

https://hdl.handle.net/10539/49894

Patel, Yaseera . (2025). Assessment of the anti-cancer potential of mushroom extracts in A549 lung cancer cells and the efficacy of doxorubicin [Master's dissertation, University of the Witwatersrand, Johannesburg]. WIReDSpace. https://hdl.handle.net/10539/49894

Downloaded from a DSpace repository. https://dspace.org/

Assessment of the anti-cancer potential of mushroom extracts in A549 lung cancer cells and the efficacy of doxorubicin.





Yaseera Patel

Supervisors: Dr Gary Gabriels and Dr Leonie Harmse

A dissertation submitted to the Faculty of Health Sciences, University of the Witwatersrand, in fulfilment of the requirements for the degree of

Masters of Science in Medicine

2025

DECLARATION

I, Yaseera Patel, declare that this Dissertation is my own, unaided work. It is being submitted for the Degree of Master of Science in Medicine at the University of the Witwatersrand, Johannesburg. It has not been submitted before for any degree or examination at any other University.



……

Yaseera Patel

On this….23rd….day of ….March…..2025

DEDICATION

I dedicate this dissertation to the students of Gaza—past, present, and future—who continue to dream despite the unimaginable hardships they face.

To Mostafa al-Sawaf, a 17-year-old boy who aspired to become a pharmacologist but was martyred on September 18th, 2024. To the countless other students whose aspirations have been stolen, but whose resilience and spirit remain unbreakable. If I were to name each martyr my thesis would stretch for thousands of pages. You are not forgotten. Your dreams, your struggles, and your strength deserve to be recognized.

As Angelina Jolie once said, "Across the world, there is a woman just like me, with the same abilities, and the same desires, the same work ethic and love for her family, only she sits in a refugee camp."

This dissertation is a tribute to those who have been denied the privilege of education and a normal life—not for lack of talent or ambition, but because of circumstances beyond their control.

May their dreams never be forgotten, and may justice and freedom prevail.

تحيا فلسطين

ABSTRACT

Introduction: The five-year survival rate for metastatic lung cancer is 18.6%. In Eastern medicine, mushrooms have been used as a treatment for various cancer types. Among these are *Ganoderma lucidum* and *Trametes versicolour*, which contain bioactive molecules with proposed anticancer and immunomodulatory properties. In this study, commercially available mushroom products were evaluated for their potential cytotoxic effects against the A549 lung cancer cell line and the results were compared to a normal cell line (HEK293).

Methods: The mushroom products underwent dual extraction using methanol and dichloromethane which was evaporated. The final dried extracts were redissolved in sterile distilled water (*I. obliquus*) or a DMSO:ethanol mixture (*T. versicolour* and *G. lucidum*).A549 cells were maintained aseptically in culture. The MTT cell viability assay was used to determine the cytotoxic effect and the 50% inhibitory concentrations (IC_{50}) of the mushroom extracts. Doxorubicin was used as a positive control. Cell morphology was evaluated using fluorescent probes, Hoechst 33342, propidium iodide, and acridine orange, to assess the mode of cell death when cells were exposed to concentrations equivalent to IC_{80} values of the mushroom extracts and doxorubicin. The expression of phosphatidylserine on cell membranes was detected with FITC-labelled annexin-V, caspase-3/7 expression was assessed using the CellEvent™ Caspase-3/7 Green Detection Reagent, and reactive oxygen species formation was measured using the CellROX™ Deep Red Reagent. P-glycoprotein expression levels were determined using immunofluorescence techniques.

Results: *G. lucidum* was the most active mushroom extract in A549 and HEK293 cells at 24 h (IC_{50} value = 0.255 mg/mL and 0.591 mg/mL, respectively). When combined with doxorubicin in A549 cells, both *G. lucidum* and *T. versicolour* decreased the efficacy of doxorubicin. In HEK293 cells, the mushroom extracts increased the efficacy of doxorubicin. According to FTIR analysis, extracts were most stable when stored at 4°C. Morphological evaluation showed apoptosis in A549 cells treated with *T. versicolour* at 0.5 mg/ml, whereas *G. lucidum* caused concentration dependent necrosis. Annexin-V staining confirmed apoptosis in *G. lucidum* and *T. versicolour* treated cells, along with an increase in caspase-3/7 activity in A549 cells. HEK293 cells underwent necrosis when treated with the extracts for 24 h. Reactive oxygen species production was also elevated in both A549 and HEK293 treated cells. Immunofluorescence analysis showed no significant changes in P-glycoprotein expression.

Conclusion: The cytotoxic effects of *G. lucidum* and *T. versicolour* on both cancerous and non-cancerous cells highlight their lack of selectivity, raising significant safety concerns regarding their use. Given their potential to harm normal tissues, further research is necessary to establish safe exposure limits and regulatory guidelines are needed to protect consumers from unverified or misleading health claims.

ACKNOWLEDGEMENTS

I would like to express my deepest gratitude to the people who have supported and shaped me throughout this journey.

- To my grandmother, Amina, who raised me with love and strength. I would be nothing without you. Everything I do is in the hope of making your world a better place.
- To my sister, Shaakira, who is the best friend and sister a girl could ask for. Your unwavering support and encouragement kept me going, even when things felt impossible.
- To my friends, old and new, thank you for your kindness, patience, and companionship during the most challenging times of my life. Your presence made all the difference.
- To Rafiyya, whose humour and perspective have taught me not to take life too seriously. Only you could convince me to adopt six rats - and somehow, I have no regrets.
- To Muhammad, for the encouragement, the laughter, and for always offering a listening ear without judgment. Your friendship has been invaluable.

Special thanks to

- My supervisor, Dr Gary Gabriels, I am deeply grateful for your guidance, kindness, and unwavering support in making this project a reality. Your willingness to assist with every challenge along the way has meant so much to me.
- My supervisor, Dr Leonie Harmse, for never holding back, your honesty and high standards have made me a better researcher and scientific writer. It has been an honour to be one of your students, and I wish you a very happy retirement. Thank you for your contributions not only to this project but to science as a whole.
- Funding support from the Wits Postgraduate Scholarship, the McGill Bequest to the Pharmacology Division, Wits FHS research fund and South African National Research Foundation.

Research Outputs

1. Attendance at the African Centre for Gene Technologies Regional Plant Biotechnology Forum – 2022
2. Patel, Y., Gabriels, G. and Harmse, L. (2023). The potential anti-cancer effect of fungal extracts from Chinese complementary medicine on A549 lung cancer cells. Poster presentation at South African Society for Basic and Clinical Pharmacology, 24 – 26 August.
3. Patel, Y., Gabriels, G. and Harmse, L. (2023). The effect of fungal extracts from Chinese complementary medicine on A549 lung cancer cells. Poster presentation at the WITS Faculty of Health Sciences, School of Therapeutic Sciences Biennial Research Day, 5 September.
4. Patel, Y., Gabriels, G. and Harmse, L. (2023). There's mush-room for improvement in current cancer treatment. Oral presentation at the WITS Pharmacology Research Day, 9 November 2023.
5. Patel, Y., Gabriels, G. and Harmse, L. (2025). The effect of selected mushrooms on the efficacy of cancer chemotherapeutic agents in A549 lung cancer cells. Oral presentation at the Indigenous Plant Use Forum, 10 – 14 August.
6. Patel, Y., Gabriels, G. and Harmse, L. (2025). Evaluating the Impact of Selected Mushrooms on Chemotherapy Effectiveness in A549 Lung Cancer Cells. Oral presentation at the WITS Faculty of Health Sciences, School of Therapeutic Sciences Biennial Research Day, 2 September.

Table of Contents

CHAPTER 1: INTRODUCTION

1.1. Lung Cancer ……1

1.1.1. Lung Cancer Classification……..1

1.1.1.1. Adenocarcinoma……..2

1.1.1.2. Squamous cell carcinoma ……..……..2

1.1.1.3. Large cell carcinoma…….……...3

1.1.2. Lung Cancer Treatment……..…….……..…3

1.1.2.1. Radiotherapy……..……..….4

1.1.2.2. Chemotherapy……..……..……..….4

1.1.2.2.1. Combination Chemotherapy……..…….……..……6

1.1.2.3. Targeted Molecular Therapies……..……..…..7

1.1.2.3.1. Epidermal Growth Factor Receptor Mutations.....7

1.1.2.3.2. Anaplastic Lymphoma Kinase Mutations.....8

1.1.2.3.3. Immune checkpoint inhibitors.....9

1.2. Drug Resistance.....10

1.2.1. P-glycoprotein.....11

1.3. Cell Death.....12

1.3.1. Apoptosis.....12

1.3.2. Necrosis.....14

1.3.3. Autophagy.....15

1.4. Complementary and Alternative Medicine.....16

1.4.1. Health Supplement Market and Regulation.....17

1.5. Mushrooms for medicinal use.....18

1.5.1. *Trametes versicolour*.....19

1.5.2. *Ganoderma lucidum*.....22

1.5.3. *Inonotus obiquus*.....24

1.6. Problem Statement.....24

1.7. Research Aims.....26

1.8. Research Objectives.....26

CHAPTER 2: METHODOLOGY

2.1. Assessment of information provided on the labels of commercial preparations of mushrooms…….....28

2.2. Extraction preparation.....28

2.2.1. Procedure for extraction from dried material or capsules…….……..……29

2.2.2. Procedure for extraction from tinctures……..…29

2.3. Fourier Transform Infrared Spectroscopy 29
2.3.1. FTIR inter-batch analysis.....30
2.3.2. Stability assessment of the mushroom extracts by FTIR.....30
2.4. Cell culture.....30
2.4.1. Maintenance and Sub-culturing.....31
2.4.2. Cryopreservation.....31
2.4.3. Determination of cell numbers and viability prior to experimental use.....31
2.5. Cell viability assay.....32
2.5.1. Evaluation of active chemotherapeutic agents and mushroom extracts.....32
2.5.2. Vehicle control.....33
2.5.3. Determining IC_{50} values.....33
2.5.4. Combination studies.....33
2.6. Assessment of the effects of extracts on cell morphology 34
2.7. Annexin-V assay……..….....35
2.8. The detection of caspase 3/7 expression caused by mushroom extracts and doxorubicin.....35
2.9. Reactive Oxygen Species detection.....36
2.10. The detection of P-glycoprotein expression in A549 and HEK293 cells after treatment with mushroom extracts and doxorubicin.....37
2.11. Statistical Analysis……38

CHAPTER 3: RESULTS

3.1. An assessment of the labelling information of commercially available mushroom products.....39
3.1.1. Product warning statements.....39
3.1.2. Product disclaimers 39
3.1.3. Product claims.....40
3.2. Extract preparation.....41
3.3. The effect of mushroom extracts and chemotherapeutic drugs on A549 and HEK293 cell viability.....42
3.3.1. The identification of chemotherapeutic drugs against the A549 cell line.....42
3.3.2. The identification of active mushroom extracts against the A549 and HEK293 cell lines.....44
3.3.3. Determination of IC_{50} values of *G. lucidum*, *T. versicolour* and doxorubicin against A549 and HEK293 cells.....47
3.3.3.1. Determination of IC_{50} values of *G. lucidum*, *T. versicolour* and doxorubicin against A549 cells.....47

3.3.3.2. Determination of IC_{50} values of *G. lucidum*, *T. versicolour* and doxorubicin against HEK293 cells……49
3.3.4. The effect of *G. lucidum* and *T. versicolour* on the cytotoxic efficacy of doxorubicin in A549 and HEK293 cells....50
3.3.5. Stability assessment of *G. lucidum* and *T. versicolour* stored for 13 weeks....54
3.4. FTIR analysis....55
3.4.1. Batch consistency analysis of *G. lucidum* and *T. versicolour* tincture from the same manufacturer....56
3.4.2. Extract stability assessment....59
3.4.2.1. Using FTIR to measure extract profile over time....59
3.4.2.1.1. Extracts stored at room temperature....60
3.4.2.1.2. Extracts stored at -18°C....63
3.4.2.1.3. Extracts stored at 4°C....65
3.5. Assessment of cytotoxic effects by evaluating the morphology of A549 and HEK293 cells....67
3.5.1. The cytotoxic effects of *G. lucidum* and *T. versicolour* on A549 cell morphology....67
3.5.2. The cytotoxic effects of *G. lucidum* and *T. versicolour* on HEK293 cell morphology....73
3.6. The effect of the mushroom extracts and doxorubicin on Annexin-V binding to phosphatidylserine....80
3.6.1. Annexin-V binding to phosphatidylserine in A549 cells....81
3.6.2. Annexin-V binding to phosphatidylserine in HEK293 cells....84
3.7. The activation of caspase-3/7 in cells treated with *G. lucidum* and *T. versicolour*....87
3.7.1. The activation of caspase 3/7 in A549 cells after treatment with *G. lucidum* and *T. versicolour*....88
3.7.2. The activation of caspase-3/7 in HEK293 cells treated with *G. lucidum* and *T. versicolour*....90
3.8. Determination of the effect of ROS level caused by *G. lucidum* and *T. versicolour* treatment....93
3.8.1. Reactive oxygen species levels in A549 cells treated with *G. lucidum* and *T. versicolour*....94
3.8.2. Reactive oxygen species levels in HEK293 cells treated with *G. lucidum* and *T. versicolour*....96
3.9. The detection of P-glycoprotein levels in A549 and HEK293 cells....98

CHAPTER 4: DISCUSSION

4.1. Assessment of information provided on the labels of commercial preparations of mushrooms……99
4.2. Extract Preparation and Solubility Considerations....100
4.3. Consistency of Mushroom Tincture across 3 batches....100
4.4. Extract stability under different storage conditions....101
4.4.1. Summary....102
4.5. The cytotoxic effects of chemotherapeutic drugs and mushroom extracts towards the A549 and HEK293 cell lines....102
4.5.1. Doxorubicin....102
4.5.2. *G. lucidum*....103
4.5.3. *T. versicolour* 104
4.5.4. *I. obliquus* 105
4.5.5. Summary 105
4.6. The effect of mushroom extracts on doxorubicin efficacy in A549 and HEK293 cells....106
4.6.1. *G. lucidum*....106
4.6.2. *T. versicolour* 107
4.6.3. Summary....107
4.7. Cytotoxic Effects of *G. lucidum*, *T. versicolour* and doxorubicin on A549 and HEK293 Cells....108
4.7.1. Doxorubicin....108
4.7.2. *G. lucidum*....109
4.7.3. *T. versicolour*....109
4.7.4. Summary....110
4.8. The effect of *G. lucidum* and *T. versicolour* extracts on phosphatidylserine translocation....110
4.8.1. Doxorubicin....111
4.8.2. *G. lucidum*....111
4.8.3. *T. versicolour*....112
4.8.4. Summary....112
4.9. The effect of *G. lucidum*, *T. versicolour* and doxorubicin on caspase-3/7 activity....113
4.9.1. Doxorubicin....113
4.9.2. *G. lucidum*....113
4.9.3. *T. versicolour*....114
4.9.4. Summary....114
4.10. The effect of *G. lucidum* and *T. versicolour* in A549 and HEK293 Cells on ROS levels....115

4.10.1. Doxorubicin.....115
4.10.2. *G. lucidum*.....116
4.10.3. *T. versicolour*.....116
4.10.4. Summary and comparison.....117
4.11. The effect of doxorubicin, *G. lucidum* and *T. versicolour* on P-glycoprotein expression in A549 and HEK293 cells.....117
4.12. Integrated discussion……...118

CHAPTER 5: CONCLUSION

5.1. Limitations.....122
5.2. Future studies.....122

REFERENCES.....124

Appendix

Appendix A: Research Ethics Approval ……..…..140

Appendix B: The detection of P-glycoprotein levels in A549 cells……..…141

Appendix C: The detection of P-glycoprotein levels in HEK293 cells……..….142

Appendix D: Turnitin Report……..143

List of Figures

CHAPTER 1: INTRODUCTION

Figure 1.1 Schematic representation of apoptotic events…….…….13

Figure 1.2 The 2D structure of β-glucan……...18

Figure 1.3 *T. versicolour* fruiting body……..…….…….…..…19

Figure 1.4 The 2D structure of PSK…….….20

Figure 1.5 *G. lucidum* fruiting body……..……22

Figure 1.6 Ganoderic acid 2-D Structure…….……..…23

Figure 1.7 *I. obliquus* fruiting body…….…….24

CHAPTER 3: RESULTS

Figure 3.1 The effect of anticancer drugs: doxorubicin, camptothecin and irinotecan on A549 cell viability.……..…….…….40

Figure 3.2 The effect of mushroom extracts and doxorubicin on (A) A549 and (B) HEK293 cell viability……..…….…….41

Figure 3.3 Representative dose response curves of doxorubicin, *G. lucidum* and *T. versicolour* against the A549 cell line……..……43

Figure 3.4 Representative dose response curves of doxorubicin, *G. lucidum* and *T. versicolour* against the HEK293 cell line……..…….……..……..…45

Figure 3.5 Representative dose response curves of doxorubicin and mushroom extracts……..…47

Figure 3.6 Representative dose response curves of combination experiments of doxorubicin and mushroom extracts…….….48

Figure 3.7 Bar graphs showing the percentage cell viability vs extract storage time for *G. lucidum* (A) and *T. versicolour* (B) treated cells at 1mg/mL for 24 h on A549 cells…….…….51

Figure 3.8 FTIR spectrum of three batches of *G. lucidum* tinctures from the same manufacturer……..52

Figure 3.9 FTIR spectrum of three batches of *T. versicolour* tinctures……53

Figure 3.10 FTIR profiles for *T. versicolour* extracts stored at room temperature……..…..55

Figure 3.11 FTIR profiles for *G. lucidum* extracts stored at room temperature…….……..57

Figure 3.12 FTIR profiles for *T. versicolour* extracts stored at -18℃…….…….58

Figure 3.13 FTIR profiles for *G. lucidum* extracts stored at -18℃……..59

Figure 3.14 FTIR profiles for *T. versicolour* extracts stored at 4℃…….…61

Figure 3.15 FTIR profiles for *G. lucidum* extracts stored at 4℃…….61

Figure 3.16 Representative photomicrographs showing the morphological changes caused by *G. lucidum*, *T. versicolour* and doxorubicin on A549 cells after 18 h treatment ……..……...65

Figure 3.17 Representative photomicrographs showing the morphological changes caused by *G. lucidum*, *T. versicolour* and doxorubicin on A549 cells after 24 h treatment …….67

Figure 3.18 Representative photomicrographs showing the morphologic changes caused by *G. lucidum*, *T. versicolour* and doxorubicin on HEK293 cells after 18 h treatment ……..……..70

Figure 3.19 Representative photomicrographs showing the morphological changes caused by *G. lucidum*, *T. versicolour* and doxorubicin on HEK293 cells after 24 h treatment ……..……..73

Figure 3.20 Average percentage of cells that underwent apoptosis or necrosis when treated with *G. lucidum* and *T. versicolour*……...75

Figure 3.21 Representative photomicrographs showing binding of annexin-V to phosphatidylserine in A549 cells when treated with doxorubicin, *G. lucidum* and *T. versicolour*…….…….78

Figure 3.22 Representative photomicrographs showing binding of annexin-V to phosphatidylserine in HEK293 cells when treated with doxorubicin, *G. lucidum* and *T. versicolour*…….…….80

Figure 3.23 Average percentage of (A) A549 and (B) HEK293 cells positive for Annexin-V and PI after 24 h exposure to doxorubicin, *G. lucidum* and *T. versicolour*……..…….81

Figure 3.24 Representative photomicrographs showing the expression of Caspase-3/7 in A549 cells when treated with mushroom extracts and doxorubicin…….83

Figure 3.25 The average percentages of A549 cells with caspase-3/7 activity…….…85

Figure 3.26 Representative photomicrographs showing the expression of Caspase-3/7 on HEK293 cells when treated with mushroom extracts and doxorubicin ……..……..…86

Figure 3.27 The average percentages of HEK293 cells with caspase-3/7 activity……87

Figure 3.28 Photomicrographs showing the detection of reactive oxygen species in A549 cells when treated with doxorubicin, *T. versicolour* and *G. lucidum* for 4 h……..89

Figure 3.29 Representative photomicrographs showing the detection of reactive oxygen species in HEK293 cells when treated with doxorubicin, *G. lucidum* and *T. versicolour*…..……..……91

List of Tables

CHAPTER 1: INTRODUCTION

Table 1.1 Common Chemotherapeutic drugs used to treat NSCLC……5

Table 1.2 NSCLC treatments by individual molecular marker types……...…….10

Table 1.3 The five subcategories of CAMs and a description of each subcategory…….…….16

CHAPTER 3: RESULTS

Table 3.1 The warning categories assessed on the product labels (n=15)……...…..36

Table 3.2 Description of different disclaimers on product labels (n=15)…….…..37

Table 3.3 Description of specific claims on product labels (n=15)…….38

Table 3.4 The IC_{50} values (mg/mL) of *G. lucidum*, *T. versicolour* and doxorubicin on A549 cells and the statistical comparison to doxorubicin……..44

Table 3.5 The IC_{50} values (mg/mL) of mushroom extracts (*G. lucidum* and *T. versicolour* extracts) and doxorubicin on HEK293 cells…….……46

Table 3.6 The IC_{50} values (µM) of doxorubicin when combined with *G. lucidum* and *T. versicolour* on A549 and HEK293 cells……....49

Table 3.7 Table showing three randomly selected points from the *G. lucidum* spectrum……..…53

Table 3.8 Table showing three randomly selected points from the *T. versicolour* overlapped spectrum……...……..54

Table 3.9 The peak wavenumbers observed in the FTIR spectrum of *T. versicolour* extract when stored for 5 weeks at room temperature compared to the day of preparation (week 0)……..……..56

Table 3.10 The peak wavenumbers observed in *G. lucidum* when stored for 5 weeks at room temperature compared to the day of preparation (week 0)……..58

Table 3.11 The peak wavenumbers observed in *T. versicolour* when stored for 5 weeks at -18°C compared to the day of preparation (week 0)……59

Table 3.12 A comparison of %T on the FTIR spectrum for *G. lucidum* stored at -18°C for 5-weeks compared to extracts the day of preparation (week 0)…….60

List of abbreviations

A

ABC - ATP-Binding Cassette

ACD - Autophagic Cell Death

ALK-A - Anaplastic Lymphoma Kinase - Active

ALK-R - Anaplastic Lymphoma Kinase - Resistant

AO - Acridine Orange

Atgs - Autophagy-Related Genes

ATP - Adenosine Triphosphate

B

Bcl-2 - B-Cell Lymphoma 2

Bak - Bcl-2 Antagonistic Killer 1

Bax - Bcl-2-Associated X Protein

BSA - Bovine Serum Albumin

C

CAMs – Complementary and Alternative Medicines

C1156Y - Cysteine 1156 Tyrosine Mutation

D

D1203N - Aspartic Acid 1203 Asparagine Mutation

DEVD - Aspartic Acid-Glutamic Acid-Valine-Aspartic Acid

DMSO - Dimethyl Sulfoxide

DMEM - Dulbecco's Modified Eagle Medium

DNA - Deoxyribonucleic Acid

E

EGFR - Epidermal Growth Factor Receptor

F

FADD - Fas-Associated Death Domain

FBS - Fetal Bovine Serum

FDA - Food and Drug Administration

F1174L - Phenylalanine 1174 Leucine Mutation

FTIR - Fourier Transform Infrared Spectroscopy

G

G1269A - Glycine 1269 Alanine Mutation

G719X - Glycine 719 Mutation

H

HO – Hoechst

I

I1171T - Isoleucine 1171 Threonine Mutation

IL – Interleukin (-2,4,6,10,13)

IOPS – *Inonotus Obliquus* Polysacharride

J

JNK - c-Jun N-terminal Kinase

L

L858R - Leucine 858 Arginine Mutation

L861Q - Leucine 861 Glutamine Mutation

M

MDR1 - Multi-Drug Resistance Protein 1

MMPs - Matrix Metalloproteinases

MDR- Multi-Drug Resistance

MTT - 3-(4,5-Dimethylthiazol-2-yl)-2,5-Diphenyltetrazolium Bromide

P

PD-L1- Programmed death ligand 1

PD-1 - Programmed death 1

pH - Potential of Hydrogen

PI - Propidium Iodide

PSK - Polysaccharide-Krestin

PBS - Phosphate-Buffered Saline

Q

QR - Quick Response

R

RIP1 - Receptor-Interacting Protein 1

RIPK - Receptor-Interacting Protein Kinase

ROS - Reactive Oxygen Species

RP – Relative Potency

S

SAHPRA - South African Health Products Regulatory Authority

S768I - Serine 768 Isoleucine Mutation

S1206Y - Serine 1206 Tyrosine Mutation

SHP - Src Homology Phosphatase

SCLC - Small Cell Lung Cancer

T

T790M - Threonine 790 Methionine Mutation

TGF-β - Transforming Growth Factor Beta

TLR - Toll-Like Receptor

TNF - Tumour Necrosis Factor

TNFR1 - Tumour Necrosis Factor Receptor 1

TRAIL - TNF-Related Apoptosis-Inducing Ligand

TRAIL-R - TRAIL Receptor

CHAPTER 1: INTRODUCTION

1.1 Lung Cancer

Lung cancer is one of the most prevalent cancers worldwide and is associated with high morbidity and mortality. Tobacco exposure is the primary risk factor, responsible for approximately 70% of cases. The remaining 30% occur in individuals with no smoking history, with a higher incidence observed in Asian populations, where driver gene alterations, particularly mutations in the epidermal growth factor receptor (EGFR), are common (Meyer *et al*., 2024). Additionally, air pollution has been identified as a significant contributing factor (Meyer *et al*., 2024). Despite advances in cancer diagnostics and treatment, lung cancer remains a leading cause of cancer-related deaths globally.

According to Globocan 2020 data, lung cancer was the second most diagnosed cancer worldwide, with an incidence rate of 11.4% (Sung *et al*., 2021). It was also the leading cause of cancer-related deaths, contributing to 18% of cancer mortality in the same year (Sung *et al*., 2021). In South Africa, lung cancer was the fourth most diagnosed cancer in 2020, accounting for 8.3% of cases, but it ranked first in cancer-related mortality at 13.6% (Sung *et al*., 2021). Among males, it was the second most common cancer (12%), following prostate cancer (25.8%). Among females, lung cancer ranked fourth (4.9%), with breast (27.1%), cervical (28.7%), and colorectal (6.3%) cancers taking the top three positions (Sung *et al*., 2021).

The 5-year overall survival rate for lung cancer patients across all stages (I-IV) is 19%, with survival rates declining as the disease progresses. For patients with stage IA lung cancer, the 5-year survival rate exceeds 75%, whereas it drops to less than 10% for stage IV patients (Li *et al*., 2022).

Lung cancer often remains asymptomatic until advanced stages, making early detection critical for improving outcomes (Li *et al*., 2022). Advanced-stage lung cancer is associated with tumour invasion of surrounding tissues, metastasis, and complications such as paraneoplastic syndromes, which contribute to its poor prognosis (Li *et al*., 2022). Additionally, higher tumour mutation burdens and genetic instability in advanced disease stages promote cancer progression. Cancer cells may also evade the immune system by creating an immunosuppressive tumour microenvironment, which accelerates tumour growth and reduces the efficacy of treatment (Li *et al*., 2022).

1.1.1 Lung Cancer Classification

Lung cancers are typically diagnosed through histopathological examination, involving microscopic evaluation of biopsy samples (Lemjabbar-Alaoui *et al*., 2015). They are classified as small-cell lung carcinoma (SCLC) or non-small-cell lung carcinoma (NSCLC), with SCLC accounting for 15% and NSCLC comprising 85% of cases (Rodrigues-Canales *et al*., 2016). Molecular profiling is now routinely performed alongside histopathology to further classify lung cancers and guide treatment decisions (Rodrigues-Canales *et al*., 2016). NSCLCs are further subdivided into three main histopathological types: adenocarcinoma, squamous cell carcinoma, and large cell carcinoma (Watanabe *et al*., 2010).

1.1.1.1 Adenocarcinoma

Adenocarcinoma is the most common type of lung cancer in non-smoking patients and accounts for ~50% of all lung cancer cases (Myers and Wallen, 2023). It usually occurs in peripheral regions of the lung and can often be found at sites of chronic inflammation and in scar tissue (Myers and Wallen, 2023). Adenocarcinoma can present with diverse histological patterns, sometimes intermixed within the same tumour. These histological patterns are acinar, papillary, micropapillary, lepidic and solid patterns (Inamura, 2017). Solid pattern adenocarcinoma can be difficult to distinguish from large cell and squamous cell carcinomas based on histology alone. To aid in diagnosis, pneumocyte markers are evaluated, including mucin production and immunohistochemical expression of napsin A or thyroid transcription factor 1, which are specific to solid pattern adenocarcinoma (Rodrigues-Canales *et al*., 2016). Additionally, adenocarcinoma is a malignant tumour characterized by glandular differentiation of epithelial cells (Rodrigues-Canales *et al*., 2016).

1.1.1.2 Squamous cell carcinoma

Squamous cell carcinoma is the second most common lung cancer subtype and accounts for approximately 30% of all lung cancer cases (Sabbula *et al*., 2024). Squamous cell carcinoma is more strongly associated with smoking than adenocarcinoma and large cell carcinoma types of NSCLCs (Sabbula *et al*., 2024).

Squamous cell carcinoma affects squamous cells which make up the lining of airways as well as other organs in the human body. Squamous cell carcinomas usually occur in main airways or central parts of the lung, such as the bronchus (Sabbula *et al*., 2024). This subtype is characterized by the expression of p40/p63, intercellular bridges and cytokeratin 5/6 which may result in keratinization (Villalobos and Wistuba, 2017). Although keratinization is a hallmark of squamous cell carcinoma, it does not always present with the morphological

features of keratinization. There are three histological variants of squamous cell carcinoma: basaloid, keratinizing, and non-keratinizing (Sabbula *et al*., 2024).

1.1.1.3 Large cell carcinoma

Large cell carcinoma is uncommon, and accounts for a minute percentage of all lung cancers (approximately 2%) (Rodriques-Canales *et al*., 2016). This cancer type is defined as an undifferentiated NSCLC and does not show immunohistochemical evidence of small cell, glandular or squamous cell differentiation (Rodriques-Canales *et al*., 2016). Diagnosing large cell carcinomas cannot be done on cytology samples and core needle biopsies, instead extensive sampling of a surgically resected specimen is required after ruling out adenocarcinoma, squamous cell carcinoma and SCLCs (Rodriques-Canales *et al*., 2016).

Distinguishing between large cell carcinoma, adenocarcinoma, squamous cell carcinoma and SCLCs is aided by the diagnostic markers mentioned previously (Section 1.1.1.1 and 1.1.1.2). Large cell carcinoma may be positive for cytokeratin but will be negative for p40 which distinguishes it from squamous cell carcinoma. Large cell carcinoma further is negative for TTF-1 which distinguishes it from adenocarcinoma (Rodriques-Canales *et al*., 2016).

1.1.2 Lung Cancer Treatment

Treatment for lung cancer is determined by several factors, including tumour stage, size, location, the patient's overall health, and the cancer type (NSCLC or SCLC) (Lemjabbar-Alaoui *et al.,* 2015). Surgery is the preferred and most effective treatment option for early-stage, resectable lung cancer (Lemjabbar-Alaoui *et al.,* 2015). Resectable tumours are those that can be surgically removed with clear margins and without causing significant damage to surrounding vital structures. These tumours are typically localized, have not spread extensively to lymph nodes or distant organs, and are often found in patients with adequate lung function and general health to tolerate surgery (Goldstraw *et al*., 2011).

In contrast, non-resectable tumours are those that cannot be safely or completely removed due to factors such as large tumour size, invasion into nearby critical structures (e.g., major blood vessels or the heart), extensive lymph node involvement, or distant metastasis. These tumours are commonly found in more advanced stages of lung cancer and often require non-surgical treatments (Goldstraw *et al*., 2011).

For patients with non-resectable tumours, chemotherapy and radiation are commonly used, either sequentially or concurrently, depending on the clinical scenario. Radiotherapy,

chemotherapy, and surgery remain the primary treatment modalities, often used in combination based on the cancer type and stage (Lemjabbar-Alaoui *et al.,* 2015). Approximately 40% of lung cancer cases are diagnosed at advanced stages, with most patients presenting with non-resectable disease, excluding surgery as a treatment option (Provencio *et al*., 2011). Advances in molecular profiling have enabled the identification of key biomarkers, such as anaplastic lymphoma kinase (ALK) translocations, epidermal growth factor receptor (EGFR) mutations, and overexpression of Programmed death 1 (PD-1) or Programmed death ligand 1 (PD-L1) immune checkpoints, leading to the development of targeted therapies (Villalobos and Wistuba, 2017).

1.1.2.1 Radiotherapy

Radiotherapy is often used in combination with surgery or chemotherapy. Nonetheless, for advanced stages of NSCLC (stage III) the survival rates are poor, and radiotherapy is not effective in treating the late stages of lung cancer (Provencio *et al*., 2011).

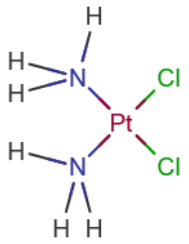
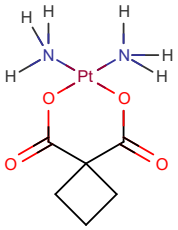
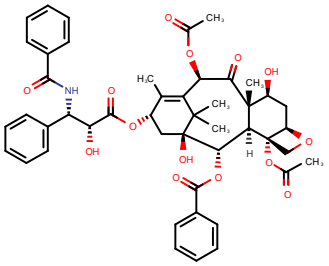
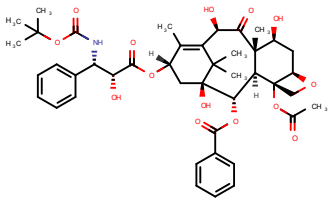
1.1.2.2 Chemotherapy

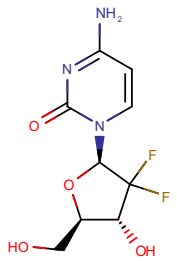
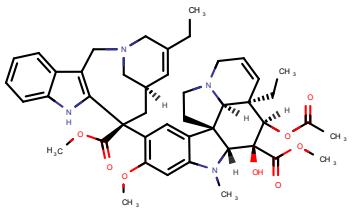
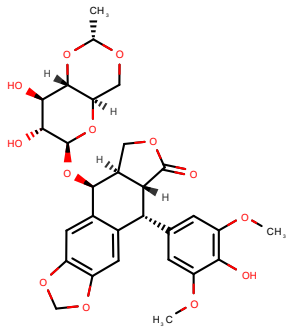
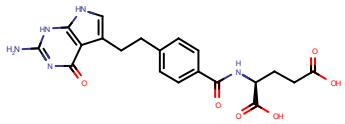
Chemotherapy is a systemic cancer treatment that involves administering drugs, either intravenously or orally, to target and kill cancer cells. In the case of NSCLC, chemotherapy plays a vital role in several stages of treatment depending on tumour size, stage, spread, and patient health status. Its primary goal is to shrink tumours, control the disease, or eliminate microscopic cancer cells that may not be visible on imaging tests (Araujo *et al*., 2020).

Chemotherapy may be recommended for NSCLC in several clinical situations. Neoadjuvant chemotherapy is administered before surgery, often in combination with radiation therapy, to shrink the tumour and improve the chances of successful surgical removal (Chiang *et al*., 2019). This approach may also allow for less extensive surgery or make previously inoperable tumours eligible for resection (Chiang *et al*., 2019). Adjuvant chemotherapy is given after surgery to eliminate any remaining cancer cells and reduce the risk of recurrence (Chiang *et al*., 2019). Even if there is no visible evidence of cancer post-surgery, it is often recommended due to the possibility of microscopic cancer cells remaining (Chiang *et al*., 2019). For patients with locally advanced NSCLC, where tumours have invaded nearby structures or surgery is not an option, chemotherapy is typically combined with radiation as the main treatment. In metastatic NSCLC (Stage IV), where the cancer has spread to distant organs, chemotherapy is frequently used as the primary treatment to control disease progression and relieve symptoms (National Comprehensive Cancer Network, 2024). This can be done alone or in combination with

targeted therapies or immunotherapies, depending on the tumour's molecular profile. Several drugs are commonly used to treat NSCLC, either alone or in combination (National Cancer Institute, 2024):

Table 1.1 Common Chemotherapeutic drugs used to treat NSCLC

Common Chemotherapeutic Drugs for NSCLC	Description	Structures	PubChem CID
Cisplatin	A platinum-based chemotherapy agent that interferes with deoxyribonucleic acid (DNA) replication, leading to cancer cell death.		546003
Carboplatin	Another platinum-based drug, often used as an alternative to cisplatin, especially for patients who may not tolerate cisplatin's side effects.		426756
Paclitaxel	A taxane drug that prevents cancer cells from dividing by stabilizing their microtubules.		36314
Docetaxel	Another taxane that works similarly to paclitaxel by inhibiting cell division.		148124

Gemcitabine	An antimetabolite that disrupts DNA synthesis, leading to cell death.		60750
Vinorelbine	A vinca alkaloid that blocks the formation of microtubules, preventing cell division.		5311497
Etoposide	A topoisomerase inhibitor that prevents DNA unwinding, leading to DNA damage and cell death.		36462
Pemetrexed	An antimetabolite that disrupts folate-dependent processes critical for DNA synthesis, often used in combination with cisplatin or carboplatin.		135410875

1.1.2.2.1 Combination Chemotherapy

Combination chemotherapy refers to using two or more drugs simultaneously to target cancer cells through different mechanisms, enhancing the overall effectiveness (Araujo *et al*., 2020). The most common combinations for NSCLC typically include a platinum-based drug (cisplatin or carboplatin) plus another agent, such as: (i) Cisplatin + Pemetrexed: A preferred combination for adenocarcinoma or large-cell NSCLC. (ii) Cisplatin or Carboplatin + Paclitaxel: Commonly used for squamous cell carcinoma. (iii) Carboplatin + Docetaxel or

Gemcitabine: Alternatives for patients who may not tolerate cisplatin (Araujo *et al*., 2020; National Comprehensive Cancer Network, 2024).

Combination treatments are often chosen to improve outcomes, but they can also increase the risk of side effects, which must be carefully managed (National Cancer Institute, 2024; National Comprehensive Cancer Network, 2024). Chemotherapy remains an essential component of lung cancer management, particularly for patients with unresectable or advanced disease. With ongoing advancements in supportive care and treatment combinations, the side effects of chemotherapy can be managed more effectively to enhance patients' quality of life during treatment (National Cancer Institute, 2024; National Comprehensive Cancer Network, 2024).

1.1.2.3 Targeted molecular therapies.

1.1.2.3.1 Epidermal growth factor receptor mutations

Epidermal growth factor receptor (EGFR) is a protein found on cell surfaces that helps control signals for cell survival, growth, and division (Iyer *et al*., 2024). In many NSCLCs, EGFR undergoes mutations that drive cancer growth (Iyer *et al*., 2024). Tyrosine kinase inhibitors (eg. Erlotinib and gefitinib) are drugs used to block these abnormal signals, effectively targeting mutated EGFR. However, over time, cancer cells often develop resistance to tyrosine kinase inhibitors, which reduces the treatment’s effectiveness (Iyer *et al*., 2024).

The most common EGFR mutations, known as "classic mutations," are exon 19 deletions and exon 21 L858R substitutions, accounting for about 90% of EGFR mutations (Zhang *et al*., 2019). An L858R substitution is a specific mutation where the amino acid leucine (L) is replaced by arginine (R) at position 858 in exon 21. This leads to excessive signalling for cell growth and survival. Patients with these mutations generally respond well to tyrosine kinase inhibitors and often have longer progression-free survival compared to patients treated with traditional chemotherapy. Second-generation tyrosine kinase inhibitors, such as afatinib and dacomitinib, have shown better outcomes when used as first-line treatments for patients with classic EGFR mutations (Zhang *et al*., 2019).

Uncommon EGFR mutations, which include G719X, L861Q, S768I, complex mutations, and exon 20 insertions, vary in their response to EGFR-targeted therapies. G719X is a mutation on exon 18 in which glycine (G) at position 719 is replaced by another amino acid, L861Q is a

substitution of leucine (L) at position 861 with glutamine (Q) in exon 21, S768I is a mutation in exon 20 where serine (S) at position 768 is replaced by isoleucine (I) (Zhang *et al*., 2019).

The effectiveness of treatment depends on the specific mutation within exons 18-21, though the reasons for these differences are not fully understood (Zhang *et al*., 2019). First-generation tyrosine kinase inhibitors, like gefitinib and erlotinib, can benefit patients with some uncommon mutations, and second-generation tyrosine kinase inhibitors have shown improved outcomes for mutations such as G719X, L861Q, and S768I. However, exon 20 insertion mutations are generally resistant to EGFR-targeted drugs. In 2021, the Food and Drug Administration (FDA) granted accelerated approval for mobocertinib to treat NSCLC patients with exon 20 insertion mutations (Duke *et al*., 2023). Currently, there is no universally accepted treatment strategy for patients with uncommon EGFR mutations (Zhang *et al*., 2019).

1.1.2.3.2 Anaplastic lymphoma kinase mutations

ALK is a member of the tyrosine kinase receptor superfamily, which plays a critical role in the cell signalling processes that regulate cell survival, growth, and division (Du *et al*., 2018). Under normal conditions, ALK helps control these cellular functions, but genetic alterations can lead to its abnormal activation, driving cancer cell proliferation.

There are three primary types of ALK gene mutations: amplifications, rearrangements, and point mutations (Du *et al*., 2018). ALK amplification (ALK-A) mutations result in multiple extra copies of the ALK gene, leading to constitutive activation of the ALK receptor. This activation selectively triggers downstream signalling pathways, including the activation of Sec homology 2 domain-containing transforming protein C, a substrate of the ALK receptor, which promotes uncontrolled cell proliferation. ALK amplifications have been observed in various cancers, such as NSCLC, pulmonary sarcomatoid carcinomas, and anaplastic large-cell lymphoma (Du *et al*., 2018). ALK rearrangements (ALK-R) occur when parts of the ALK gene are fused with another gene, creating an oncogenic fusion protein (Du *et al*., 2018). This fusion leads to abnormal ALK activation, driving cancer cell survival and proliferation. ALK rearrangements are commonly observed in a subset of NSCLCs (Du *et al*., 2018). Point mutations are single nucleotide changes in the ALK gene that lead to the substitution of one amino acid for another in the ALK protein. These mutations are often associated with acquired resistance to ALK inhibitors (Du *et al*., 2018). For example, specific point mutations such as V1180L (Valine (V) is replaced by leucine (L) at position 1180), D1203N (Aspartic acid (D) is replaced by asparagine (N) at position 1203), S1206Y (Serine (S) is replaced by tyrosine (Y)

at position 1206), I1171T (Isoleucine (I) is replaced by threonine (T) at position 1171), G1269A (Glycine (G) is replaced by alanine (A) at position 1269), F1174L (Phenylalanine (F) is replaced by leucine (L) at position 1174), and C1156Y (Cysteine (C) is replaced by tyrosine (Y) at position 1156) have been identified in NSCLC patients who develop resistance to ALK-targeted therapies (Du *et al*., 2018). Point mutations are clinically significant because they influence the effectiveness of ALK inhibitors and necessitate adjustments in treatment strategy (Du *et al*., 2018).

Several ALK inhibitors have been developed to target abnormal ALK signalling in NSCLC and other cancers. These include first-generation ALK inhibitors: crizotinib, which effectively blocks ALK but may lead to drug resistance over time. Second-generation ALK inhibitors: alectinib and ceritinib, which are more potent and can target some resistance mutations. Third-generation ALK inhibitors: Designed to overcome resistance from certain point mutations, offering options for patients whose cancers have progressed on earlier treatments (Du *et al*., 2018).

1.1.2.3.3 Immune checkpoint inhibitors

Programmed death-1 (PD-1) is a T-cell inhibitory checkpoint molecule. The role of PD-1 was better understood when its ligands, PD-L1 and PD-L2, were discovered. PD-1 binds to these ligands to maintain immune tolerance, preventing T-cells from attacking normal tissue (Sharma *et al*., 2022). When PD-1 engages with its ligand, it inhibits T-cell activation by blocking signals from the T-cell receptor. This is done through the recruitment of proteins called SHP-1 and SHP-2, which deactivate key molecules involved in T-cell receptor signalling, such as CD3 epsilon chain and zeta-chain-associated protein kinase 70 (Sharma *et al*., 2022).

In cancer, PD-1 is often overexpressed on tumour infiltrating T-cells, especially “exhausted” T-cells that are less effective at fighting tumours (Sharma *et al*., 2022). Tumour cells and other cells in the tumour microenvironment, such as endothelial and myeloid cells, frequently express PD-L1. PD-L2 is mostly found on antigen-presenting cells. When PD-1 binds to PD-L1 in the tumour microenvironment, it supresses the T-cells’ ability to mount an anti-tumour response (Sharma *et al*., 2022).

Blocking the interaction between PD-1 and PD-L1 using anti-PD-1 or anti-PD-L1 antibodies has been shown in animal studies to improve T-cell responses and shrink tumours. Clinical trials later confirmed the effectiveness of these antibodies in patients with various cancers, including melanoma, renal cell carcinoma, and NSCLC. The FDA first approved monoclonal

anti-PD-1 antibodies for metastatic melanoma in 2014, followed by approval of multiple PD-1/PD-L1 inhibitors for other cancers (Sharma *et al*., 2022).

PD-1 and PD-L1 therapies work by blocking signals that reduce T-cell activity, helping the immune system better attack tumours. PD-1 works after T-cells have already recognized and targeted a tumour (Sharma *et al*., 2022). It acts during the effector phase of the T-cell response, mainly affecting exhausted CD8 T-cells, which are less effective in fighting cancer. Blocking PD-1 or PD-L1 helps these exhausted T-cells regain their ability to attack tumour cells (Sharma *et al*., 2022).

Hence, based on the molecular markers expressed in the cancer, different chemotherapeutic drugs are used as presented in Table 1.2.

Table 1.2: NSCLC treatments by individual molecular marker types. Table adapted from Goodman & Gillman's: The Pharmacological Basis of Therapeutics, Chapter 69: General Principles in the Pharmacotherapy of Cancer (Chabner and Barnes, 2018).

Cancer indication	**Individual molecular marker (DNA, mRNA, protein)**	**TARGET: drugs**
Lung NSCLC	ALK translocation	ALK: alectinib, ceritinib, crizotinib
Lung NSCLC	EGFR deletion of exon 19 or L858R mutation	EGFR: afatinib, dacomitinib, erlotinib, gef itinib
Lung NSCLC	EGFR T790M mutation	EGFR: osimertinib
Lung NSCLC	PD-L1* expression	PD-1*, PD-L1: pembrolizumab

*PD-L1 – Programmed death ligand 1, PD-1 – programmed death-1

Tailoring treatments based on the molecular profile of NSCLC has significantly improved patient outcomes by targeting specific drivers of cancer growth and overcoming mechanisms of drug resistance (Du *et al*., 2018).

1.2 Drug Resistance

Cancer drug resistance is a complex and multifactorial process that can be either intrinsic or acquired during treatment (Mansoori *et al*., 2017). While many cancers initially respond to therapy, resistance often develops over time, leading to treatment failure. This phenomenon is driven by various mechanisms, including increased drug efflux, alterations in drug targets, enhanced DNA repair, and activation of survival pathways (Mansoori *et al*., 2017).

One of the most well-characterized resistance mechanisms is the active efflux of xenobiotics from a cell, primarily mediated by adenosine triphosphate (ATP)-binding cassette (ABC) transporters. These transmembrane proteins actively expel chemotherapeutic agents from

cancer cells, thereby reducing intracellular drug accumulation and limiting cytotoxic efficacy (Bukowski *et al*., 2020). The ABC transporter superfamily in humans consists of 49 members, including key transporters such as multidrug resistance protein 1 (MDR1/P-glycoprotein), multidrug resistance-associated protein 1 (MRP1), and breast cancer resistance protein (Housman *et al*., 2014). These transporters perform essential physiological functions, such as maintaining the integrity of the blood-brain barrier, and protecting cells against toxic effects of xenobiotics making them important in the development of drug resistance (Housman *et al*., 2014).

The overexpression of ABC transporters in tumours is frequently associated with poor clinical outcomes due to decreased intracellular drug retention and efficacy. Strategies to overcome efflux-mediated resistance include the use of transporter inhibitors, such as gefitinib, which targets breast cancer resistance protein to enhance drug sensitivity (Housman *et al*., 2014; Bukowski *et al*., 2020). Furthermore, oncogenic signalling pathways, including the mitogen-activated protein kinase cascade, regulate the expression of ABC transporters, with kinase overactivation further promoting resistance (Housman *et al*., 2014; Bukowski *et al*., 2020). Targeting these signalling pathways presents a potential therapeutic strategy to counteract drug efflux and improve chemotherapy outcomes (Housman *et al*., 2014; Bukowski *et al*., 2020).

1.2.1 P-Glycoprotein

P-glycoprotein is a major contributor to drug efflux-mediated resistance and belongs to the ABC transporter superfamily, the largest class of membrane transporters responsible for the translocation of diverse substrates, including sugars, peptides, amino acids, proteins, and metabolites, across intra- and extracellular membranes (Pasquier *et al*., 2013).

P-glycoprotein is capable of recognizing and exporting a broad spectrum of chemotherapeutic agents with varying chemical structures and molecular weights (250–1202 Da) (Pasquier *et al*., 2013). By actively pumping these compounds out of cells, P-glycoprotein serves as a critical mediator of multidrug resistance and is widely recognized as a biomarker for treatment failure in cancer therapy. Consequently, targeting P-glycoprotein function has been a major focus in efforts to enhance drug retention and restore chemotherapy sensitivity.

Given that the current study investigates the effects of selected medicinal mushrooms on lung cancer cells, evaluating their potential to modulate P-glycoprotein expression or function is particularly relevant. If certain mushroom-derived compounds are able to inhibit or suppress

the expression P-glycoprotein, they may help reverse drug resistance and improve the efficacy of chemotherapeutic agents.

1.3 Cell death

Cell death is a fundamental biological process essential for maintaining tissue homeostasis, eliminating damaged or harmful cells, and shaping immune responses. It can occur through various mechanisms, including apoptosis, a highly regulated process of programmed cell death; necroptosis, a form of inflammatory cell death that shares features with necrosis but is genetically controlled; pyroptosis, which is triggered by infections and involves the activation of inflammatory caspases; and ferroptosis, a form of iron-dependent cell death driven by lipid peroxidation (Strasser and Vaux, 2020). Understanding these distinct pathways is crucial, as dysregulation in cell death contribute to diseases such as cancer, neurodegeneration, and autoimmune disorders. The following sections will explore specific forms of cell death, highlighting their unique characteristics and significance in cancer (Strasser and Vaux, 2020).

1.3.1 Apoptosis

Apoptosis, first described by Kerr, Wyllie, and Currie (1972), is a distinct form of programmed cell death that plays a fundamental role in development, tissue homeostasis, and disease. Unlike necrosis, which is characterized by uncontrolled cell lysis and inflammation, apoptosis is a tightly regulated process that facilitates the systematic elimination of cells without eliciting an immune response (Kerr *et al*., 1972; Festjens *et al*., 2006).

Cells undergoing apoptosis experience morphological and biochemical changes that occur in two distinct phases. The first phase is characterized by nuclear and cytoplasmic condensation, followed by the formation of membrane-bound apoptotic bodies. These apoptotic bodies contain cellular fragments that maintain structural integrity (Kerr *et al*., 1972). In the second phase, phagocytic cells such as macrophages recognize and engulf these apoptotic bodies, facilitating their degradation via lysosomal enzymes (Kerr *et al*., 1972; Silva, 2010). The absence of inflammatory responses in apoptosis highlights its physiological importance in regulating cell numbers and eliminating damaged or potentially harmful cells (Festjens *et al*., 2006).

Apoptotic cell clearance is mediated by apoptotic cell-associated molecular patterns, which signal phagocytes to recognize and engulf dying cells (Silva, 2010). One of the most well-characterized apoptotic cell-associated molecular patterns is phosphatidylserine, which is

translocated from the inner to the outer leaflet of the plasma membrane early in apoptosis, serving as an “eat me” signal for macrophages (Silva, 2010).

Apoptosis is primarily regulated by two distinct but interconnected pathways: the intrinsic (mitochondrial) pathway and the extrinsic (death receptor) pathway (Elmore, 2007) (Figure 1.1). The intrinsic pathway is governed by the B-cell lymphoma 2 (Bcl-2) family of proteins, which regulate mitochondrial outer membrane permeabilization. In response to stimuli such as DNA damage, oxidative stress, or growth factor deprivation, pro-apoptotic proteins (e.g., Bcl-2-Associated X Protein (Bax), Bcl-2 Antagonist/Killer (Bak)) induce mitochondrial permeability, leading to the release of cytochrome c and other apoptogenic factors (Elmore, 2007). Cytochrome c associates with apoptotic protease-activating factor-1 to form the apoptosome, which activates caspase-9 and subsequently caspase-3, initiating the execution phase of apoptosis (Elmore, 2007).

The extrinsic pathway is initiated by the activation of death receptors belonging to the tumour necrosis factor (TNF) receptor superfamily, including Fas (CD95) and TNF-related apoptosis-inducing ligand (TRAIL) receptors (Elmore, 2007). Upon ligand binding, these receptors recruit adaptor proteins such as Fas-associated death domain (FADD) and TNF receptor-associated death domain, leading to the activation of caspase-8 (Elmore, 2007). Caspase-8 can directly activate executioner caspases or engage the intrinsic pathway by cleaving BH3 interacting-domain death agonist, a pro-apoptotic Bcl-2 family member, thereby amplifying the apoptotic response (Elmore, 2007).

Apoptosis plays a critical role in preventing tumorigenesis, as the loss of apoptotic regulation is a hallmark of cancer (Pfeffer and Singh, 2018). Cancer cells evade apoptosis through various mechanisms, including overexpression of anti-apoptotic Bcl-2 proteins, and the overexpression of apoptotic inhibitor proteins like cIAP-1/2 and XIAP which inhibit caspase, in addition a loss of pro-apoptotic factors such as Bax and Bak is common (Pfeffer and Singh, 2018). Understanding apoptotic signalling pathways is therefore essential for developing targeted cancer therapies aimed at restoring apoptotic sensitivity in malignant cells.

Research suggests that apoptosis is not the only form of programmed cell death, as necroptosis and other caspase-independent mechanisms have been identified (Festjens *et al*., 2006). Unlike apoptosis, necroptosis is a regulated form of necrosis that involves receptor-interacting protein kinases (RIPK1 and RIPK3), leading to membrane rupture and inflammation (Festjens *et al*., 2006). The interplay between apoptotic and non-apoptotic cell death pathways underscores the

complexity of cellular homeostasis and the need for further investigation into their regulatory mechanisms.

In summary, apoptosis is a highly conserved and tightly regulated process that ensures cellular turnover, maintains tissue integrity, and prevents disease. Its dysregulation contributes to a range of pathologies, from cancer to neurodegenerative disorders, making it a crucial focus of biomedical research.

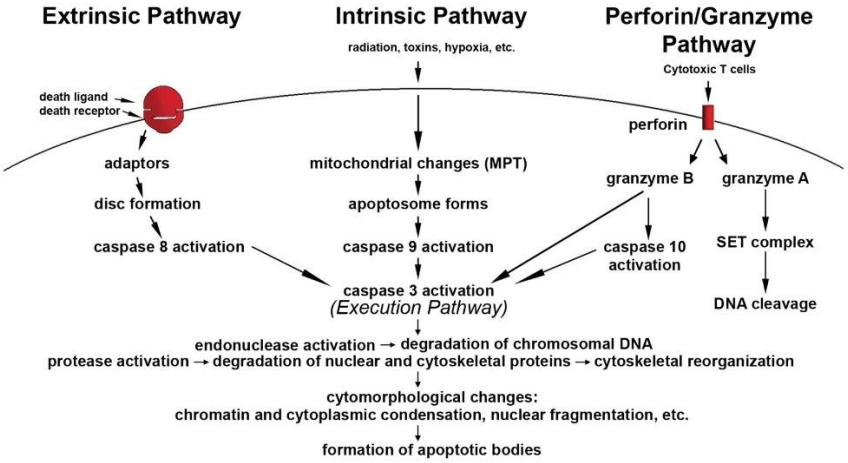


Figure 1.1 Schematic representation of apoptotic events. Adapted from Elmore S. Apoptosis: A review of programmed cell death. Toxicologic Pathology. 2007;35(4):495–516. © 2007 SAGE Publications. Used with permission.

1.3.2 Necrosis

The term "necrosis" is derived from a Greek word, "nekros" which means corpse. Necrosis is a form of pathological cell death which has been described as an unprogrammed cell death, as a result of physio-chemical stress (Zong and Thompson, 2006). Necrosis being thought of as "unprogrammed" is a concept which is reinforced by the fact that the exposure of cells to supraphysiological conditions would lead to necrotic cell death (Zong and Thompson, 2006). More recently, it has been shown that the response to a death stimulus is often a continuum of apoptosis and necrosis (Zong and Thompson, 2006). Many substances cause apoptosis at lower doses while causing necrosis at higher doses (Zong and Thompson, 2006). *In vivo*, if a cell is not engulfed by a phagocyte or in-vitro, where phagocytosis does not happen, dead cells in a late stage of apoptosis may present with features of necrosis (Zong and Thompson, 2006). This is due to the loss of plasma membrane integrity and the loss of cellular energy. The process by which this occurs is called "secondary necrosis" or "apoptotic necrosis" (Zong and Thompson, 2006).

The morphological features of necrosis include irreversible plasma membrane damage, cytoplasmic and nuclear swelling both of which leads to an increase in cell volume, karyorrhexis (nuclear fragmentation), karyolysis (nuclear dissolution), nuclear pyknosis, cytoplasmic vacuoles and organelle breakdown (Kroemer *et al*., 2009; Khalid and Azimpouran, 2023). As a result of all the morphological changes, necrotic cells appear to be more vacuolated and eosinophilic (Khalid and Azimpouran, 2023). There are three phases during necrosis: (i) initiation, (ii) propagation, and (iii) execution. The phases cannot be easily distinguished, especially propagation and execution. This is because many cellular events are initiated and occur simultaneously (Khalid and Azimpouran, 2023).

Necrotic cell death is regulated by a set of catabolic mechanisms and signal transduction pathways. Toll-like receptors (TLR3 and TLR4) and death domain receptors (tumour necrosis factor receptor 1 (TNFR1), (TNF-related apoptosis-inducing ligand receptor)TRAIL-R and Fas/CD95) have been shown to elicit necrosis in the presence of caspase inhibitors (Degterev *et al*., 2008). TLR3, TRAILR, Fas/CD95 and TNFR1-mediated cell death depend on the kinase called RIP1. This has been shown in studies using necrostatin-1 to knockout and chemically inhibit RIP1 (Degterev *et al*., 2008). This can be used to discriminate between programmed necrosis (necroptosis) and accidental necrosis, since necroptosis is avoided by inhibiting RIP1 (Kroemer *et al*., 2009).

FADD is a crucial adaptor molecule at the crossroads of apoptotic and necrotic cell death. FADD contains both a death effector domain for initiating apoptotic signalling and a death domain for initiating necrotic signalling. Hindering caspase activation switches cell death from apoptosis to necrosis (Festjens *et al*., 2006). Necrotic cell death is not due to one signalling cascade but rather a result of the interplay between several signalling pathways. The RIP1 kinase is a central initiator of necrosis and has a role in the TNFα-induced necrosis as well as for TRAIL-R, TF-R1, and Fas-induced necrosis. The identification of RIP1 substrates will give more insight into the downstream signalling pathways which contribute to death receptor-induced necrotic cell death (Festjens *et al*., 2006).

1.3.3 Autophagy

Autophagy is a lysosome-dependent catabolic process characterized by the formation of double-membrane autophagosomes that sequester and degrade cytoplasmic components (Jung *et al*., 2020). It occurs at a basal level for cellular homeostasis and under stress conditions as a survival mechanism by recycling cellular components for energy and metabolism (Jung *et al*.,

2020). However, excessive autophagy can lead to autophagic cell death (ACD) (Shimizu *et al*., 2014).

Autophagy is regulated by extracellular signals, including cytokines and hormones. Th1 cytokines (interleukin-2 (IL-2), interferon-γ, TNF-α, TGF-β) induce autophagy, while Th2 cytokines (IL-4, IL-10, IL-13), insulin, and insulin-like growth factor-1 inhibit it (Jung *et al*., 2020). Morphologically, ACD involves extensive autophagic vacuolization without chromatin condensation and lacks phagocytic clearance (Kroemer *et al*., 2009).

Over 30 autophagy-related proteins (Atgs) regulate autophagy. Atg1 initiates the process, while Beclin1 (Atg6) and phosphatidylinositol 3-kinase facilitate membrane invagination (Shimizu *et al*., 2014). The Atg5-Atg12 and microtubule-associated protein 1A/1B-light chain 3-phosphatidylethanolamine conjugation pathways drive autophagosome formation, with microtubule-associated protein 1A/1B-light chain 3 translocation serving as an autophagy marker (Shimizu *et al*., 2014).

ACD requires both autophagy activation and specific death signals. Jun N-terminal kinase (JNK) phosphorylation is crucial, as Bax or Bak deficient cells exposed to apoptotic stimuli undergo ACD only when JNK is activated (Shimizu *et al*., 2014). Nutrient-starved cells with autophagic structures do not undergo ACD in the absence of JNK activation, highlighting its essential role (Shimizu *et al*., 2014).

1.4 Complementary and Alternative Medicine

The South African Health Products Regulatory Authority (SAHPRA) defines "complementary medicine" as any substance or mixture of substances derived from natural sources such as algae, fungi, plants, lichens, seaweed, minerals, and animals, which are used outside the framework of conventional pharmaceutical drugs. Further, the substance must be used, manufactured or sold for the use in complementing or assisting the mental or physical state (SAHPRA, 2020). Whereas "alternative medicine" refers to treatments that are used as a replacement for conventional therapies.

Complementary and Alternative Medicines (CAMs) are classified into five subcategories, (i) alternative whole medicine systems, (ii) mind-body interventions, (iii) biologically based therapies, (iv) energy therapies, and (v) manipulative and body-based methods (Ventola, 2010). Health supplements fall into the "biologically based therapies" subcategory (Table 1.3).

Table 1.3 The five subcategories of CAMs and a description of each subcategory. CAM subcategories and descriptions obtained from Ventola, 2010.

CAM subcategory	Description
Alternative Whole Medicine Systems	Ayuverdic, Chinese, naturopathic and homeopathic medicines
Mind-Body Interventions	Prayer, mental healing, dance therapy, music and meditation
Biologically Based Therapies	Food, herbs, vitamins and health supplements
Energy Therapies	Reiki, electromagnetic field exposure and therapeutic touch
Manipulative and Body-Based Methods	Osteopathic and chiropractic manipulation and massage

1.4.1 Health Supplement Market and Regulation

In 2020, the global health supplement market size accounted for $191.1 billion (United States Dollar) and is expected to grow to $307.8 billion by 2028 at a compound annual growth rate (CAGR) of 5.9% between 2021 and 2028 (Zion Market Research, 2021). In South Africa, the Vitamins and Minerals segment of the health supplement industry accounts for $231.5 million (United States Dollar) and is expected to grow annually by 4.3% (CAGR 2023-2027) (Statista, 2023).

A large amount of the South African population consumes some type of health supplement daily (Modhia, 2022). Vitamins and minerals are utilized most often and is followed by traditional medicine and speciality supplements such as probiotics and omega-3s (Modhia, 2022). Online sales in web retailers and supplement websites have expanded substantially over the years (Dunn *et al*., 2005). The emergence of popularity surrounding health supplements has identified a gap in both knowledge and communication for health professionals with regards to being able to provide patients with advice about these treatments (Dunn *et al*., 2005). There is a lack of evidence-based information about the safety, drug-interactions and efficacy of health supplements, especially the complementary and alternative medicines (Ventola, 2010).

In the United States, health supplements are classified as “functional foods” and are regulated as food rather than pharmaceuticals. The FDA does not require supplements to undergo efficacy evaluation and mandates only minimal safety data for new ingredients (Starr, 2015). Products without new ingredients require no testing or safety data (Starr, 2015).

While mandates exist for introducing new supplement ingredients, their implementation remains incomplete due to the absence of finalized guidelines defining sufficient safety evidence (Starr, 2015). Even if fully enforced, these guidelines may improve but not fully address safety concerns. Key regulatory shortcomings include manufacturers selectively submitting favourable data, the lack of mandatory premarket human safety studies, and the reliance on historical use as evidence of safety (Starr, 2015). Despite FDA oversight, companies can legally market supplements with new ingredients, even if later found to be unsafe (Starr, 2015).

In South Africa, CAMs and health supplements are regulated under the Medicines and Related Substances Act 101 of 1965 (SAHPRA, 2020). Health supplements are regulated less strictly than scheduled medicines. “Health supplements” is defined by SAHPRA as any substance, mixture of substances or extract as determined by the Authority, sold in dosage forms used or purported for use in restoring, correcting or modifying any mental or physical state by either, (i) supplementing the diet, (ii) having a nutritional effect or (iii) complementing health. The definition excludes medicines or substances which are listed as Schedule 1 or higher in the Medicines and Related Substances Act, 1965 (Act 101 of 1965) and further excludes injectable preparations.

Supplements have been subjected to registration since 2013 by virtue of SAHPRA under section 14(2) of the Act. In registering supplements, SAHPRA require that all manufacturers, importers, exporters, and wholesalers of complementary medicines are licensed as per section 22C(1)(b) of The Medicines Act. The registration and licensing process must be preceded by a confirmation of compliance with good pharmacy practice from South African Pharmacy Council and a Pharmacy Premises Licence through the National Department of Health.

1.5 Mushrooms for medicinal use

Mushrooms are the fruiting bodies of fungi and are highly valued worldwide for their nutritional properties and palatability (Saritha *et al*., 2016). They contain a diverse range of bioactive compounds, including both primary and secondary metabolites (Saritha *et al*., 2016). Primary metabolites, which constitute a significant portion of mushroom biomass, include peptides, proteins, β-glucans (Figure 1.2), and oxalic acid (Kirha *et al*., 2023). β-glucans function as immune adjuvants, stimulating both innate and adaptive immune responses (Kirha *et al*., 2023).

Mushrooms also produce secondary metabolites such as steroids, quinolones, terpenes, anthraquinones, and benzoic acid derivatives, many of which have antimicrobial properties, inhibiting the growth of various microbes (Kirha *et al*., 2023).

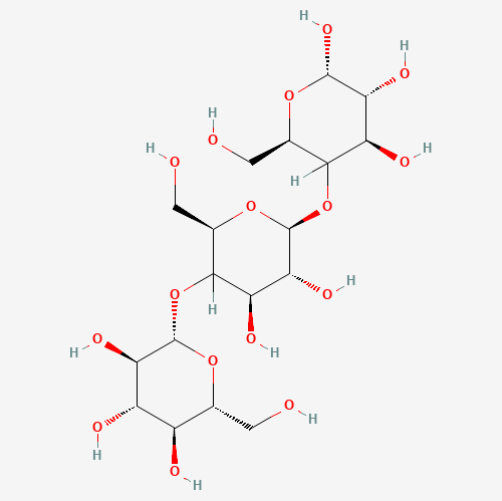


Figure 1.2 The two dimensional structure of β-glucan. The molecular formula is $C_{18}H_{32}O_{16}$, PubChem CID 439262**.** It is a glucose polymer consisting of a beta (1 – 3) linked beta-D-glucopyranosyl unit with beta (1-6) linked side chains of varying lengths.

In addition to their nutritional value, certain mushrooms have been used as adjuvant therapy in Eastern medicine to enhance the efficacy of conventional cancer treatments or mitigate their adverse effects (Habtemariam, 2020; Jeitler *et al*., 2020). The bioactive compounds attributed with anticancer properties include fungus-derived glucans such as grifolan, lentinan, polysaccharide peptides, proteoglycans, glycan, as well as triterpenoids, triterpenes, and flavonoids (Kirha *et al*., 2023).

Fungi have also been a significant source of drug discovery, contributing not only to anticancer agents but also to antibiotics, antifungals, antivirals, immunosuppressants, and treatments for malaria and diabetes (Brunton *et al*., 2023; Habtemariam, 2020). Notable FDA-approved drugs derived from fungi include anthracyclines (chemotherapy), penicillin (antibiotic), cyclosporine (immunosuppressant), and lovastatin (cholesterol-lowering agent) (Brunton *et al*., 2023).

Many mushrooms are classified as “medicinal mushrooms” due to their use in traditional medicine. Certain bioactive molecules, such as β-glucans, regulate immune cell development, differentiation, and proliferation, thereby activating immune responses and inhibiting cancer metastasis and growth (Kirha *et al*., 2023). Polysaccharides are among the most effective and widely studied mushroom-derived compounds with immunomodulatory and antitumor

properties, with their biological activity influenced by variations in monosaccharide composition and structure (Lu *et al*., 2021).

Currently, a variety of commercialized mushroom products, including tinctures, capsules, powders, and teas, are marketed as health supplements with claimed pharmacological benefits. Three of the most widely used medicinal mushrooms are *Trametes versicolour* (*T. versicolour*), *Ganoderma lucidum* (*G. lucidum*), and *Inonotus obliquus* (*I. obliquus*).

1.5.1 *T. versicolour*

T. versicolour (Figure 1.3) is a species of fungus in the *Polyporaceae* family and has been under intensive investigation in recent years (Habtemariam, 2020). *T. versicolour* grows in many countries around the world, including South Africa. Eastern medicine has made use of the proposed medicinal properties of *T. versicolour* and other fungi for well over 2000 years (Habtemariam, 2020).



Figure 1.3 *Trametes versicolour* fruiting body. Image obtained from Biomons website. (https://biomons.com/en/colorful-flat-tube-trametes-versicolor-mushroom-of-vitality/)

The main biomolecules associated with these mushrooms are polysaccharides in the form of β-glucans which are homopolysaccharides consisting of D-glucose monomers linked through β-glycosidic bonds (β-1,3, β-1,4, β-1,6) (Friedman, 2016; Du *et al*., 2019). Other polysaccharides found in mushrooms include heteropolysaccharides such as polysaccharide-krestin (PSK) and an analogous compound polysaccharide peptide (PSP) is found in some strains of *T. versicolour* (Friedman, 2016). While both PSK and PSP contain β-1,3, β-1,4, and β-1,6 glycosidic linkages, they differ in their sugar composition: PSK includes fucose, fructose, galactose, mannose, and xylose, whereas PSP contains rhamnose and arabinose (López-Gil *et al*., 2024). Structurally, PSK consists of a β-glucan backbone with β-1,4 main chains and β-1,3 and β-1,6 side chains, with a protein component attached at the β-1,6 side chain (Friedman, 2016). It has an approximate molecular weight of 100,000 Da. PSP, on the other hand, contains

the amino acid sequence Aspartic Acid-Cysteine-Proline-Proline-Cysteine-Glutamic Acid (Nation Center for Biotechnology Information, 2025).

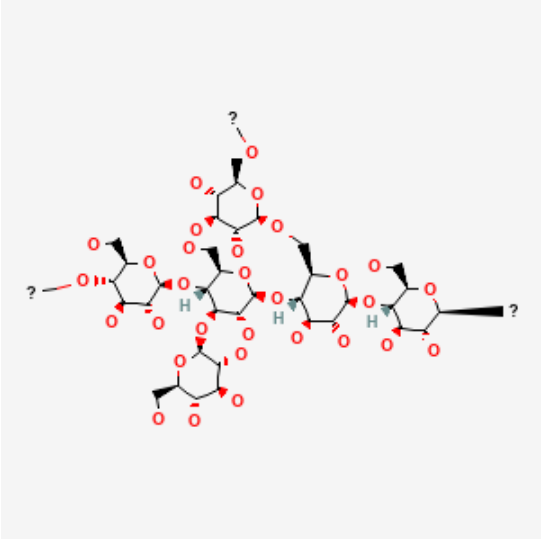


Figure 1.4 The two-dimensional structure of polysaccharide krestin. Polysaccharide krestin is a protein bound polysaccharide extracted from *Trametes versicolour*. The protein component is located at the β-1,6 side chain. It has a molecular weight of 94kDa. PubChem SID 135316798.

PSK has been widely adopted as an adjunctive and adjuvant therapy in oncology, particularly in Japan, where it has been approved as an anticancer drug since 1977, and in China since 1987 (Winder *et al*., 2021). Initially used as an adjuvant treatment for gastric cancer, PSK has showed significant clinical benefits, including improved disease-free survival and overall survival in colorectal cancer patients, as shown in meta-analyses (Sakamoto *et al*., 2006). Additionally, the use of adjuvant PSK has been associated with increased five-year survival rates in patients with recurrent breast cancer (Sugimachi *et al*., 1984). Decades of research in Asian countries have confirmed the efficacy of T. versicolor components as supportive therapy for various cancers, including those of the stomach, nasopharynx, rectum, colon, and lungs (Winder *et al*., 2021).

The immunomodulatory properties of *T. versicolour* are largely attributed to its polysaccharide constituents, particularly PSK and PSP, which enhance both innate and adaptive immune responses. PSK has been shown to activate TLRs, primarily TLR2 and TLR4, leading to the maturation of dendritic cells and the subsequent release of pro-inflammatory cytokines such as IL-12, TNF-α, and IL-6 (Engel *et al*., 2013). This activation mechanism is critical, as TLR engagement on antigen-presenting cells serves as a bridge between innate and adaptive immunity, promoting the activation of T and B lymphocytes (Lu *et al*., 2011). Furthermore, β-

glucans present in PSK and PSP are recognized by immune receptors, stimulating macrophages, monocytes, and natural killer cells, which further contribute to an antitumor immune response (Standish *et al*., 2008). Notably, PSK has been reported to enhance IL-2 production in Cluster of differentiation 4 Positive T cells through modulation of T-cell receptor signalling rather than direct TLR engagement, suggesting a more complex mechanism of action beyond simple pattern recognition receptor activation (Asai *et al*., 2008). However, despite the extensive documentation of PSK's immunostimulatory effects, critical gaps remain in understanding its precise molecular interactions, particularly its dependency on TLR2/TLR4 versus alternative pathways. Moreover, while preclinical and clinical studies suggest a role for PSK in augmenting immune responses in cancer therapy, standardized methodologies for evaluating its efficacy and safety in different patient populations are still needed.

The anticancer activity of these compounds is observed in concentrations less than 1 mg/mL and many experiments have shown activity at concentrations ≤ 100 μg/mL (Pawlikowska *et al*., 2020; Roca-Lema *et al*., 2019). Roca-Lema *et al*. (2019) investigated the effects of polysaccharide-rich extracts from *T. versicolour* in human colon cancer cell lines (LoVo and HT-29). Their study found that *T. versicolour* extracts inhibited proliferation and induced cytotoxicity in a dose-dependent manner, with significant effects observed at concentrations as low as 10 μg/mL. The extracts suppressed anchorage-independent cell growth, indicating a reduction in tumorigenic potential. Migration and invasion assays showed that *T. versicolour* extracts inhibited metastatic behaviour by increasing E-cadherin expression and decreasing matrix metalloproteinase-2 activity (Roca-Lema *et al*., 2019). When combined with 5-fluorouracil, *T. versicolour* extracts enhanced cytotoxicity, suggesting a potential role as an adjuvant therapy in colorectal cancer (Roca-Lema *et al*., 2019). The concentrations at which *T. versicolour* has anticancer activity in A549 cells will be determined in this study.

1.5.2 *G. lucidum*

Ganoderma lucidum (Figure 1.5), commonly known as Ling-zhi in China and Reishi in Japan, belongs to the *Ganodermataceae* family within the Basidiomycetes class. This edible mushroom has been widely used in Traditional Chinese Medicine and other Eastern medical practices for centuries due to its diverse pharmacological properties (Jin *et al*., 2016).



Figure 1.5 *Ganoderma lucidum* fruiting body (obtained from Zeng *et al*., 2019).

Research has showed that *G. lucidum* has antitumor, anti-inflammatory, and antioxidant properties, making it a promising candidate for complementary and alternative medicine (Heah *et al*., 2020). The prominent bioactive compounds responsible for the proposed immunomodulatory and anticancer properties of this species are polysaccharides, in the form of β-glucans, and triterpenes (Jin *et al*., 2016).

As previously stated, β-glucans have been shown to stimulate both adaptive and innate immunity by targeting dendritic cells, neutrophils, macrophages, monocytes and natural killer cells (Jin *et al*., 2016). The β-glucan binds to receptors on immune cells which triggers a series of molecular pathways such as the protein kinase C, NFκB and mitogen-activated protein kinase which would ultimately lead to activation of the host immune system and proliferation of immune cells (Jin *et al*., 2016).

The basic chemical structure of triterpenoids found in *G. lucidum* is that of an oxygenated lanostane (Feng *et al*., 2013). Ganoderic acid is the most studied triterpenoid in *G. lucidum* (Figure 1.6) (Feng *et al*., 2013). Structure-activity relationship assays of 43 triterpenoids extracted from *G. lucidum* showed that the side-chain, C-3 carbonyl group, hydroxyl groups and double bonds are important in the cytotoxicity of *G. lucidum* triterpenoids (Feng *et al*., 2013; Liang *et al*., 2019). The anticancer activity of *G. lucidum* extracts such as ganoderic acid, was shown by Liu *et al*. (2012). In this study LC-MS/MS was used to identify α and β-tubulin as a target for ganoderic acid. Ganoderic acid interacts with the subunits of α and β-tubulin, thereby affecting microtubule function and achieving anticancer activity (Liu *et al*., 2012). Polysaccharides of *G. lucidum*, mainly act as immunomodulators or antioxidants while triterpenoids function to inhibit cancer cell proliferation and metastasis (Xu *et al*., 2011; Camargo and Kaneno, 2011).

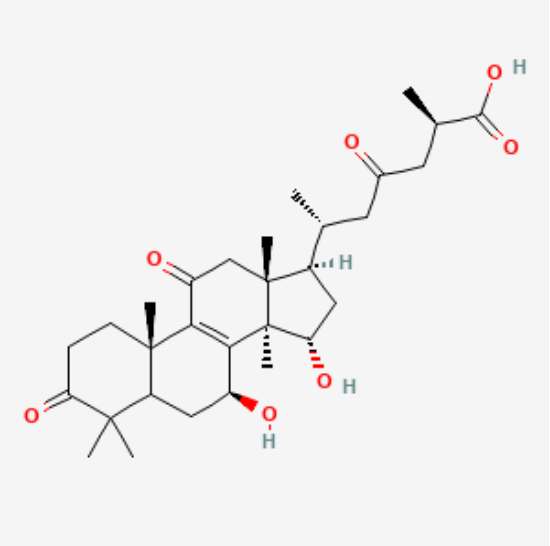


Figure 1.6 Ganoderic acid two-dimensional structure. Ganderic acid is the main triterpenoid in *Ganoderma lucidum*. It has the molecular formula C33H44O7, PubChem CID 73554535 and a molecular weight of 516.7 g/mol.

In addition to its anticancer potential, *G. lucidum* has been used to manage a range of health conditions, including hypertension, gastric ulcers, bronchitis, arthritis, chronic hepatitis, immunological disorders, and hypercholesterolemia (Heah *et al*., 2020). Studies suggest that its immunomodulatory effects enhance the body's defence mechanisms by stimulating the activity of macrophages, natural killer cells, and T lymphocytes (Heah *et al*., 2020). Furthermore, polysaccharides found in *G. lucidum* have been shown to improve gut microbiota balance, which plays a crucial role in immune system regulation and overall health (Heah *et al*., 2020).

1.5.3 *I. obliquus*

Inonotus obliquus, commonly known as Chaga, is a parasitic fungus that predominantly colonizes the trunks of birch trees in cold climates (Figure 1.7). The fungus aids in the absorption of moisture and nutrients, facilitating tree recovery, although prolonged colonization can ultimately lead to tree decay (Arata *et al*., 2016). Traditionally used in Eastern medicine, *I. obliquus* has been recognized for its anticancer, antioxidant, and immunomodulatory properties (Arata *et al*., 2016). Its bioactive constituents include *I. obliquus* polysaccharides (IOPS), polyphenols, triterpenoids, and melanin, each contributing to its therapeutic potential.



Figure 1.7 *Inonotus obliquus* fruiting body. Image obtained from Herbal Reality website. (https://www.herbalreality.com/herbalism/western-herbal-medicine/chaga-mushroom-medicinal-properties/).

IOPS, a major bioactive component, has a relative molecular mass of 156,611 Da and exerts anticancer effects through the regulation of matrix metalloproteinases (MMPs) (Lu *et al*., 2021). MMPs, such as MMP-2, MMP-7, and MMP-9, play a crucial role in extracellular matrix degradation, which facilitates tumour invasion and metastasis (Lu *et al*., 2021). IOPS has been shown to suppress MMP activity while upregulating tissue inhibitor of metalloproteinases-2, thereby reducing cancer cell migration and invasion (Lu *et al*., 2021). Additionally, IOPS downregulates nuclear factor kappa B (NF-κB), a key transcription factor involved in tumour progression and inflammation, further contributing to its antitumor effects (Lu *et al*., 2021).

Al-Tuwaijri *et al*. (2021) showed that half maximal inhibitory concentrations (IC_{50})values for *I. obliquus* extracts ranged from 1.27 to 1.80 mg/mL depending on the method of extraction. Other studies have shown that extracts had cytotoxic activity against A549 cells at IC_{50} values of 0.02 mg/ml at 48 h (Zhong *et al*., 2009).

1.6 Problem Statement

Lung cancer remains the leading cause of cancer-related mortality worldwide, with poor prognosis and limited treatment efficacy, particularly when diagnosed at advanced stages. Conventional therapies, including chemotherapy and radiotherapy, often fail due to drug resistance and inadequate tumour suppression.

Medicinal mushrooms, such as *Ganoderma lucidum*, *Trametes versicolour*, and *Inonotus obliquus*, have a long history of use in traditional medicine systems for managing respiratory illnesses, enhancing immunity, and promoting general wellbeing. In traditional Chinese medicine, *G. lucidum* has been used to treat respiratory conditions such as asthma, coughs, and lung deficiency syndromes. Similarly, *T. versicolour* has traditionally been employed as

an immune tonic and as an adjunct in treating pulmonary infections. *I. obliquus*, widely used in Siberian and Eastern European folk medicine, has been consumed for ailments including persistent cough, bronchitis, and other lung-related complaints. These ethnomedicinal applications suggest potential relevance to lung health and offers a rationale for investigating these species in the context of lung cancer.

While *G. lucidum* has been investigated for its effects on A549 lung cancer cells, the comparative effects of other mushrooms like T. versicolour and I. obliquus, as well as their potential to modulate drug resistance remains undescribed. However, the effects of other mushrooms like *T. versicolour* and *I. obliquus*, as well as their potential to modulate drug resistance, remain unknown. Further investigation is needed to determine anticancer activity and efficacy of these species, particularly in the context of lung cancer treatment.

This study aims to evaluate the effect of *G. lucidum*, *T. versicolour* and *I. obliquus* on the viability and proliferation of A549 lung adenocarcinoma cells, with a particular focus on apoptosis induction and potential modulation of drug resistance pathways, including P-glycoprotein expression. By systematically assessing these effects, this research will contribute to understanding whether these natural compounds have measurable anticancer activity, in addition to their traditional use in complementary medicine.

1.7 Research Aim

This study aims to evaluate the effect of mushroom extracts (*G. lucidum*, *T. versicolour* and *I. obliquus* extracts) obtained from commercially available supplements on the A549 lung adenocarcinoma cell line and on a non-cancerous cell line (HEK293 cells).

1.8 Research Objectives

I. To assess labelling information on selected commercially available mushroom supplement products.
II. To assess the uniformity of mushroom extracts obtained from different sources using Fourier Transform Infrared spectroscopy (FTIR).
III. To evaluate the stability of the mushroom extracts over time, using FTIR.
IV. To determine IC_{50} values of the mushroom extracts (*T. versicolour* extracts, *G. lucidum* extracts and *I. obliquus* extracts) and doxorubicin against the A549 and HEK293 cell lines.
V. To determine whether mushroom extracts cause necrosis.

VI. To determine the expression of reactive oxygen species (ROS) in A549 and HEK293 cells when treated with doxorubicin and mushroom extracts.

VII. To determine if extracts induce P-glycoprotein resistance genes by measuring P-glycoprotein expression caused by the mushroom extracts and doxorubicin against A549 and HEK293 cells.

VIII. Determine whether cells were undergoing apoptosis by using two methods (Annexin-V and Caspase-3/7 Assay).

IX. To determine the effect of the mushroom extracts and doxorubicin on membrane phosphatidylserine expression and Caspase-3/7 activity in A549 and HEK293 cells.

X. To determine if the mushroom extracts have any effect on the efficacy of doxorubicin.

CHAPTER 2: METHODOLOGY

2.1 Assessment of information provided on the labels of commercial preparations of mushrooms.

Mushroom products were purchased from an online health foods store called 'Faithful To Nature' (www.faithfultonature.co.za) which is based in Cape Town, Western Cape, South Africa. The products were supplied in three forms: tinctures (dual extracts), dried raw material, and powdered extracts encapsulated in vegetarian capsules. The product labels indicated that each preparation contained the respective mushroom species with no other additives, and they were minimally processed with no fillers or preservatives added. The products consisted of locally manufactured, internationally imported and locally assembled products. The purchase was determined by popularity of the products as shown by the "filter" search results on the website. The three mushroom types were selected based on claims of anticancer and immunomodulatory properties.

The information on labels was assessed according to specific predetermined categories which included the following: general information, warnings, claims, disclaimers, quality assurance and scientific pledge. For this study, a warning is defined as a statement of caution to the consumer, a disclaimer is a statement which denies responsibility and is an act of repudiating a claim, a claim is defined as an assertion that something is true - typically without providing evidence, quality assurance refers to the standard of the product according to the manufacturer and a scientific pledge refers to a guarantee by the manufacturer.

This assessment method was informed by the general regulations made under the Medicines and Related Substances Act, 1965 (Act 101 of 1965), particularly Regulation 10, which outlines the required labelling elements for human-use medicines and health supplements. Notably, Regulation 10(1)(cc)(iii) requires unregistered complementary medicines to carry the disclaimer: "This unregistered medicine has not been evaluated by the SAHPRA for its quality, safety or intended use."

Each supplement was evaluated for the presence or absence of the aforementioned labelling categories. The information was transcribed into a Microsoft Office Excel 2016 spreadsheet (Excel©, 1985-2024 Microsoft Corporation). Statements were captured as either "yes" or "no" statements. Percentage values were then assigned to each category and investigated for statistical analysis.

2.2 Extract preparation.

In preparation of all aqueous extracts, Milli-Q™ (Millipore Elix 3 Water Purification System) water was used. The storage instructions found on product labels for the mushroom supplements were followed if provided by the manufacturer. Products of different dosage forms were used for extract preparation. The dosage forms used were tinctures, capsules, and powders. All mushroom extracts and tinctures used were stored at 4°C. Extracts made from powders followed the same procedures as those for capsules.

A dual extraction method using methanol and dichloromethane was used for powders and capsules. Methanol is a polar, water soluble solvent while dichloromethane (also called methylene chloride) is slightly polar and not miscible in water (Cequier-Sánchez *et al*., 2008). This polarity range allows for the extraction of a wide range of compounds with both polar and non-polar constituents. Additionally, having the mixture of methanol and dichloromethane allows for improved solubility of compounds which may not be soluble in either solvent alone (Cequier-Sánchez *et al*., 2008).

2.2.1 Procedure for extraction from dried material or capsules

Capsules were emptied and 2 g of dry mushroom mass was weighed out into a beaker (Figure 2A). To this, 50 ml of a 1:1 dichloromethane: methanol mixture was added and left to stir overnight, covered to prevent evaporation. The mixture was then filtered using 8-12 µm filter paper (Ahlstrom Munksjö, Lasec, South Africa) and the filtrate was left to evaporate in a fume hood overnight. The residue was resuspended in either water (*I. obliquus*) or 7:3 ethanol: Dimethyl Sulfoxide (DMSO) (*G. lucidum* and *T. versicolour*). The resuspended solutions were then filtered through a Acrodisc® PF Syringe Filter 0.8/0.2 µm Supor® Membrane and stored in a tube at 4°C until use (Figure 2.2 A).

2.2.2 Procedure from extractions from tinctures

Ten millilitres of each tincture was evaporated in a fume hood overnight (Figure 1B). The residue was weighed and redissolved in either water (*I. obliquus*) or a 7:3 mixture of ethanol: DMSO (*G. lucidum and T. versicolour*) to make a stock concentration of 20 mg/ml. Extracts were then stored at 4°C.

2.3 Fourier Transform Infrared Spectroscopy.

Fourier Transform Infrared Spectroscopy (FTIR) is used to identify polymeric, organic, and sometimes inorganic materials. The assay uses infrared light of 10 000 to 100 cm^{-1} which is transmitted through a given sample. As the radiation is transmitted through the sample, the

respective wavelength is absorbed depending on the composition of the sample (Nandiyanto *et al*., 2019). Different functional groups can be identified based on the wavenumber (location of the x-axis). Single bonds lie between 2500 – 4000 cm^{-1}, triple bonds lie between 2000 – 2500 cm^{-1}, double bonds span from 1500 – 2500 cm^{-1} (Nandiyanto *et al*., 2019). This absorbed radiation is converted into vibrational and/or rotational energy by the sample molecules. A spectrum is generated from this which typically ranges from 4000 cm^{-1} to 400 cm^{-1} and acts as a fingerprint for the sample being investigated (Nandiyanto *et al*., 2019). The fingerprint region can be found from 600 – 1500 cm^{-1}. Fingerprints are unique to different molecular structures which makes FTIR a qualitative technique which can be used for the identification of different compounds, batch consistency analysis, and the assessment of stability of compounds (Nandiyanto *et al*., 2019).

2.3.1 FTIR inter-batch analysis.

FTIR analysis was performed on liquid samples from three batches of tinctures. No modifications were made to the tinctures. Fifty microliters of each tincture and/or extract sample were used. The Perkin Elmer Spectrum GX (Perkin-Elmer, Beaconsfield, BUCKS, UK) was used to analyse samples. Twenty scans per sample in the region 4000 – 650 cm^{-1} were performed. The Spectrum software (PerkinElmer, Inc. Version 10.4.1) was used to obtain spectra.

2.3.2 Stability assessment of the mushroom extracts by FTIR.

The stability of the mushroom extracts (*G. lucidum* and *T. versicolour*) were assessed over a period of 5 weeks. FTIR analysis was performed on liquid samples stored at various temperatures. Samples were stored at room temperature, at 4 °C, and at -18°C. The first analysis was done on the day the extracts were prepared (week 0) and subsequently once a week thereafter. The region 4000 – 650 cm^{-1} was used, and twenty scans were done for each sample.

2.4 Cell culture.

The A549 lung cancer and HEK293 cell lines were purchased from the American Type Culture Collection and verified for authentication by short tandem repeat analysis by Inqaba biotec, South Africa. Both cell lines were cultured in a 1:1 (v/v) solution of Dulbecco's Modified Eagles Medium (DMEM) (Sigma-Aldrich, Johannesburg, South Africa) and Ham F12 culture media (Sigma-Aldrich, Johannesburg, South Africa), supplemented with 10% (v/v) foetal bovine serum (FBS) (Thermo Fisher Scientific, Johannesburg, South Africa). Heat-inactivated FBS (Thermo Fisher Scientific, Johannesburg, South Africa) was purchased and stored at -

20℃. The Olympus DP72 inverted phase contrast microscope was used to observe cells daily to monitor growth and evaluate microbial contamination. The ethics waiver: W-CBP-220831-01, for the use of the cells in this study was granted by the Faculty of Health Sciences, University of the Witwatersrand (Appendix A).

The culture media for both A549 and HEK293 cells was supplemented with 1% (v/v) sodium pyruvate (Merck, Johannesburg, South Africa), 1% (v/v) L-glutamine (Merck, Johannesburg, South Africa), 1% (v/v) nonessential amino acids (Merck, Johannesburg, South Africa).

2.4.1 Maintenance and Sub-culturing.

Cells were grown in 75 cm^2 Greiner bio-one culture flasks (Lasec SA, Johannesburg, South Africa) in culture media supplemented with 10% FBS (Thermo Fisher Scientific, Johannesburg, South Africa) at 37℃ and 5% CO_2 humidified atmosphere. Cells were trypsizined using Trypsin-Ethylenediaminetetraacetic acid (Sigma-Aldrich, Johannesburg, South Africa) when 80-90% confluent. Cells were then either reseeded at an appropriate density for maintaining the culture or used for experimental assays.

2.4.2 Cryopreservation.

Cells were trypsinized and centrifuged at 1500 rpm for 5 minutes. The pellet was resuspended in freezing medium which contains 6% (v/v) cell culture grade DMSO (MW=78.13 $g \cdot mol^{-1}$) and HAM/DMEM cell culture media supplemented with 20% (v/v) FBS. The suspension was placed in Nest cryovials (Whitehead Scientific, Cape Town, South Africa) and stored at -70℃ in a cryo freezer box. A steady drop in temperature of 1℃ per minute is used to ensure maximal survival (Whaley *et al*., 2021). For long-term storage, cells were kept in liquid nitrogen at -140 to -196℃.

2.4.3 Determination of cell numbers and viability prior to experimental use.

Trypan blue ($C_{34}H_{28}N_6O_{14}S_4$) is a toluidine-derived dye. The trypan blue exclusion method was used to assess the viability of cells after trypsinisation and before cells were plated for experiments. Trypan blue is impermeable to cell membranes and enters cells with a compromised membrane integrity binding to intracellular proteins (Piccinini *et al*., 2017). Using phase contrast microscopy, the non-viable cells can be observed by their blue colouring while viable cells remain transparent (Piccinini *et al*., 2017).

A 1:1 (v/v) dilution was made with cell suspension and trypan blue (Sigma-Aldrich, Johannesburg, South Africa), the final concentration of trypan blue was 0.2% (w/v) in phosphate buffered saline (PBS). The cell suspension was placed on a haemocytometer and counted using a Nikon microscope by phase contrast microscopy (Magnification: 100x). Cells in the eight corners of the grid of the haemocytometer were counted and the average calculated. The following formula was used to determine the number of cells per ml of suspension:

$$\#cells\ per\ ml\ of\ cell\ suspension: Average\ number\ of\ cells\ counted\ \times 2 \times 10\ 000$$

2.5 Cell Viability Assay.

The 3-(4,5-dimethylthiazol-2-yl)-2,5-diphenyltetrazolium bromide (MTT) assay is used for the measurement of cell proliferation and cytotoxicity. The reduction of the yellow water-soluble tetrazolium dye (MTT) into an insoluble purple formazan crystal by mitochondrial dehydrogenases is an indication of viable cells (Mosmann, 1983).

A549 and HEK293 cells were seeded in 96-well microtiter plates (NEST Bio-tech Co., Ltd) at a density of 1×10^4 cells per well in 100 µl of culture media and incubated overnight at 5% CO_2 and 37°C. A549 and HEK294 cells were treated with a concentration range (0.000125 - 1 mg/ml) of mushroom extracts diluted in complete media. Each concentration was done in quadruplicate and incubated for 24 or 48 h. Doxorubicin was used as a positive control. A negative control containing untreated cells was included.

MTT (Sigma-Aldrich, Johannesburg, South Africa) was prepared at a concentration of 5 mg/ml (w/v in PBS), filtered through a 0.22 µm membrane and stored at 4˚C protected from light. Four h prior to the end of each incubation period, 40 µL MTT solution was added into each well and the plates incubated for 4 h. Following the incubation, plates were centrifuged at 1500 rpm for 7 minutes. The media was carefully aspirated, and the formazan crystals were dissolved in 200 µL DMSO. The plates were then agitated on an orbital plate shaker (Thermoshaker MRC) for 5 minutes at 1000 rpm. The absorbance (Optical Density at 540 nm and 690 nm) of each well of the 96 well-plate was measured at 540 nm and 690 nm on the Labysystems iEMS micro-plate reader. Blank wells contained no cells but did contain culture media and MTT solution.

2.5.1 Evaluation of active chemotherapeutic agents and mushroom extracts.

Extracts from three mushrooms, *Ganoderma lucidum*, *Trametes versicolour*, and *Inonotus obliquus*, were evaluated at concentrations ranging from 0.000125 to 1 mg/mL. This range was

selected to capture both low-dose and higher-dose effects commonly used in in vitro cytotoxicity studies and is consistent with previously published work on natural product screening. However, it is important to note that such concentrations may exceed physiologically achievable levels in vivo, particularly in the case of crude extracts, due to factors like poor absorption and rapid metabolism.

Doxorubicin, camptothecin, and irinotecan were used as positive controls. Doxorubicin was tested between 0.001 and 60 μM, while camptothecin and irinotecan were evaluated over a range of 0.1 to 100 μM. These concentrations encompass and extend slightly beyond therapeutically relevant plasma concentrations for these agents, ensuring detection of both cytotoxic and sub-cytotoxic effects in vitro.

2.5.2 Vehicle controls.

Vehicle controls are used in studies in which inert substances are used to solubilize a test substance (Johnson and Besselsen, 2002). To perform a vehicle control, the substance is used unaccompanied by the active test compound (Johnson and Besselsen, 2002).

Using the same concentration range of ethanol (0.000875 – 7 %) and DMSO (0.000375 – 3 %) used in the treatments, a vehicle control was performed. The percentage cell viability of the vehicle control was compared to that of the negative control to determine the effect of ethanol and DMSO in the A549 and HEK293 cell lines.

2.5.3 Determining IC_{50} values.

The IC_{50} value is defined as the half-maximal inhibitory concentration and were obtained by treating A549 and HEK293 cells to a range of concentrations of the active mushroom extracts identified as presented in Section 2.5.1 using the MTT assay.

The range of concentrations for *G. lucidum* and *T. versicolour* extracts was 0.000125 – 1 mg/ml whilst the concentration range for the positive control, doxorubicin, was 5.44×10^{-7} – 0.04 mg/ml (0.001 – 60 μM). Each concentration was performed in quadruplicate. Non-linear regression analysis was used to determine IC_{50} values, and a sigmoidal dose-response curve was constructed using GraphPad Prism Version 5.0. A Student's t-test was performed to determine whether the differences between IC_{50} values was significant. GraphPad Prism was used and a p-value of < 0.05 was considered statistically significant.

2.5.4 Combination studies.

A common practice in cancer treatment is to use a combination of compounds/drugs with different targets. This method of combination therapy is done with the aim of reducing the development of drug resistance, decreasing toxicity towards the patient, and increasing the therapeutic efficacy of the treatments (Fan *et al*., 1998).

A549 and HEK293 cells were treated with fixed concentrations (equivalent to IC_{50} values) of *G. lucidum* and *T. versicolour* extracts, while doxorubicin was tested across a range of concentrations (0.001–60 μM) to determine its IC_{50} value when combined with the extracts. This concentration range was the same as was used to construct the dose-response curve in Section 2.5.3. The design was informed by the concept of relative potency (RP), where a shift in the IC_{50} value of doxorubicin in the presence of the extract indicates a potential interaction. A decrease in IC_{50} suggests increased potency (potential synergy), while an increase suggests reduced efficacy (potential antagonism) (Villeneuve *et al*., 2000: Bijnsdorp *et al*., 2011).

2.6 Assessment of the effects of extracts on cell morphology

Morphological features of apoptosis and necrosis are well known. Three diffused dyes are used to assess the morphology of cells. These dyes are acridine orange (AO), Hoechst 33342 (HO) and propidium iodide (PI) (Foglieni *et al*., 2001).

In cells, AO accumulates in lysosomes due to the weak basic properties of the dye and the low internal potential of hydrogen (pH) of the lysosomes. Within the lysosomes, AO becomes protonated and trapped. The entrapment of AO is a feature of apoptosis and can be exploited for discrimination between apoptosis and necrosis (Vermes and Haanen, 1994). HO is a bis-benzimidazole dye which shows strong fluorescence when bound to DNA (Latt *et al*., 1975). The dye fluoresces at 461 nm when excited by UV light and emits a blue fluorescence (460-490 nm) (Atale *et al*., 2014; Crowley *et al*., 2016). Because of the DNA binding properties of HO, the dye can be used to observe nuclear condensation which is a feature of apoptosis (Crowley *et al*., 2016). PI is a membrane impermeable red-fluorescence dye which is excluded from cells with intact plasma membranes (viable cells and apoptotic cells) but will be retained in cells with impaired plasma membrane integrity (necrotic cells). PI intercalates between DNA strands and has an excitation/emission maxima of ~ 525/617 nm with bound DNA (Atale *et al*., 2014).

A549 and HEK293 cells were seeded onto sterile coverslips in 6-well plates at a density of 400 000 cells per coverslip and incubated overnight at 37°C and 5% CO_2. After the incubation period, cells were treated with *G. lucidum* and *T. versicolour* extracts at concentrations of 0.25

mg/ml and 0.5 mg/ml and the positive control, doxorubicin, at concentrations equivalent to the IC_{80} values. Treatments were done at 18 h and 24 h incubation periods. After the incubations, the diffused dyes AO, HO and PI were combined in PBS using the following ratio: 0.5% (v/v) AO, 0.2% (v/v) HO and 0.1% (v/v) PI. The fluorescent stain mixture was added to each well and incubated in the dark for 30 minutes at room temperature. Following the incubation, cells were mounted onto microscope slides using mounting solution (Sigma Alrdrich/Merck). Cells were viewed on the Olympus CKX41 microscope. Filter cube sets, U-MNIB3 (Excitation:480/20, Emission: 510/50) for AO, U-MWU2 (Excitation365/10, Emission 420 long pass) for HO 33342 and U-MWIG2 (Exitation535/30, Emission: 580 long pass) for PI were used. Images were captured using the Olympus DP72 camera and analysed using the Olympus CellSens Software package (Olympus, Tokyo, Japan).

2.7 Annexin-V assay

Annexin-V is a calcium-dependent protein that binds specifically to phosphatidylserine, which becomes exposed on the outer leaflet of the membrane during early apoptosis (Demchenko, 2013). Because annexin-V cannot permeate intact cell membranes, it only labels apoptotic cells while excluding viable ones. To distinguish apoptotic from necrotic or dead cells, PI is added, as it only stains cells that have lost membrane integrity.

A549 and HEK293 cells were seeded onto sterile coverslips within 6-well plates at a density of 400 000 cells per well and incubated overnight at 37°C and 5% CO_2. Cells were then treated with doxorubicin at concentrations equivalent to the IC_{80} values and incubated for 18 and 24 h, this served as the positive control. Cells were also treated with 0.25 mg/ml and 0.5 mg/ml of *T. versicolour* and *G. lucidum* and incubated for 18 and 24 h. An untreated negative control was included. The Invitrogen annexin V, Alexa Fluor™ 488 conjugate (Thermo-Fisher Scientific) was used to bind and detected translocated PS. The detection reagent was prepared by combining the conjugated Alexa Fluor 488-annexin-V reagent and PI to a 1× annexin-binding buffer (Thermo-Fisher Scientific). Coverslips were washed with PBS solution (pH 7.4). Next, 100 µl of the solution containing PI (1% v/v), Alexa Fluor 488-annexin-V conjugate (6% v/v) was added to each coverslip and incubated for 15 minutes in the dark. Coverslips were mounted onto microscope slides using mounting media and viewed using the Olympus BX41 microscope and images were captured using the Olympus DP72 camera. Images were analysed and processed using the Olympus CellSens Software.

2.8 The detection of caspase 3/7 activation caused by mushroom extracts and doxorubicin.

Caspase-3 is a member of the Cysteine-Aspartic acid protease family (Eskandari and Eaves, 2022). Caspases are produced as inactive zymogens which are then subjected to activation by a range of specific internal and/or external signals.

A549 and HEK293 cells were seeded onto sterile coverslips in 6-well plates at a density of 400 000 cells per well. Cells were treated at concentrations equivalent to the IC_{80} values of doxorubicin and concentrations of 0.25 mg/ml and 0.5 mg/ml of both *G. lucidum* and *T. versicolour* and incubated for 18 and 24 h. The CellEvent™ Caspase-3/7 Green Detection Reagent (Thermo-Fisher Scientific) was prepared in 5% (v/v) FBS. Media was aspirated from each well and the diluted Caspase-3/7 Green Detection Reagent was added to each coverslip. The plate was incubated in a 37°C incubator for 30 minutes, covered in foil. Coverslips were mounted onto microscope slides and viewed using the Olympus BX41 microscope and images were captured using the Olympus DP72 camera. The green, fluorescent signal confirms the activation of caspase-3/7. Caspase-3/7 is localized in the cytoplasm, where it cleaves downstream substrates that facilitate apoptotic cell disassembly. Images were analysed and processed using the Olympus CellSens Software.

2.9 Reactive Oxygen Species detection

ROS, also referred to as "free radicals", describes an array of oxygen-containing molecules which are highly reactive (Glorieux *et al*., 2024). ROS are produced in the mitochondria as a result of normal metabolism and the mitochondria are both the source and the target of ROS (Nakamura and Takada, 2021). A disruption in redox homeostasis has been linked to many diseases including cancer (Glorieux *et al*., 2024). ROS act as secondary messengers in both normal and cancer cell signalling (Nakamura and Takada, 2021).

In excess, ROS causes cells to undergo apoptosis due to damaged membranes, organelles, proteins and nucleic acids. At low levels, ROS acts as a signal transducer to activate angiogenesis, cell proliferation, migration, and invasion (Nakamura and Takada, 2021).

A549 and HEK293 cells were seeded at a density of 200 000 cells per well onto sterile coverslips within 6-well plates and incubated overnight at 37°C and 5% CO_2. The CellROX™ Deep Red Reagent (ThermoFisher Scientific, Invitrogen) was used. The reagent was prepared in culture media composed of 1:1 (v:v) DMEM (Sigma-Aldrich, Johannesburg, South Africa) and Ham F-12 media (Sigma-Aldrich, Johannesburg, South Africa). The treatments, *i.e.* doxorubicin, *G. lucidum*, and *T. versicolour* extracts were then added to the reagent and culture media. Doxorubicin was used as the positive control at concentrations equivalent to the IC_{80}

values while *G. lucidum* and *T. versicolour* extracts were used at both 0.25 mg/ml and 0.5 mg/ml. Cells were incubated with the CellROX™ Deep Red Reagent and the respective treatment compounds for 4 h. The Olympus CKX41 microscope was used to view cells. Images were captured using the DP72 camera.

2.10 The detection of P-glycoprotein expression in A549 and HEK293 cells after treatment with mushroom extracts and doxorubicin.

Immunofluorescence is an immunochemical technique used for the detection and localization of specific proteins in cell preparations and tissues (Im *et al*., 2019). Immunofluorescence is based on the use of antibodies that will recognize and bind to a specific target protein (Im *et al*., 2019).

Cells were seeded at a density of 200 000 cells per well in a 6 well plate onto sterile coverslips and incubated overnight at 37°C and 5% CO_2. After incubation, cells were treated with 0.25 and 0.5 mg/ml *T. versicolour* and *G. lucidum* extracts. Doxorubicin was used as the positive control and cells were treated at concentrations equivalent to the IC_{80} values. An antibody control which contained no primary antibody was included. Cells were incubated for 18 and 24 h. Thereafter, cells were washed with PBS twice. Cells were then fixed using 3.7% (v/v) formaldehyde and incubated for 20 minutes at room temperature. Formaldehyde was aspirated from all the wells and cells were washed with PBS twice. To permeabilize cell membranes, 0.25% (v/v) triton-X was added to cells and left to incubate for 20 minutes at room temperature. Cells were then washed twice using PBS. A solution containing 0.5% (v/v) bovine serum albumin (BSA) was used to block nonspecific binding of antibodies to the cell structure. Coverslips were incubated with the blocking solution for one hour at room temperature. Cells were then washed using PBS.

The primary antibody, 0.43 mg/ml mouse anti-human P-glycoprotein monoclonal Ab (MAS-12854) (Thermo Fisher Scientific, Johannesburg South Africa) was prepared as a 1:200 dilution in 0.5% (v/v) BSA. The negative control contained 0.5% (v/v) BSA but no primary antibody. This was done to check for non-specific binding of the secondary antibody and to assess the background fluorescence. Cells were incubated with the primary antibody overnight at 4°C. The following day, the primary antibody solution was removed from cells and cells were washed using PBS. The secondary antibody, 2 mg/ml goat anti-mouse polyclonal Ab (ab150113) (Thermo Fisher Scientific, Johannesburg South Africa) was prepared as a 1:800 dilution in 0.5% (v/v) BSA. Cells were incubated with secondary antibody in the dark and at

room temperature for one hour. Hoechst 33342 was added to cells to stain nuclei. Coverslips were mounted onto microscope slides using mounting solution (Sigma-Aldrich, Johannesburg, South Africa). Slides were stored at 4°C. The Olympus CKX41 microscope was used to view cells. Images were captured using the DP72 camera. The following filter cube sets were used: U-MWU2 (Excitation: 365/10, Emission: 420 long pass) for Hoechst 33342, and U-MNIB3 (Excitation: 480/20, Emission: 510/50) for Alexa Fluor 488.

2.11 Statistical Analysis

All experiments were repeated independently at least three times (n = 3). Results are expressed as mean ± standard error of the mean (SEM). Statistical analyses were performed using GraphPad Prism (version 5). For dose–response curves, non-linear regression analysis (log(inhibitor) vs. normalized response – variable slope) was used to calculate IC_{50} values. Comparisons between multiple groups were performed using One-way ANOVA assuming Gaussian distribution with Geisser-Greenhouse correction to determine statistical significance. For comparisons between two groups, unpaired two-tailed Student's t-tests were used when appropriate. For combination studies, shifts in IC_{50} values of doxorubicin in the presence of mushroom extracts were assessed using relative potency analysis. A statistically significant decrease or increase in IC_{50} was interpreted as a potential synergistic or antagonistic interaction, respectively. Differences were considered statistically significant at $p < 0.05$.

CHAPTER 3: RESULTS

3.1 Assessment of information provided on the labels of commercial preparations of mushrooms.

The information on labels was assessed according to specific predetermined categories which included the following: general information, warnings, claims, disclaimers, quality assurance and scientific pledge?. For this study, a warning is defined as a statement of caution to the consumer, a disclaimer is a statement which denies responsibility and is an act of repudiating a claim, a claim is defined as an assertion that something is true - typically without providing evidence, quality assurance refers to the standard of the product according to the manufacturer and a scientific pledge refers to a guarantee by the manufacturer.

Fifteen mushroom products were selected for analysis, of which 7 (46.67%) were manufactured locally, 2 (13.33%) were internationally imported products, and 6 (40%) did not indicate where the products were manufactured. Formulations consisted of powders 2 (13.33%), capsules 5 (33.33%), and tinctures 8 (53.3%). Of the 15 products, only 7 (46.67%) had product labels with instructions on the procedure to use the product.

All product labels 15 (100%) had recommended daily amounts. Only 13 (86.67%) product labels had ingredient lists. Seven (46.67%) product labels indicated expiration dates while two had “best before” dates. Seven (46.67%) product labels had batch numbers, and four (26.67%) product labels indicated storage instructions.

3.1.1 Product warning statements

Five (33.33%) product labels had warning statements, and one product (6.67%) listed a contraindication on the label. The warning categories are shown in Table 3.1.

Table 3.1 The warning categories indicated on the product labels (n=15).

Warning descriptions	Total	%
“Keep out of reach of children”	3	20
“Use with caution during pregnancy and lactation”	5	33.33
“Consultation with healthcare professionals”	2	13.33

3.1.2 Product disclaimers

Eight (53.33%) products contained a disclaimer on the label. A disclaimer is defined as a statement intended to specify or delimit the scope of rights and obligations that may be exercised and enforced by parties in a legally recognised relationship (Gabriels *et al*., 2012). Disclaimers observed on the eight labels were as described in Table 3.2 as follows:

Table 3.2 Description of different disclaimers on product labels (n=15).

Disclaimer descriptions	**Total**	**%**
"The product has not been evaluated by the Medical Controls Council/ SAHPRA"	8	53.33
"The product is not intended/certified to diagnose, treat, cure or prevent any disease"	8	53.33
"This medicine is not a substitute for medical attention"	1	6.67
"Consult a practitioner if symptoms persist"	1	6.67
"Health supplements are intended only to compliment health or supplement the diet"	3	20
"Consult a complimentary health practitioner regarding the use of the product during pregnancy"	3	20

The disclaimer advising individuals to consult a "complementary health practitioner" during pregnancy can be misleading and potentially dangerous (Table 3.2). Complementary health practitioners, such as naturopaths or herbalists, have no official medical training or qualifications of licensed medical doctors. They are not equipped to diagnose or manage health conditions during pregnancy, which requires specialized knowledge of both maternal and foetal health. Relying on their advice instead of consulting a qualified healthcare provider could lead to risks for both the mother and the baby, as they lack the necessary expertise to safely navigate the complexities of pregnancy-related health issues. It is crucial for expectant mothers to seek guidance from healthcare professionals who are trained and licensed in medical care, especially during such a critical time.

3.1.3 Product claims

Eight (53.33%) products contained a claim on the label. These claims were not necessarily backed by rigorous scientific investigation. One product (6.67%) contained a quick response (QR) code to view "lab results". Upon scanning the QR code, an error message appeared. The different categories of claims are shown in Table 3.3.

Table 3.3 Description of specific claims on product labels (n=15).

Claim description	Total	%
“Cancer support”	3	20
“Provides immune support / immune booster”	4	26.67
“Antioxidative properties”	4	26.67
“Stress reduction”	3	20
“Anti-inflammatory”	2	13.33
“Provides increased energy”	2	13.33
“Increased/renewed vitality”	3	20
“Reduces fatigue”	1	6.67
“Improves sleep”	1	6.67
“Improves gut balance”	1	6.67
“Tonic medicinal properties”	2	13.33
“Anti-viral properties”	1	6.67
“Enhances physical endurance”	1	6.67
“Adaptogen”	2	13.33
“Anti-aging”	1	6.67
“Supports longevity”	1	6.67
“Promotes peace of mind”	1	6.67

The claim of "cancer support" on supplement labels is vague and potentially misleading, as it fails to specify what kind of support is being offered or how the supplement is meant to help the patient with cancer. Without clear details on the active ingredients, their mechanisms of action, or scientific evidence supporting their effectiveness, consumers are left uncertain about how the product might benefit them in the context of cancer. This lack of transparency can give false hope and lead people to rely on unproven remedies instead of seeking appropriate medical treatment. It is essential for supplement manufacturers to provide more specific, evidence-based information about their products, especially when making claims related to serious health conditions like cancer.

3.2 Extract preparation

The dosage forms used for extraction included tinctures, capsules, and powders. Extracts made from powders followed the same procedures as those made from capsule.

For the dual extraction method, a mixture of methanol and dichloromethane (1:1) was used for both powders and capsules. After emptying the contents of the capsules, 2 g of dry mushroom mass was dissolved in 50 mL of the solvent mixture and stirred overnight. The resulting filtrate was allowed to evaporate in a fume hood. On average, 5.4% of the original weight of dry *I. obliquus*, 1.65% of *G. lucidum* and 4.45% of *T. versicolour* remained in the beaker after being evaporated. This residue was then resuspended in either water (*I. obliquus*) or a 70% ethanol: 30% DMSO solution (*G. lucidum* and *T. versicolour*), yielding final concentrations of 20 mg/mL. *I obliquus* was insoluble in the mixture of ethanol and DMSO while *G. lucidum* and *T. versicolour* were insoluble in water.

Most mushroom supplements, such as tinctures and capsules, are typically consumed with water, which is a common practice for ease of ingestion. However, the observed solubility issues, with some extracts being insoluble in water, pose a potential concern. Since many of the bioactive compounds in these extracts may not dissolve in water, their absorption, bioavailability and effectiveness could be compromised when taken in the typical manner. This emphasizes the need for careful consideration of the solubility properties of these extracts to ensure their optimal use in supplementation.

Tincture extracts (10 mL) were evaporated overnight, and the average weight of the residue obtained was 0.06 g for *I. obliquus*, 0.05 g for *G. lucidum* and 0.08 for *T. versicolour*. This residue was then resuspended in either water (*I. obliquus*) or a 70% ethanol: 30% DMSO solution (*G. lucidum* and *T. versicolour*), yielding final concentrations of 20 mg/mL.

To determine the optimal temperature for extract storage, additional experiments were conducted.

3.3 The effect of mushroom extracts and chemotherapeutic drugs on A549 and HEK293 cell viability.

3.3.1 The identification of chemotherapeutic drugs against the A549 cell line.

The effects of chemotherapeutic drugs and mushroom extracts on cell viability was evaluated against A549 lung cancer cells. The initial evaluation was done at a treatment period of 24 h to determine the IC_{50} values of active compounds. Doxorubicin was the most active chemotherapeutic agent against the A549 cells with a percentage cell viability of 20% at 20 µM and 38% at 10 µM (Figure 3.1) and was therefore selected as the positive control for this study. At 20 µM, camptothecin showed a moderate decrease in cell viability with 50% of cells

being viable (Figure 3.1). Camptothecin (10 µM) and irinotecan at 10 µM as well as irinotecan at 20 µM showed a marginal decrease in cell viability with 78%, 99% and 91% of cells being viable, respectively (Figure 3.1).

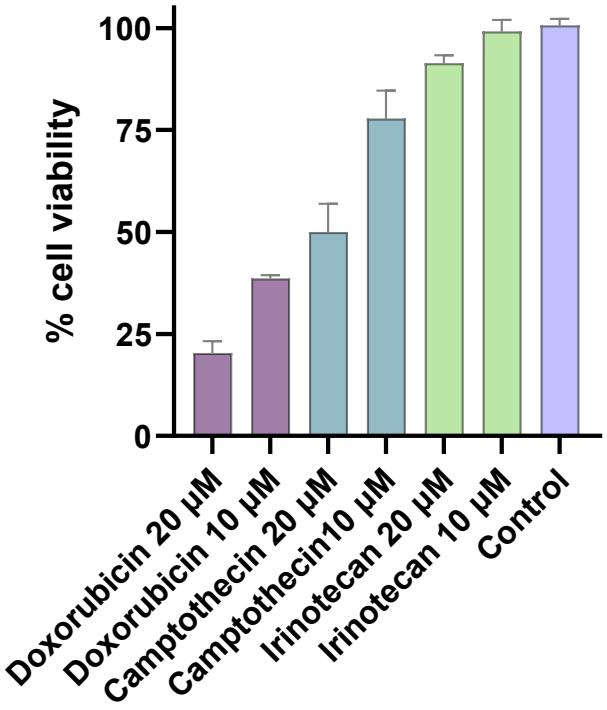


Figure 3.1 The effect of anticancer drugs: doxorubicin, camptothecin and irinotecan on A549 cell viability. A549 cells were treated with chemotherapeutic drugs (doxorubicin, camptothecin and irinotecan) for 24 h. A control with no treatment was included. Error bars represent the mean ± SEM and was obtained from three independent experiments (n=3).

3.3.2 The identification of active mushroom extracts against the A549 and HEK293 cell lines.

Mushroom extracts (*G. lucidum*, *T. versicolour* and *I. oliquus*) were tested against A549 and HEK293 cells, and the results are shown in Figure 3.2. Human embryonic kidney cells (HEK293) were used as a control cell line to evaluate the toxicity of the mushroom extracts on non-cancerous cells. To determine whether an extract was considered active, the study followed the general guideline that extracts with IC_{50} values ≤ 1 mg/mL are regarded as biologically active, as proposed in several phytopharmacological studies. This threshold is commonly used in the early stages of natural product screening to identify promising candidates for further purification and mechanistic studies (Kuete, 2010). While there is no standard classification of the activity of compounds based on percentage cell viability, the framework used in this study is: a percentage cell viability of less than 30% at a concentration of 0.5 mg/mL was considered to be strongly active, 30-50% at 0.5 mg/mL was considered moderately active, and 50-90% was considered poorly active. A percentage cell viability > 90% was considered inactive. Additionally, results at a lower concentration of 0.25 mg/mL were also presented to show the concentration-dependent effects of the extracts, as variations in cytotoxicity may occur at different doses.

Doxorubicin was used as the positive control. In A549 cells, doxorubicin had a percentage cell viability of 0.56% at 0.5 mg/mL and 2.3% at 0.25 mg/mL, whereas in HEK293 cells, the percentage cell viability was higher, indicating reduces sensitivity of non-cancerous cells to doxorubicin (Figure 3.2).

G. lucidum extracts were the most active mushroom extracts in A549 cells, causing the suppression of cell viability to 20% at 0.5 mg/mL and 68% at 0.25 mg/mL (Figure 3.2 A). In HEK293 cells, however, *G. lucidum* extracts were less effective inhibitors of proliferation with 75.08% and 84.45% cell viability at 0.5 mg/mL and 0.25 mg/mL, respectively (Figure 3.2 B).

T. versicolour extracts were moderately active against A549 cells, with a percentage cell viability of 41% at 0.5 mg/mL and 64% at 0.25 mg/mL (Figure 3.2 A). In HEK293 cells, *T. versicolour* activity was lower, with a percentage cell viability of 55.79% at 0.5 mg/mL and 67.82% at 0.25 mg/mL (Figure 3.2 B).

I. obliquus extracts were very poorly active against A549 cells. At 0.5 mg/mL a percentage cell viability of 82% was observed, which increased to 98% at 0.25 mg/mL (Figure 3.2 A). *I.*

obliquus extracts were inactive against HEK293 cells. At 0.5 mg/mL a percentage cell viability of 94.21% was observed and 98.61% at 0.25 mg/mL (Figure 3.2 B).

The vehicle control for the 0.5 mg/mL mushroom extracts consisted of 3.5% ethanol and 1.5% cell culture grade DMSO and this mixture had a percentage cell viability of 78.63% in A549 cells and 82.13% in HEK293 cells. The vehicle control which consisted of the equivalent percentage of ethanol and DMSO as in the 0.25 mg/mL extracts, i.e. 1.75% and 0.75%, had a percentage cell viability of 81.53% and 85.51% in A549 and HEK293 cells, respectively (Figure 3.2). Although the vehicle control exhibits minimal cytotoxicity in both A549 and HEK293 cells, the increased loss of viability observed with the corresponding extract concentrations indicates that the bioactive compounds are primarily responsible for the enhanced cytotoxic effects.

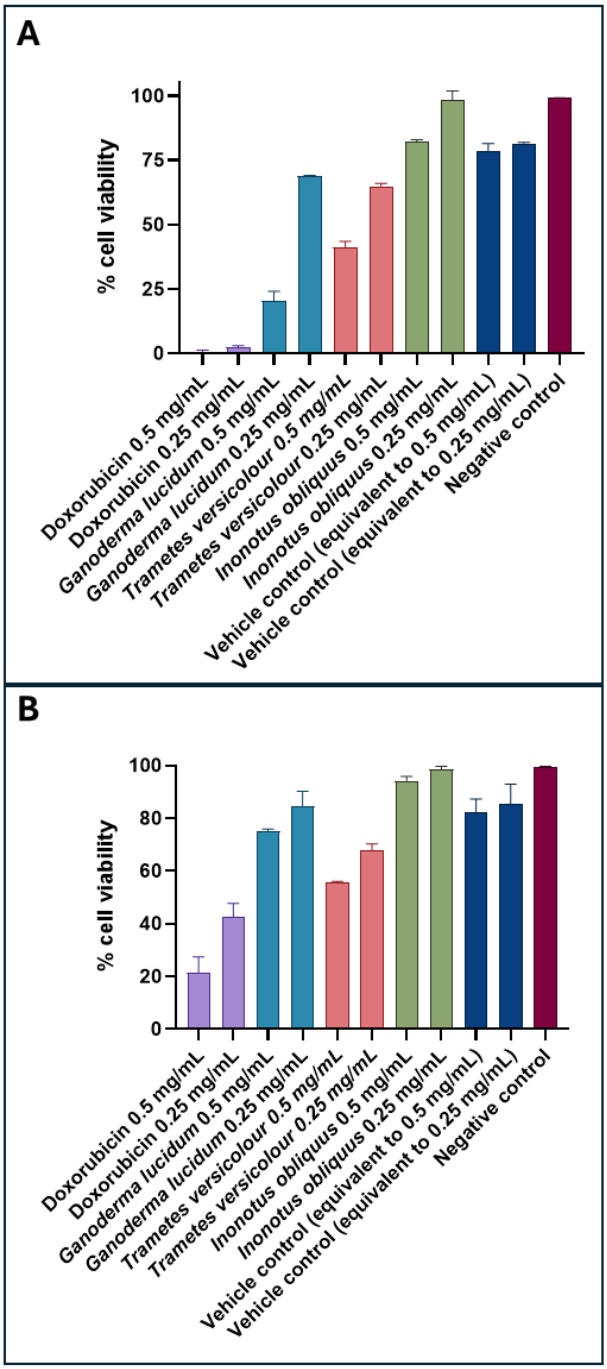


Figure 3.2 The effect of mushroom extracts and doxorubicin on (A) A549 and (B) HEK293 cell viability. A549 and HEK293 cells were treated for 24 h with *Ganoderma lucidum*, *Trametes versicolour* and *Inonotus obliquus* extracts with the equivalent amounts of vehicle (ethanol and DMSO at a 7:3 ratio (v/v)) to match each concentration. Doxorubicin was used as a positive control. Error bars represent the mean ± SEM and were obtained from three independent experiments (n=3).

In summary, *T. versicolour* was the most active mushroom extract in HEK293 cells, whereas *G. lucidum* was the most active in A549 cells. Both *G. lucidum* and *T. versicolour* extracts were less active in HEK293 cells than in A549 cells.

3.3.3 Determination of IC_{50} values of *G. lucidum*, *T. versicolour* and doxorubicin against A549 and HEK293 cells.

3.3.3.1 Determination of IC_{50} values of *G. lucidum*, *T. versicolour* and doxorubicin against A549 cells

I. obliquus extracts were poorly active in A549 cells, therefore, no further evaluation was done on this mushroom. Dose response curves of A549 cells were obtained by treating the cells with a range of concentrations of *G. lucidum* extracts (0.000125 – 2 mg/mL), *T. versicolour* extracts (0.000125 mg/mL – 3 mg/mL) and doxorubicin (0.001 – 100 µM) which equates to 5.44×10^{-7} – 0.05 mg/mL for 24 h and 48 h. Each experiment was repeated at least three times and the representative dose response curves are shown in Figure 3.3.

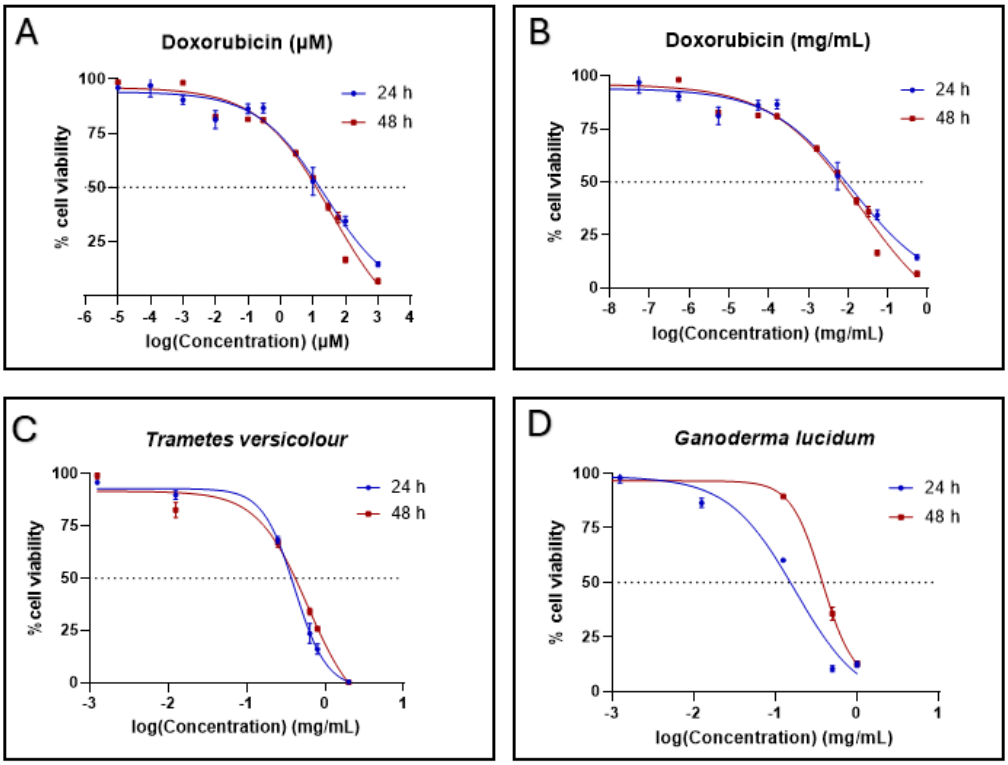


Figure 3.3 Representative dose response curves of doxorubicin, *Ganoderma lucidum* and *Trametes versicolour* against the A549 cell line. Cells were treated at a range of concentrations of (A) doxorubicin at 0.00001 – 100 µM, (B) doxorubicin at 5.44×10^{-7} – 0.05 mg/mL (C) *Ganoderma lucidum* at 0.000125 – 2 mg/mL and (D) *Trametes versicolour* at 0.000125 – 3 mg/mL. Each point along the curve represents the mean while the error bars represent the SEM. The dose response curves are a representation of three independent experiments (n=3).

Non-linear regression analysis in GraphPad Prism Version 5.1 (GraphPad Prism Software, San Diego, USA) was used to calculate IC_{50} values (Table 3.4). *G. lucidum* was the most active

mushroom extract and had lower IC_{50} values for both the 24 and 48 h treatment periods when compared to *T. versicolour* i.e., 0.26 ± 0.02 mg/mL and 0.25 ± 0.05 mg/mL, compared to 0.30 ± 0.01 mg/mL and 0.61 ± 0.04 mg/mL (Table 3.4). *T. versicolour* had a higher IC_{50} value under the 48 h treatment period (0.61 ± 0.04 mg/mL) compared to the 24 h treatment period (0.30 ± 0.01 mg/mL) (Table 3.4). Both *G. lucidum* and doxorubicin had lower IC_{50} values when cells were treated for 48 h compared to 24 h (Table 3.4).

Table 3.4 The IC_{50} values (mg/mL) of *Ganoderma lucidum*, *Trametes versicolour* and doxorubicin on A549 cells and the statistical comparison to doxorubicin. Concentrations are in mg/mL unless specified otherwise. Doxorubicin values are given in both mg/mL and µM. Values are shown as mean ± SEM. The p-values were obtained by using the Student's t-test with Welch's correction. The Student's t-test compared the IC_{50} values of the mushroom extracts to that of doxorubicin.

	Doxorubicin			***Ganoderma lucidum***		***Trametes versicolour***	
Treatment period	**IC_{50} value (µM)**	**IC_{50} value (mg/mL)**	**p-value**	**IC_{50} value (mg/mL)**	**p-value**	**IC_{50} value (mg/mL)**	**p-value**
24 h	9.85 ± 1.56	0.005 ± 0.001	-	0.255 ± 0.022	Significant**	0.304 ± 0.007	Significant ***
48 h	5.51 ± 0.93	0.003 ± 0.001	-	0.246 ± 0.049	Significant*	0.613 ± 0.040	Significant **

Significance was set at $p<0.05$ (*) while p-values less than 0.01 (**) and 0.001 (***) were highly significant.

The IC_{50} values of the extracts *G. lucidum* and *T. versicolour* in mg/mL were compared to the IC_{50} value of doxorubicin at 24 and 48 h. To determine whether the difference between treatments was significant, a Student's t-test with Welch's correction was used, and p-values are shown in Table 3.4.

The IC_{50} values of both *G. lucidum* and *T. versicolour* extracts were significantly higher than that of doxorubicin for both the 24 h and 48 h time periods (Table 3.4). The IC_{50} value of *G. lucidum* was 51- and 82-fold greater than that of doxorubicin at 24 h ($p<0.01$) and 48 h ($p<0.05$), respectively.

T. versicolour had IC_{50} values which were 61- and 204-fold greater than the IC_{50} values of doxorubicin at 24 h ($p<0.001$) and 48 h ($p<0.01$). Doxorubicin had IC_{50} values significantly lower than that of both *G. lucidum* and *T. versicolour* (Table 3.4).

3.3.3.2 Determination of IC_{50} values of *G. lucidum*, *T. versicolour* and doxorubicin against HEK293 cells

Representative dose response curves are shown in Figure 3.4. *G. lucidum* and *T. versicolour* were not strongly active in the HEK293 cells. At the highest concentrations tested, a 100% cell death was not achieved. When treated at concentrations higher than 3 mg/mL there was a colour interference from the mushroom extracts. The representative dose response curves are presented as a rough comparison for the A549 cells.

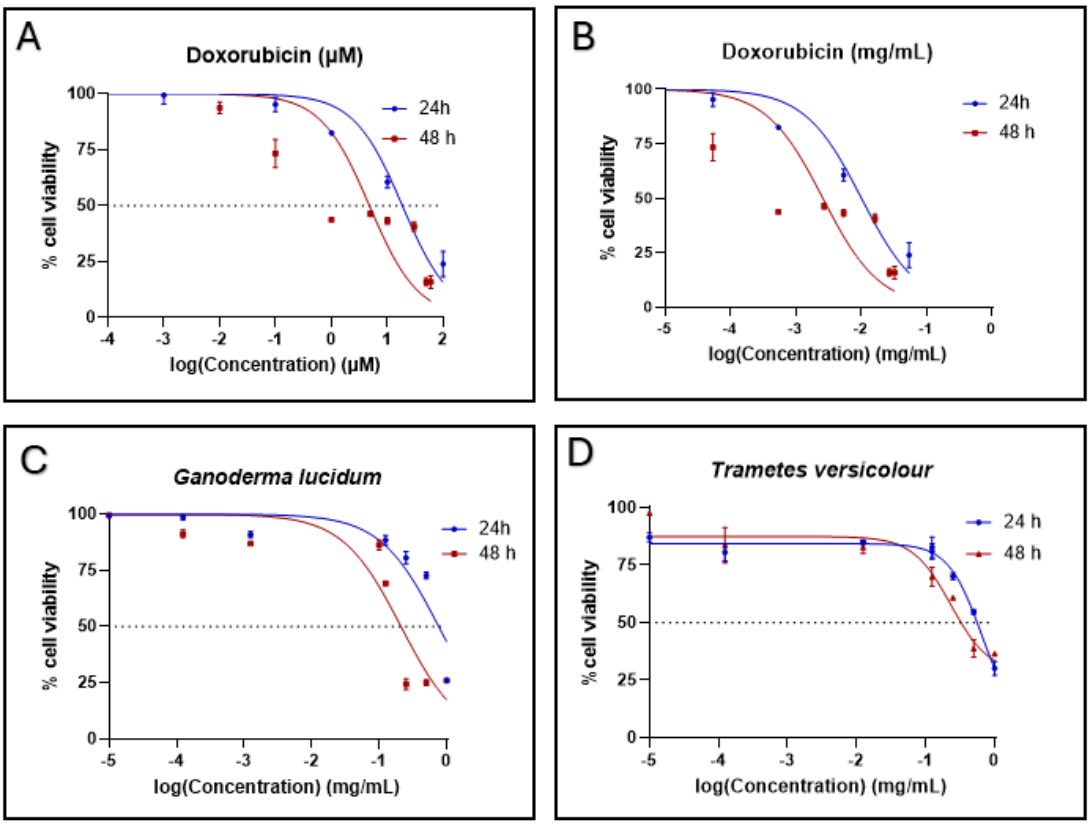


Figure 3.4 Representative dose response curves of doxorubicin, *Ganoderma lucidum* and *Trametes versicolour* against the HEK293 cell line. Cells were treated with a range of concentrations of (A) doxorubicin at 0.00001 – 100 µM, (B) doxorubicin at 5.44×10^{-7} – 0.05 mg/mL (C) *Ganoderma lucidum* at 0.000125 – 2 mg/mL and (D) *Trametes versicolour* at 0.000125 – 3 mg/mL. Each point along the curve represents the mean while the error bars represent the SEM. The dose response curves are a representation of three independent experiments (n=3).

The IC_{50} values for *G. lucidum*, *T. versicolour* and doxorubicin are shown in Table 3.5. The IC_{50} value of *G. lucidum* extracts in HEK293 cells was 0.591 ± 0.101 mg/mL at 24 h and 0.151 ± 0.008 mg/mL at 48 h. *T. versicolour* extracts had an IC_{50} value of 0.880 ± 0.380 mg/mL and

0.282 ± 0.052 mg/mL at 24 and 48 h, respectively. Doxorubicin had an IC_{50} value of 0.010 ± 0.000 mg/mL at 24 h and 0.003 ± 0.001 mg/mL at 48 h.

A Student's t-test with Welch's correction was used to determine whether the differences between IC_{50} values of the mushroom extracts were significantly different from that of doxorubicin in the HEK293 cell-line. *G. lucidum* had an IC_{50} significantly higher than doxorubicin at 24 h ($p<0.05$) and 48 h ($p<0.001$) (Table 3.5). There was no significant difference between *T. versicolour* at 24 h compared with doxorubicin ($p>0.05$). At 48 h, *T. versicolour* had a significantly higher IC_{50} value when compared to doxorubicin ($p<0.05$) (Table 3.5).

Table 3.5 The IC_{50} values (mg/mL) of mushroom extracts (*Ganoderma lucidum* and *Trametes versicolour* extracts) and doxorubicin on HEK293 cells. Concentrations are in mg/mL. Values are shown as mean ± SEM. All concentrations are given in mg/mL unless otherwise specified. The p-values were obtained from the Student's t-test with Welch's Correction. The Student's t-test compared the IC_{50} values of the mushroom extracts to that of doxorubicin.

	Doxorubicin			***Ganoderma lucidum***		***Trametes versicolour***	
Treatment period	**IC_{50} value (µM)**	**IC_{50} value (mg/mL)**	**p-value**	**IC_{50} value (mg/mL)**	**p-value**	**IC_{50} value (mg/mL)**	**p-value**
24 h	18.62 ± 1.84	0.010 ± 0.000	-	0.591 ± 0.101	Significant *	0.880 ± 0.380	Not significant
48 h	4.79 ± 0.51	0.003 ± 0.001	-	0.151 ± 0.008	Significant ***	0.282 ± 0.052	Significant *

Significance was set at $p<0.05$ (*) while p-values less than 0.01 (**) and 0.001 (***) were highly significant.

A549 cells had a lower IC_{50} value for both *G. lucidum* and *T. versicolour* compared to HEK293 cells when exposed for 24 h. At an exposure time of 48 h, the inverse was true. The IC_{50} value of *G. lucidum* and *T. versicolour* in HEK293 cells was lower than in A549's when exposed for 48 h.

The IC_{50} value of doxorubicin was lower in A549 cells at 24 h compared to the IC_{50} value of doxorubicin in HEK293 cells. The IC_{50} value was similar in both cell lines at a 48 h incubation period.

3.3.4 The effect of *G. lucidum* and *T. versicolour* on the cytotoxic efficacy of doxorubicin in A549 and HEK293 cells.

Combination studies were performed to determine the effects of *G. lucidum* and *T. versicolour* on the efficacy of doxorubicin against A549 and HEK293 cells over 24 h and 48 h. Doxorubicin was used at a range of 0.0001 – 100 µM (equivalent to 5.44×10^{-7} – 0.05 mg/mL) in the presence of culture media containing *G. lucidum* or *T. versicolour* at their respective IC_{50} values as determined in Section 3.3.3.

Concentrations used against the A549 cells were, 0.255 mg/mL *G. lucidum* and 0.304 mg/mL *T. versicolour* at the 24 h treatment period. During the 48 h treatment period, *G. lucidum* and *T. versicolour* were used at 0.246 mg/mL and 0.6134 mg/mL, respectively. In order to evaluate the effect mushroom extracts had on the IC_{50} values of doxorubicin, dose-response curves were constructed (Figure 3.5).

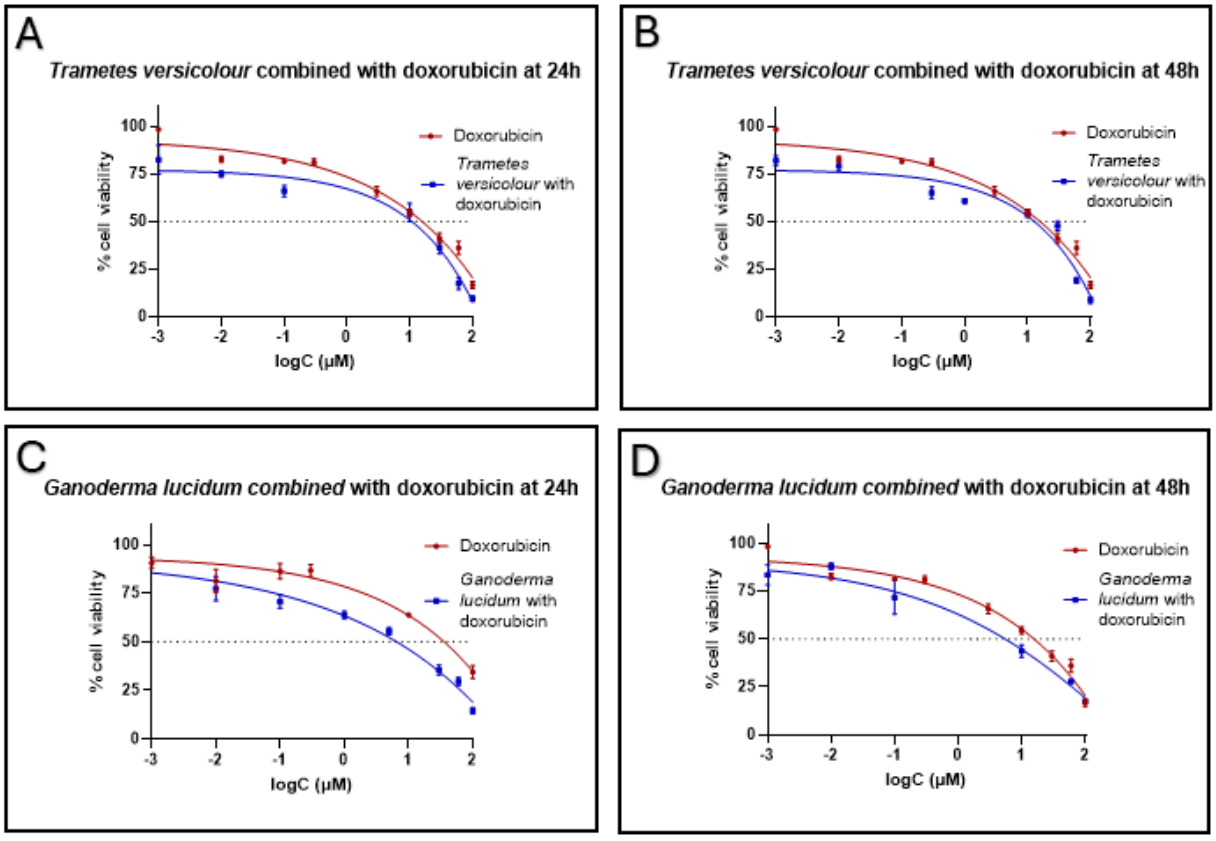


Figure 3.5 Representative dose response curves of doxorubicin and mushroom extracts. A549 cells were treated with a range of doxorubicin (0.0001 – 100 µM) and (A) *Trametes versicolour* at 0.304 mg/mL (24 h), (B) *Trametes versicolour* at 0.6134 mg/mL (48 h), (C) *Ganoderma lucidum* at 0.255 mg/mL (24 h), (D) *Ganoderma lucidum* at 0.246 mg/mL (48 h). Dose-response curves are representative of three independent experiments (n=3). Error bars indicate the SEM.

HEK293 cells were treated with *G. lucidum* and *T. versicolour* at 0.5911 mg/mL and 0.88 mg/mL, respectively for 24 h. At 48 h, doxorubicin was combined with 0.151 mg/mL *G.*

lucidum and 0.282 mg/mL *T. versicolour*. To determine if mushroom extracts influenced the IC_{50} values of doxorubicin, dose-response curves were constructed (Figure 3.6).

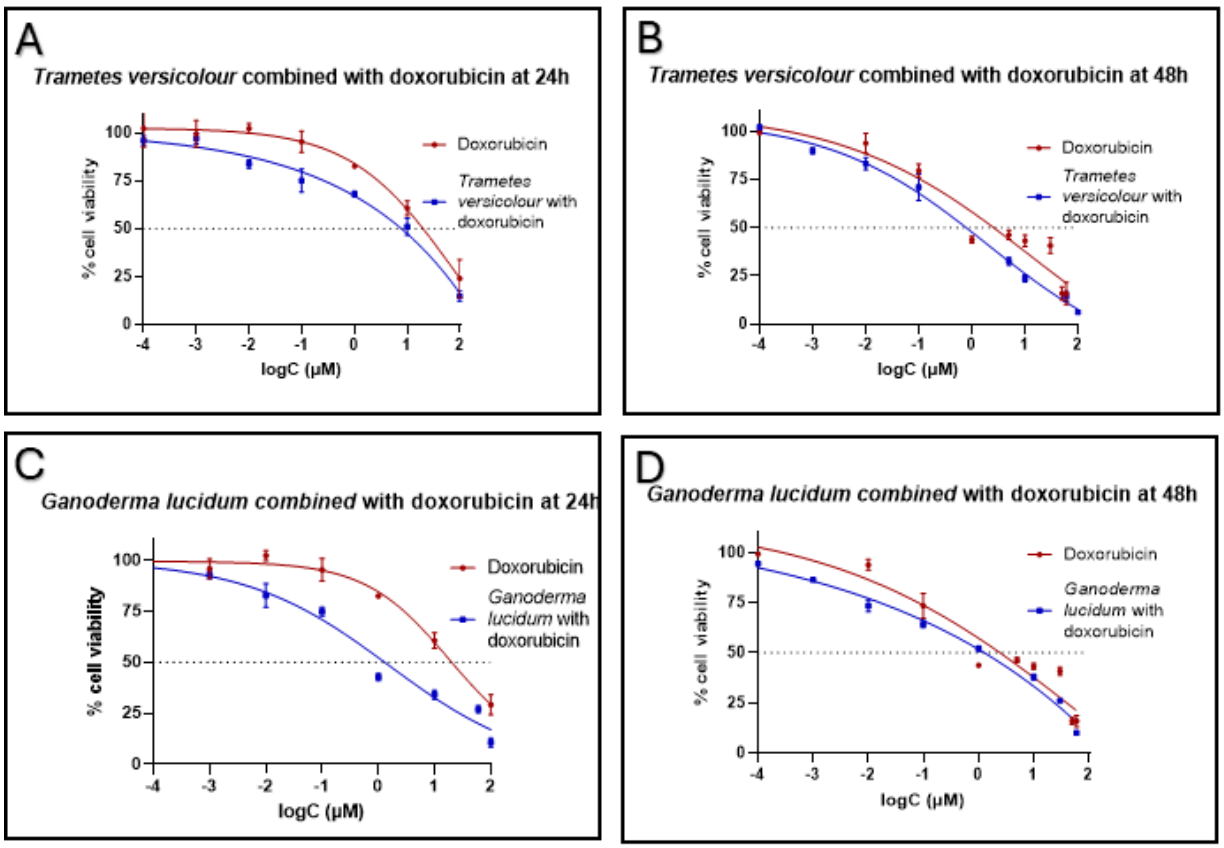


Figure 3.6 Representative dose response curves of combination experiments of doxorubicin and mushroom extracts. HEK293 cells were treated with a range of doxorubicin (0.0001 – 100 µM) and (A) *Trametes versicolour* at 0.880 mg/mL (24 h), (B) *Trametes versicolour* at 0.282 mg/mL (48 h), (C) *Ganoderma lucidum* at 0.591 mg/mL (24 h), (D) *Ganoderma lucidum* at 0.151 mg/mL (48 h). Dose-response curves are representative of three independent experiments (n=3). Error bars indicate the SEM.

Table 3.6 shows the IC_{50} values, p-values and relative potency for doxorubicin combined with the mushroom extracts after 24 h and 48 h. The IC_{50} values were used to calculate the relative potency (RP) for each combination treatment at 24 h and 48 h. Relative potency is a ratio of doses, typically the reference divided by the test compound. In this case i.e., the IC_{50} value of doxorubicin divided by the IC_{50} value of the combination (doxorubicin with either *G. lucidum*/*T. versicolour*). To evaluate the impact of *G. lucidum* and *T. versicolour* on doxorubicin efficacy, combination treatments (doxorubicin with either *G. lucidum* or *T. versicolour*) were compared to doxorubicin alone.

When tested in A549 cells, at 24 h, the combination of doxorubicin with *G. lucidum* did not cause a statistically significant difference in the IC_{50} value of doxorubicin ($p>0.05$). However,

at 48 h, there was a significant increase ($p<0.01$) in the IC_{50} value, indicating reduced cytotoxicity, and a corresponding decrease in RP (Table 3.6).

Similarly, when doxorubicin was combined with *T. versicolour*, no significant change in the IC_{50} value was observed at 24 h ($p>0.05$). At 48 h, the combination significantly increased ($p<0.001$) the IC_{50} value of doxorubicin, leading to a decrease in RP. This means that *T. versicolour* decreases the efficacy of doxorubicin.

In contrast, in HEK293 cells, the combination of doxorubicin with *G. lucidum* led to a significant decrease in the IC_{50} value of doxorubicin at both 24 h ($p<0.01$) and 48 h ($p<0.01$), resulting in an increase in RP (Table 3.6). When doxorubicin was combined with *T. versicolour*, no significant difference in the IC_{50} value was observed at 24 h ($p>0.05$). However, at 48 h, the combination significantly decreased ($p<0.01$) the IC_{50} value of doxorubicin, leading to an increase in RP.

In summary, neither combination (*G. lucidum* + doxorubicin or *T. versicolour* + doxorubicin) had a significant effect on doxorubicin's IC_{50} value at 24 h in A549 cells. However, at 48 h, both combinations resulted in a statistically significant increase in the IC_{50} value and a decreased in the efficacy of doxorubicin (Table 3.6). In HEK293 cells, *G. lucidum* significantly increased the efficacy of doxorubicin at 24 h and 48 h. *T. versicolour* had no effect on the efficacy of doxorubicin at 24 h but increased the efficacy at 48 h in HEK293 cells.

Table 3.6 The IC_{50} values (µM) of doxorubicin when combined with *Ganoderma lucidum* and *Trametes versicolour* on A549 and HEK293 cells. Values are shown as mean ± SEM. The p-values were obtained from the Student's t-test with Welch Correction assuming unequal variances. The Student's t-test was done in order to compare the IC_{50} values of the mushroom extracts combined with doxorubicin to that of doxorubicin alone.

A549 cells									
	Doxorubicin (alone)			**Doxorubicin with *Ganoderma lucidum***			**Doxorubicin with *Trametes versicolour***		
Exposure time	**IC_{50} value (µM)**	**RP**	**p-value**	**IC_{50} value (µM)**	**RP**	**p-value**	**IC_{50} value (µM)**	**RP**	**p-value**
24 h	9.85 ± 1.56	1.0	-	7.47 ± 0.29	1.3	Not significant	13.09 ± 0.58	0.8	Not significant
48 h	5.51 ± 0.93	1.0	-	9.26 ± 0.63	0.6	Significant **	13 ± 0.57	0.4	Significant ***
HEK293 cells									
	Doxorubicin (alone)			**Doxorubicin with *Ganoderma lucidum***			**Doxorubicin with *Trametes versicolour***		
Exposure time	**IC_{50} value (µM)**	**RP**	**p-value**	**IC_{50} value (µM)**	**RP**	**p-value**	**IC_{50} value (µM)**	**RP**	**p-value**

24 h	18.62 ± 1.84	1.0	-	1.882 ± 0.2	9.9	Significant **	14.93 ± 1.23	1.2	Not significant
48 h	4.79 ± 0.51	1.0	-	2.850 ± 0.3	1.7	Significant **	2.558 ± 0.2	1.9	Significant **

Significance was set at $p<0.05$ (*) while p-values less than 0.01 (**) and 0.001 (***) were highly significant.

3.3.5 Stability assessment of *G. lucidum* and *T. versicolour* stored for 13-weeks

Cell viability changes were observed over time with prolonged extract storage. As a preliminary experiment, *G. lucidum* and *T. versicolour* extracts were prepared (Chapter 2, Section 2.2) and stored at room temperature for 13 weeks. Extract stability was assessed using the MTT cell viability assay (Chapter 2, Section 2.5) against A549 cells. Cells were treated at 1 mg/mL for 24 h, and the viability was evaluated at week 1, 4 10 and 13. The results are presented in Figure 3.7 for *G. lucidum* (A) and *T. versicolour* (B).

Figure 3.7A shows the cell viability of A549 cells when treated with *G. lucidum* after storage of 1, 4, 10 and 13 weeks. A Student's t-test using Welch's correction assuming unequal variances was performed to determine whether the difference in cell viability across the 13 weeks was significant. There was no significant difference in the percentage cell viability of A549 cells when treated with *G. lucidum* extract which has been stored for up to 10 weeks (Figure 3.7 A). There was a significant increase ($p<0.005$) in percentage cell viability between week 10 and week 13. There was a 2.7-fold increase in percentage cell viability from week 10 to 13. A statistically significant increase was observed between week 1 and week 13 ($p<0.005$), with a 4-fold increase (Figure 3.7 A). *G. lucidum* extracts stored at 4°C remains stable for up to 10 weeks.

Figure 3.7 B shows the cell viability of A549 cells when treated with *T. versicolour* extract which has been stored for various lengths of time (1, 4, 10 and 13 weeks). A significant increase in cell viability was observed between weeks 1 and 4 ($p<0.005$) and subsequently between weeks 4 and 10 ($p<0.005$). There was a 17.4-fold increase in cell viability from week 1 to week 4, and a 2-fold increase from week 4 to 10 (Figure 3.7 B). The difference in cell viability between week 10 and week 13 was not statistically significant ($p>0.005$). Overall, week 1 to week 13 showed a highly significant increase in cell viability ($p<0.005$). Week 1 to week 13 showed a 36-fold increase in cell viability (Figure 3.7 B). *T. versicolour* extracts stored at 4°C were highly unstable. This indicated long term storage decreases the activity of the *T. versicolour* extracts; therefore, fresh extracts were prepared for all experiments.

In summary, cell viability increased over extract storage time implying a loss of activity for both *G. lucidum* and *T. versicolour* (Figure 3.7). Further stability assessment is required to evaluate the long-term stability of the extracts under different storage conditions.

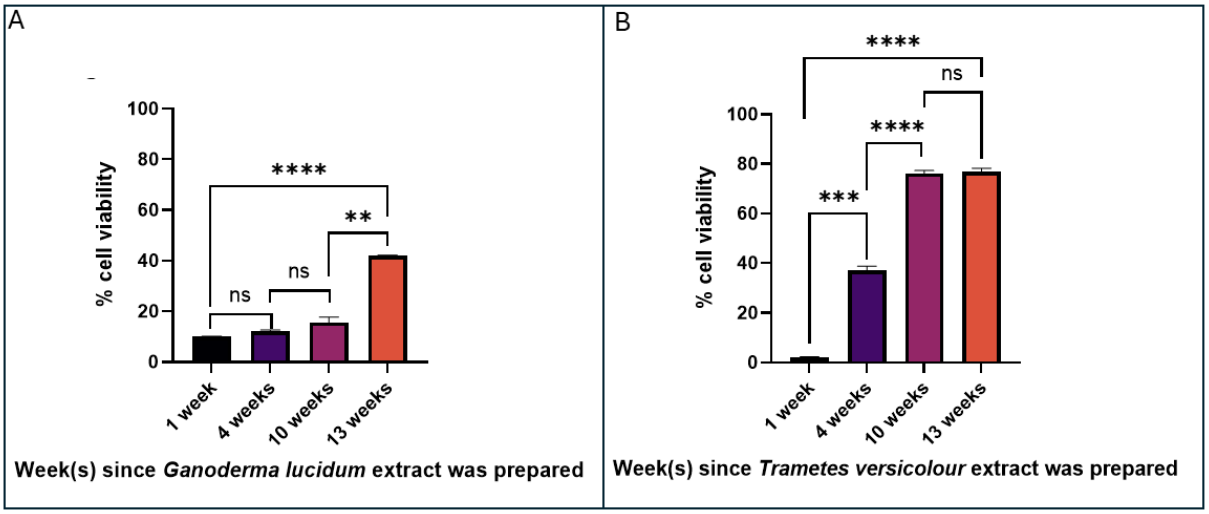


Figure 3.7 Bar graphs showing the percentage cell viability vs extract storage time for *Ganoderma lucidum* (A) and *Trametes versicolour* (B) treated cells at 1mg/mL for 24 h on A549 cells. Cells were treated with 1 mg/mL of each extract. Extracts were stored at room temperature for a period of 13 weeks. The cell viability is shown at week 1, week 4, week 10 and week 13. Error bars represent the SEM. Legends: ns= not significant. Significance was set at $p<0.05$ (*) while p-values less than 0.01 (**), 0.001 (***) and 0.0001 (****) were highly significant.

3.4. FTIR Analysis

3.4.1 Batch consistency analysis of *G. lucidum* and *T. versicolour* tincture from the same manufacturer.

Fourier Transform Infrared (FTIR) analysis was performed on three batches of the brand of tincture that showed the most activity as determined by the MTT cell viability assay (Chapter 2, Section 2.5). Liquid samples were used and unaltered from the original tinctures. Fifty microliters of each tincture was used. Twenty scans per sample in the region 4000 – 650 cm^{-1} were performed using the Perkin Elmer Spectrum GX (Perkin-Elmer, Beaconsfield, BUCKS, UK) as described in Chapter 2, Section 2.3.

In an FTIR spectrum, the x-axis represents the wavenumber (cm^{-1}), and the y-axis represents the percentage transmittance (%T). Different functional groups can be identified based on the wavenumber (location along the x-axis). The spectrum can be divided into four zones: zone 1 (single bond region) lies between 2500 – 4000 cm^{-1}, zone 2 (triple bond region) is from 2000

– 2500 cm^{-1}, zone 3 (double bond region) spans from 1500 – 2500 cm^{-1}, and zone 4 (fingerprint region) lies <1500 cm^{-1}. A high percentage transmittance means there are few bonds absorbing incidence light, whereas a low percentage transmittance means there are many bonds absorbing the incidence light. The spectrum for the inter-batch analysis of *G. lucidum* tinctures is shown in Figure 3.8. Batch 1 is shown in blue, batch 2 is shown in orange, and batch 3 is shown in green (Figure 3.8).

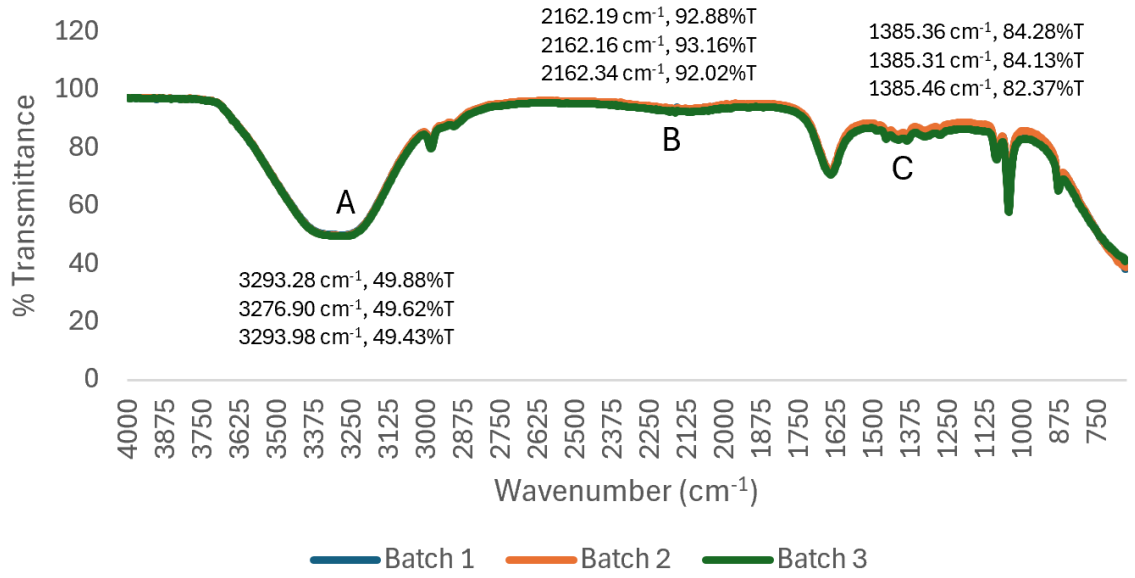


Figure 3.8 FTIR spectrum of three batches of *Ganoderma lucidum* tinctures from the same manufacturer. The x-axis represents the wavenumber (cm^{-1}) while the y-axis represents percentage transmittance (%T). Legend: blue – batch 1, orange – batch 2 and green – batch 3. Twenty scans per sample were performed using the Perkin Elmer GX.

The spectrum for each of the three batches of *G. lucidum* tinctures show little variation between overlapping spectra. A small peak shift can be observed in the 2000 - 3000 cm^{-1} region and in a few positions within the fingerprint region (<1500cm^{-1}). By performing a One-Way ANOVA assuming Gaussian distribution with the Geisser-Greenhouse correction, to compare various points (Figure 3.8, points A-C) on the overlapped spectrum, it is shown that the p-value between the wavenumber values and between the percentage transmittance is $p>0.05$ (Table 3.7). A level of significance of $p=0.05$ was used. This indicates that there was no significant difference between the three *G. lucidum* tincture batches.

Table 3.7 Table showing three randomly selected points from the *Ganoderma lucidum* spectrum. P-values from the statistical analysis to determine the difference between coordinates in the peak shifts are shown. A p-value of $p<0.05$ is considered to be statistically significant.

Point	Coordinates (x, y)	p-value (comparing wavenumber)	p-value (comparing %T)
A	(3293.28 cm^{-1}, 49.88%) (3276.90 cm^{-1}, 49.62%) (3293.98 cm^{-1}, 49.43%)	Not significant	Not significant
B	(2162.16 cm^{-1}, 93.16%) (2162.19 cm^{-1}, 92.88%) (2162.34 cm^{-1}, 92.02%)		
C	(1385.36 cm^{-1}, 84.28%) (1385.31 cm^{-1}, 84.13%) (1385.46 cm^{-1}, 82.37%)		

The spectrum for the inter-batch analysis of *T. versicolour* tinctures is shown in Figure 3.9. Batch 1 is shown in blue, batch 2 is in orange, and batch 3 is shown in green (Figure 3.9). Large peak shifts with a few areas of overlap can be observed within the spectrum (Figure 3.9).

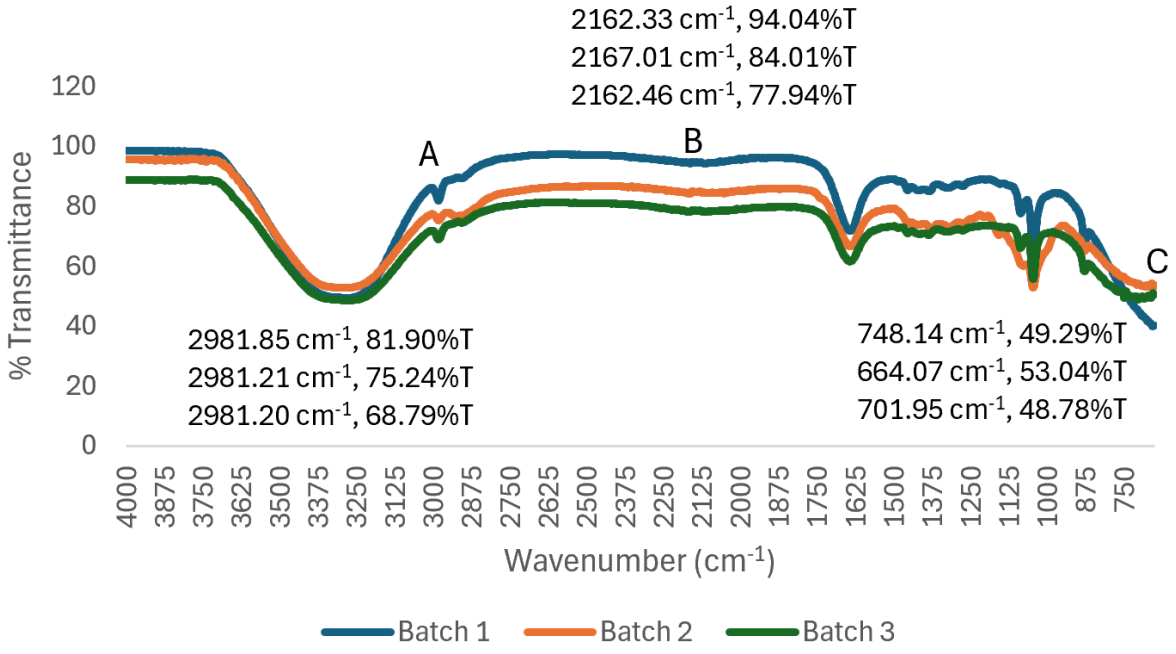


Figure 3.9 FTIR spectrum of three batches of *Trametes versicolour* tinctures. The x-axis represents the wavenumber (cm^{-1}) while the y-axis represents percentage transmittance (%T).

Legend: green – batch 1, red – batch 2 and blue – batch 3. Twenty scans per sample were performed using the Perkin Elmer GX.

One-way ANOVA assuming Gaussian distribution with Geisser-Greenhouse correction was used to compare the values between the three batches in order to determine whether the differences are statistically significant (Table 3.8). ANOVA was used to compare the means of the three groups, the Gaussian distribution is used for data that follows a normal distribution, and the Geisser-Greenhouse correction was used because the ANOVA assumes equal variances but if the assumption is invalid, the correction adjusts the result to be more reliable. P-values greater than 0.05 were obtained when comparing both the wavenumber values and percentage transmittance between points A-C, respectively (Figure 3.9).

Table 3.8 Table showing three randomly selected points from the *Trametes versicolour* overlapped spectrum. P-values from the statistical analysis to determine the difference between coordinates in the peak shifts are shown. A p-value of $p<0.05$ is considered to be statistically significant.

Point	Coordinates (x, y)	p-value (comparing wavenumber)	p-value (comparing %T)
A	(2981.85 cm^{-1}, 81.90%) (2981.21 cm^{-1}, 75.24%) (2981.20 cm^{-1}, 68.79%)	Not significant	Not significant
B	(2162.33 cm^{-1}, 94.04%) (2167.01 cm^{-1}, 84.01%) (2162.46 cm^{-1}, 77.94%)		
C	(748.14 cm^{-1}, 49.29%) (664.07 cm^{-1}, 53.04%) (701.95 cm^{-1}, 48.78%)		

3.4.2 Extract stability assessments.

3.4.2.1 Using FTIR to measure extract profiles over time.

Fourier transform infrared (FTIR) uses atomic vibrations to represent molecular structures (Nandiyanto *et al*., 2022). The peaks and spectrum of FTIR act as a fingerprint. A sufficient reference database is needed to distinguish specific molecular structures and chemical bonding. For the purposes of this study, two papers by Nandiyanto, Oktiani and Ragadhita (2019 and 2022), titled "How to Read and Interpret FTIR Spectroscope of Organic Material" and

"Interpretation of Fourier Transform Infrared Spectra (FTIR): A Practical Approach in the Polymer/Plastic Thermal Decomposition" are used. These papers address the need for a reference database and provides comprehensive strategies on how to read FTIR peaks.

G. lucidum and *T. versicolour* extracts were prepared from tinctures as described in Chapter 2, Section 2.2. Extracts were then stored at (i) room temperature, (ii) 4℃ and (iii) -18℃. FTIR analysis was done on the day extracts were prepared (week 0) and subsequently once a week thereafter for 5 consecutive weeks.

To interpret the spectrum, it is divided into four zones. Each zone corresponds to a different bond type. The fingerprint can be found in zone 1, double bonds in zone 2, triple bonds in zone 3 and single bonds in zone 4 (Nandiyanto *et al*., 2022).

3.4.2.1.1 Extracts stored at room temperature

At room temperature, there is little variation between the *T. versicolour* spectra from week 1 – 4 in comparison to week 0. Spectra can be seen overlapping (Figure 3.4). When comparing the profiles of week 0 to that of week 5 several differences were observed. Visible changes in the spectrum can be observed in the fingerprint region (zone I), between 650 – 1500 cm^{-1}. A large peak is visible in zone II on the spectrum for week 5 which is absent from week 0 (Figure 3.10).

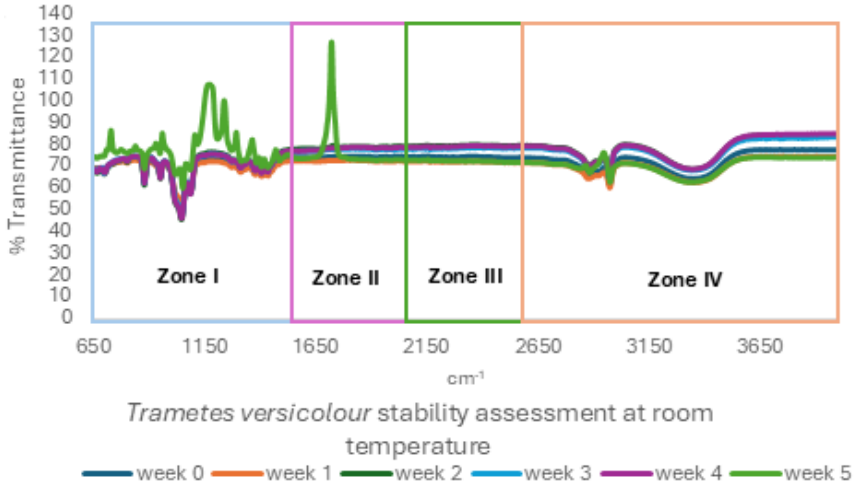


Figure 3.10 FTIR profiles for *Trametes versicolour* extracts stored at room temperature. Extracts were measured over a period of 5 weeks. The x-axis represents the wavenumber (cm^{-1}) while the y-axis represents the % transmittance. Zone I (fingerprint) is shown in blue margins, zone II (triple bonds) in pink margins, zone III (double bonds) in green margins and zone IV (single bonds) in orange margins.

To assess the difference between spectra from week 0 and week 5, points were selected to compare more closely. The peak wavenumbers and percentage transmittance of week 0 compared to week 5 can be seen in Table 3.9.

Table 3.9 The peak wavenumbers observed in the FTIR spectrum of *Trametes versicolour* extract when stored for 5 weeks at room temperature compared to the day of preparation (week 0). *Trametes versicolour* extract was stored at room temperature for 5 weeks. FTIR readings were collected weekly on the same sample. The percentage transmittance (%T) at week 5 was compared to that collected at week 0.

Wavenumber (cm^{-1})	%T (week 0)	%T (week 5)
727	70,64	83,56
953	65,22	76,12
959	68,04	82,93
1174	**73,38**	**107,5**
1240	**72,55**	**100,07**
1295	70,05	85,13
1363	69,58	81,65
1469	71,28	76,94
1722	**74,21**	**126,98**

The fingerprint region was localised between 650 and 1500 cm^{-1}. Eight peaks were identified in this area. The region from 700-1300 cm^{-1} is assigned to skeletal C-C vibrations. A C-Cl stretch can be found from 700-800 cm^{-1}. In this region (700-800cm^{-1}), a peak is observed at week 5 while a trough is observed at week 0. There was in increase in transmission at this wavenumber region. This means that there are fewer C-Cl bonds to absorb that wavenumber of light.

The area 850-995 cm^{-1} is where aromatic phosphates are located (P-O-C stretch). Cyanate (-OCN and C-OCN) is located at 1080-1190 cm^{-1}. The region from 1230-1270 cm^{-1} is where aromatic ethers are located. The point 1295 cm^{-1} falls within the aromatic primary amine (CN stretch) and the aromatic secondary amines (CN stretch). These are located at 1250-1340 and 1280-1350 cm^{-1} respectively. Sulfonates correspond to the 1340-1365 cm^{-1} region. The region 1410-1490 cm^{-1} corresponds to carbonate ions. The 1700-1725 cm^{-1} region corresponds to the carboxylic acid assignment. There is overlap in this wavenumber with ketones which exist in the region 1705-1725 cm^{-1} (Nandiyando *et al*., 2019). Overall, an increase in %T was observed in week 5 compared to week 0. This means that there are less of the respective bonds present to absorb incidence light. At 1174 cm^{-1}, 1240 cm^{-1} and 1722 cm^{-1}, where the %T is ≥100% at

week 5, indicates that all of that frequency passed through the compounds without any being absorbed.

G. lucidum extracts from week 1 - 4 show little variation when compared to week 0. Again, as with *T. versicolour*, at week 5 there is a change in the spectrum. The fingerprint region (650 - 1500 cm^{-1}) differs from week 0. At week 5 the spectrum had an upward shift when compared to week 0 (Figure 3.11). The extract started forming a precipitate at week 5 and upon closer examination it appeared to be fermenting based off the odour and gas bubbles forming with in vial.

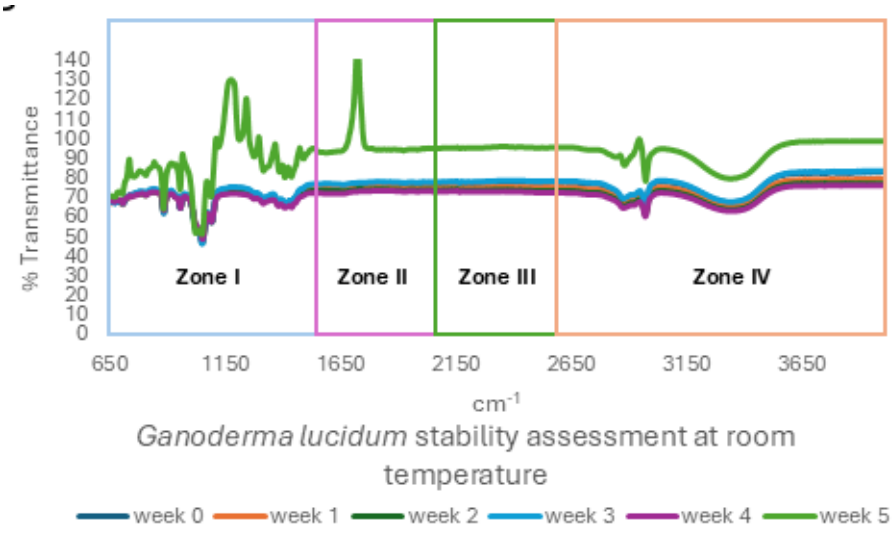


Figure 3.11 FTIR profiles for *Ganoderma lucidum* extracts stored at room temperature. Extracts were measured over a period of 5 weeks. The x-axis represents the wavenumber (cm^{-1}) while the y-axis represents the % transmittance. Zone I (fingerprint) is shown in blue margins, zone II (triple bonds) in pink margins, zone III (double bonds) in green margins and zone IV (single bonds) in orange margins.

The peak wavenumbers and percentage transmittance of week 0 compared to week 5 can be seen in Table 3.10. There were 6 peaks identified in the fingerprint region (650 – 1500 cm^{-1}). The region 700 – 800 cm^{-1} corresponds to C-Cl bonds. Cyclohexane ring vibrations are located between 1000 – 1055 cm^{-1}. Secondary amines (C-N stretch) are in the region 1130 – 1190 cm^{-1}. A big peak shift is observed at 1190 cm^{-1} in week 5 compared to week 0. Ketones and carboxylic acid overlap in wavenumber, at 1705 – 1725 cm^{-1} and 1700 – 1725 cm^{-1}, respectively. Both functional groups are categorized by carbonyl compounds. Methyl groups are located at 2950 – 2970 cm^{-1}.

Table 3.10 The peak wavenumbers observed in *Ganoderma lucidum* when stored for 5 weeks at room temperature compared to the day of preparation (week 0).

Wavenumber (cm^{-1})	%T (week 0)	%T (week 5)
733	71,1	89,12
1014	57,21	54,9
1175	**75,43**	**130,44**
1190	**75,22**	**126,26**
1240	**74,41**	**120,93**
1294	**71,72**	**101,26**
1721	**77,16**	**162,85**
1724	**77,2**	**157,97**
2945	**73,07**	**100,11**
2955	71,98	96
3995	83,4	99,08

3.4.2.1.2 Extracts stored at -18°C

At -18°C there is consistency between spectra from week 1 to 4 in *T. versicolour* extracts, when compared to week 0. At week 5 a change is observed in the fingerprint region (650 – 1500 cm^{-1}) (Figure 3.12).

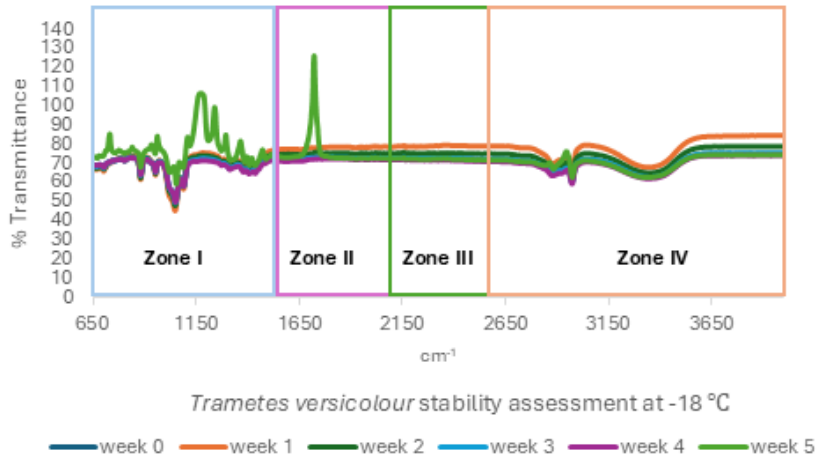


Figure 3.12 FTIR profiles for *Trametes versicolour* extracts stored at -18°C. Extracts were measured over a period of 5 weeks. The x-axis represents the wavenumber (cm^{-1}) while the y-axis represents the % transmittance. Zone I (fingerprint) is shown in blue margins, zone II (triple bonds) in pink margins, zone III (double bonds) in green margins and zone IV (single bonds) in orange margins.

The %T values for some wavenumbers which were visibly different in the spectra between week 0 and week 5 are shown in Table 3.11.

Table 3.11 The peak wavenumbers observed in *Trametes versicolour* when stored for 5 weeks at -18°C compared to the day of preparation (week 0).

Wavenumber (cm^{-1})	%T (week 0)	%T (week 5)
736	71,00	80,78
936	70,74	79,22
968	70,81	80,13
1099	64,05	75,6
1104	67,81	80,96
1176	**72,58**	**106,72**
1239	71,87	99,32
1294	69,62	84,91
1367	68,38	81,32
1420	66,27	72,92
1722	**73,00**	**126,23**

G. lucidum extracts showed variation across week 0 to week 5 (Figure 3.13). The fingerprint region (650 – 1500 cm^{-1}) showed inconsistencies from week 0, throughout to week 5. As the aim of using FTIR was to assess stability over time with storage at different temperatures, for simplicity and clarity, comparison will be made of the extracts the day of preparation (week 0) and at the end of the experiment (week 5).

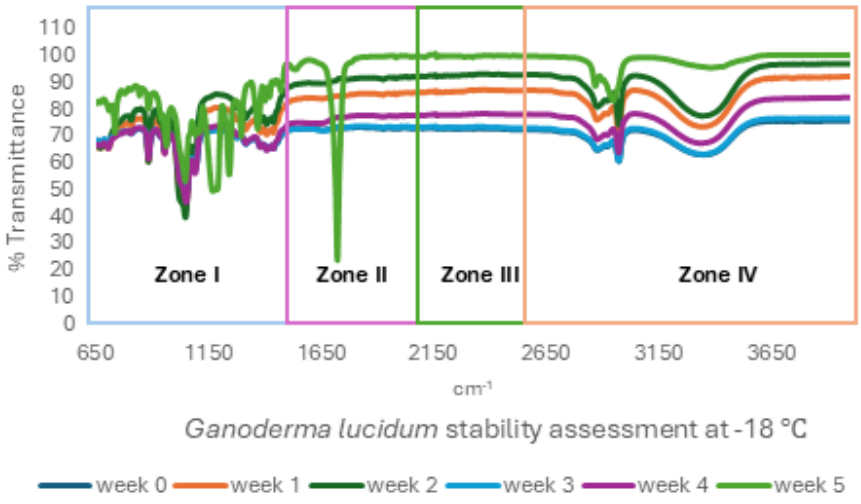


Figure 3.13 FTIR profiles for *Ganoderma lucidum* extracts stored at -18°C. Extracts were measured over a period of 5 weeks. The x-axis represents the wavenumber (cm^{-1}) while the y-axis represents the % transmittance. Zone I (fingerprint) is shown in blue margins, zone II (triple bonds) in pink, zone III (double bonds) in green and zone IV (single bonds) in orange.

The spectrum of week 5 is higher along the y-axis in comparison to the spectrum of week 0 (Figure 3.13). The spectrum for week 0 begins at 68.57 cm^{-1}, whereas week 5 beings at 82.58 cm^{-1}. Many troughs and peaks are observed in the fingerprint region (650 – 1500 cm^{-1}) in the week 5 spectrum which are not present in the week 0 spectrum (Figure 3.13). Additionally, a trough is observed at 1721 cm^{-1} on the week 5 spectrum (Figure 3.13). The spectrum shape for week 5 is similar to that of week 0 in zone III and IV, with the exception of being shifted upwards. The broad trough seen in zone IV is less prominent in week 5 compared to week 0 (Figure 3.13). All the changes at in the week 5 spectrum indicate the instability of *G. lucidum* extracts when stored at -18°C. Most of the spectrum (week 5), had a %T close to 100% which is a strong indication that the compound has degraded, as there are no bonds absorbing a wide range of wavelengths.

Table 3.12 shows the %T at week 0 compared to week 5 at a few wavenumbers which showed major differences in appearance on the spectrum.

Table 3.12 A comparison of %T on the FTIR spectrum for *Ganoderma lucidum* stored at -18°C for 5-weeks compared to extracts the day of preparation (week 0). *Ganoderma lucidum* extracts were stored at -18°C for 5 weeks and analysed using FTIR weekly.

Wavenumber (cm^{-1})	%T (week 0)	%T (week 5)
1721	73,14	23,96
1167	72,55	49,79
906	72,18	86,55
2867	65,70	89,02
2948	68,16	83,56
650	68,57	82,58

3.4.2.1.3 Extracts stored at 4°C

When stored at 4°C, there was little variation across spectra (Figure 3.14). The spectra from weeks 1 – 5 can be seen overlapping with week 0. *T. versicolour* extracts stored at 4°C were the most stable in comparison to those stored at room temperature and -18°C.

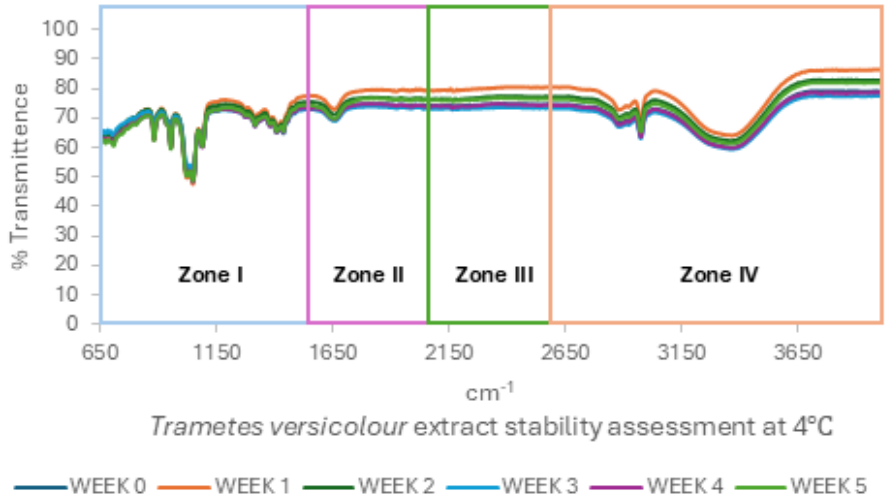


Figure 3.14 FTIR profiles for *Tramates versicolour* extracts stored at 4°C. Extracts were measured over a period of 5 weeks. The x-axis represents the wavenumber (cm^{-1}) while the y-axis represents the % transmittance. Zone I (fingerprint) is shown in blue margins, zone II (triple bonds) in pink margins, zone III (double bonds) in green margins and zone IV (single bonds) in orange margins.

When stored at 4°C, *G. lucidum* extracts showed consistency across spectra from week 1 to 5 in comparison to week 0 (Figure 3.15). *G. lucidum* extracts stored at 4°C were the most stable when compared to extracts stored at room temperature and -18°C.

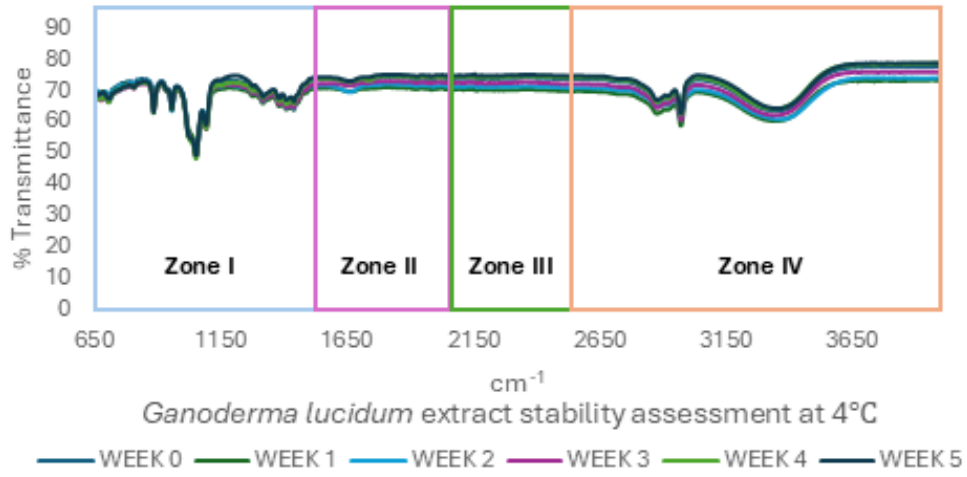


Figure 3.15 FTIR profiles for *Ganoderma lucidum* extracts stored at 4°C. Extracts were measured over a period of 5 weeks. The x-axis represents the wavenumber (cm^{-1}) while the y-axis represents the % transmittance. Zone I (fingerprint) is shown in blue margins, zone II (triple bonds) in pink margins, zone III (double bonds) in green margins and zone IV (single bonds) in orange margins.

In summary, spectral analysis showed minimal variation among *G. lucidum* and *T. versicolour* batches. At room temperature, both *T. versicolour* and *G. lucidum* extracts displayed minimal

spectral variation until week 5, at which point substantial changes were observed in the fingerprint region (650–1500 cm^{-1}). For *T. versicolour*, increased transmittance at several wavenumbers suggested degradation of specific functional groups, while for *G. lucidum*, a pronounced upward shift in the spectrum coincided with visible signs of fermentation. When stored at -18°C, *T. versicolour* remained stable up to week 5, after which peak shifts in the fingerprint region were detected, suggesting molecular changes over time. *G. lucidum* extracts stored at -18°C showed spectral inconsistencies from week 0 to week 5, with increased transmittance across a wide range of wavenumbers, indicating significant degradation. At 4°C, *T. versicolour* remained stable for the entire five-week period, with no significant spectral alterations detected. *G. lucidum* extracts stored at 4°C also showed minimal variation until week 5, at which point slight shifts in the fingerprint region suggested the onset of molecular changes, though to a lesser extent than those observed at room temperature and -18°C.

3.5 Assessment of cytotoxic effects by evaluating the morphology of A549 and HEK293 cells.

Cells were treated with 0.5 mg/mL and 0.25 mg/mL of mushroom extracts (*G. lucidum* and *T. versicolour*) and doxorubicin at concentrations equivalent to their IC_{80} values as determined in Chapter 2, Section 2.5. Cells were exposed to the compounds for a period of 18 h and 24 h. Cells were then stained using a combination of HO, AO and PI fluorescent dyes to visualise changes in the morphology of cells as described in (Chapter 2, Section 2.6). Results are shown as follows: PC merged with HO images, HO merged with PI, and PI merged with AO. The effects of *G. lucidum* and *T. versicolour* on A549 cells is shown in Figure 3.16 (18 h incubation) and 3.17 (24 h incubation) and the effect on HEK293 cells is shown in Figure 3.18 (18 h incubation) and 3.19 (24 h incubation).

3.5.1 The cytotoxic effects of *G. lucidum* and *T. versicolour* on A549 cell morphology.

Figure 3.16 shows the effect of doxorubicin, *G. lucidum* and *T. versicolour* in A549 cells at 18 h. In untreated cells (Figure 3.16, panel a and b), HO stained the nuclei evenly to show their regular ovoid shape. The absence of PI staining indicated intact plasma membranes and the absence of necrosis (Figure 3.16, panel b-c). Cells were stained green as a result of the AO dye (Figure 3.16, panel c).

Cells treated with doxorubicin at concentrations equivalent to the IC_{80} values (20 µM) showed morphological changes consistent with cellular stress (Figure 3.16, panels d-f). Under phase contrast mode, cells appear granulated (Figure 3.16, panel d). A few cells marked in panels d-

f (Figure 3.16) appear rounded as indicated by arrows. Since doxorubicin acts by inter-chelating with DNA and has an intrinsic red fluorescence, it was likely the cause of the observed red nuclei (Figure 3.16, panel e and f). The doxorubicin treated cells show a decreased staining with HO (Figure 3.16, panel e). This is because of HO binding competing with doxorubicin for the minor groove on DNA (Elgart *et al*., 2018).

Cell membranes appeared smooth, indicating the membranes were intact and the red nuclei was caused by doxorubicin and not PI (Figure 3.16, panel e). Doxorubicin accumulated in the perinuclear spaces within A549 cells but did not enter the nuclei of the majority of cells at 18 h (Figure 3.16, panel e-f).

When treated with 0.5 mg/mL *G. lucidum* extract for 18 h, cells showed nucleic changes consistent with necrosis (Figure 3.16, panels g-i). In this treatment, 59 ± 6% of cells were necrotic. Cellular membranes did not appear smooth which was indicative of compromised membrane integrity (Figure 3.16, panel g). The merged image of HO and PI was pink, indicating the presence of PI in the nuclei and necrosis of the cell (Figure 3.16, panel h). The merged image of PI and AO indicated cells stained positive for PI, confirming the compromised plasma membrane integrity (Figure 3.16, panel i). Cells were stained green as a result of AO, with the brightest green fluorescence located in the nucleus (Figure 3.16, panel i).

When cells were treated with 0.25 mg/mL of *G. lucidum* extract there was no indication of PI positive nuclei indicating the absence of necrosis. Vacuoles were present in the merged PC and HO image, indicated by the green arrows (Figure 3.16, panel j). At this treatment concentration, cells were vacuolated, and some cells were detached from the growth surface as indicated by their round shape (Figure 3.16, panel j). The cells showed changes to the nuclei, detected with HO, which were consistent with apoptotic cell death. There was an increase in the intensity of the blue, fluorescent signal and the presence of blue globules which indicated nuclear fragmentation (Figure 3.16, panel k). In the merged PI and AO image, the absence of PI indicated an intact plasma membrane, while cells were stained green with AO (Figure 3.16, panel l).

A concentration of 0.5 mg/mL *T. versicolour* extract caused some cells to detach from the growth surface, as indicated by their round shapes (Figure 3.16, panel m). At this concentration, cells showed morphological changes consistent with apoptotic cell death, such as nuclear fragmentation and an increase in blue fluorescence (Figure 3.16, panel n). Figure 3.16, panel o indicated the absence of PI while all cells were green because of AO.

A similar effect was observed at a concentration of 0.25 mg/mL *T. versicolour* extract in Figure 3.16, panel p-r. Cells in this treatment were detaching from the growth surface, as indicated by their round shape (Figure 3.16, panel p). Cells showed nuclear changes consistent with apoptosis, such as nuclear fragmentation (Figure 3.16, panel q). In the merged PI and AO image all cells were green because of the AO, the absence of PI indicated that membranes were intact (Figure 3.16, panel r).

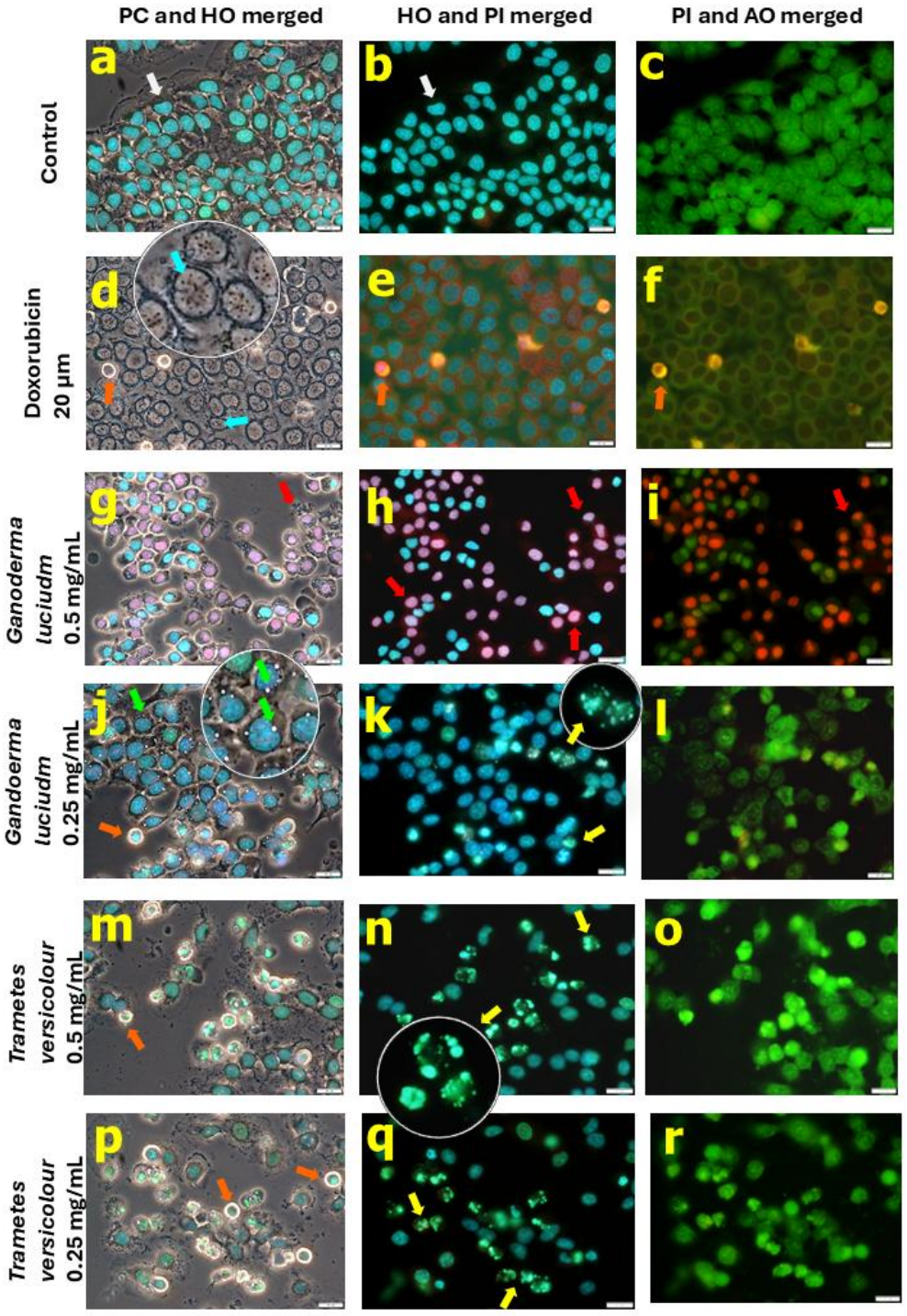


Figure 3.16 Representative photomicrographs showing the morphological changes caused by *Ganoderma lucidum*, *Trametes versicolour* and doxorubicin on A549 cells after an 18 h treatment. Panels a-c shows untreated cells, panels d-f shows the effect of 0.5 mg/mL *Ganoderma lucidum* extract, panels j-l shows the effect of 0.25 mg/mL *Ganoderma lucidum* extract, panels m-o shows the effect of 0.5 mg/mL *Trametes versicolour* extract, and panels p-r shows the effect of 0.25 mg/mL *Trametes versicolour* extract. Cells were viewed with the Olympus BX41 microscope and images were captured with the DP72 digital camera (magnification: 400×, scalebar 20µm). Legend – PC=Phase contrast, HO=Hoechst 33342, PI=Propidium iodide, and AO=Acridine orange. Arrows – white=nucleus, blue=granules, orange=rounded cell, red=necrotic cell, green=vacuoles, yellow=apoptotic cell.

Figure 3.17 shows the effect of doxorubicin, *G. lucidum* and *T. versicolour* in A549 cells at 24 h. Panels a-c represents untreated cells. Cells appeared uniform in shape and size (Figure 3.17, panel a). Cellular nuclei were stained uniformly with HO (Figure 3.17, panel b) and cell membranes were intact, indicated by the negative stain for PI (Figure 3.17, panel c). AO stained cells green (Figure 3.17, panel c). AO is an indicator of lysosome formation which presents as yellow or red granules since lysosomes are acidic.

Doxorubicin was used a positive control. When A549 cells were treated with doxorubicin for 24 h, nuclear changes consistent with apoptosis could be observed (Figure 3.17, panels d-f). Nuclei were deformed and appeared to be non-uniformly stained with HO (Figure 3.17, panel e). Since no yellow or red granules were present, doxorubicin did not increase the formation of lysosomes which is an early but not absolute indicator of autophagy.

Treatment with *G. lucidum* extracts at a concentration of 0.5 mg/mL caused cellular membranes to appear uneven, indicating that the membrane integrity was compromised (Figure 3.17, panel g). All cells stained positive for PI, this is indicative of necrosis as it suggests the plasma membrane integrity is compromised. The merged PI and AO image is orange because of the combination of the PI and AO (Figure 3.17, panel i).

At the lower concentration of *G. lucidum* extract (0.25 mg/mL), cells appeared round, and vacuoles were present (Figure 3.17, panel j). In this treatment, both apoptosis (30%) and necrosis (40%) were observed (Figure 3.17, panel k). In Figure 3.17, panel k, membrane blebbing and nuclear fragmentation can be observed which is indicative of apoptosis, while the positive stain for PI indicates necrotic cell death. In panel l (Figure 3.17) the merged PI and AO image is orange because of the combination of the PI and AO.

Similarly, treatment with *T. versicolour* extract at 0.5 mg/mL caused cells to appear granulated and vacuolated with uneven cell membranes (Figure 3.17, panel m). Cells in this treatment were necrotic as indicated by the red nuclei from PI (Figure 3.17, panel n). The merged PI and AO image is orange because of the combination of PI and AO (Figure 3.17, panel o). Green speckled regions in panel o indicate nuclear fragmentation.

At a lower concentration of *T. versicolour* (0.25 mg/mL), some cells were detached from the growth surface as indicated by their round shape (Figure 3.17, panel p). Cells showed nuclear changes consistent with apoptosis, such as an increased blue fluorescence and nuclear fragmentation seen in Figure 3.17, panel q and r.

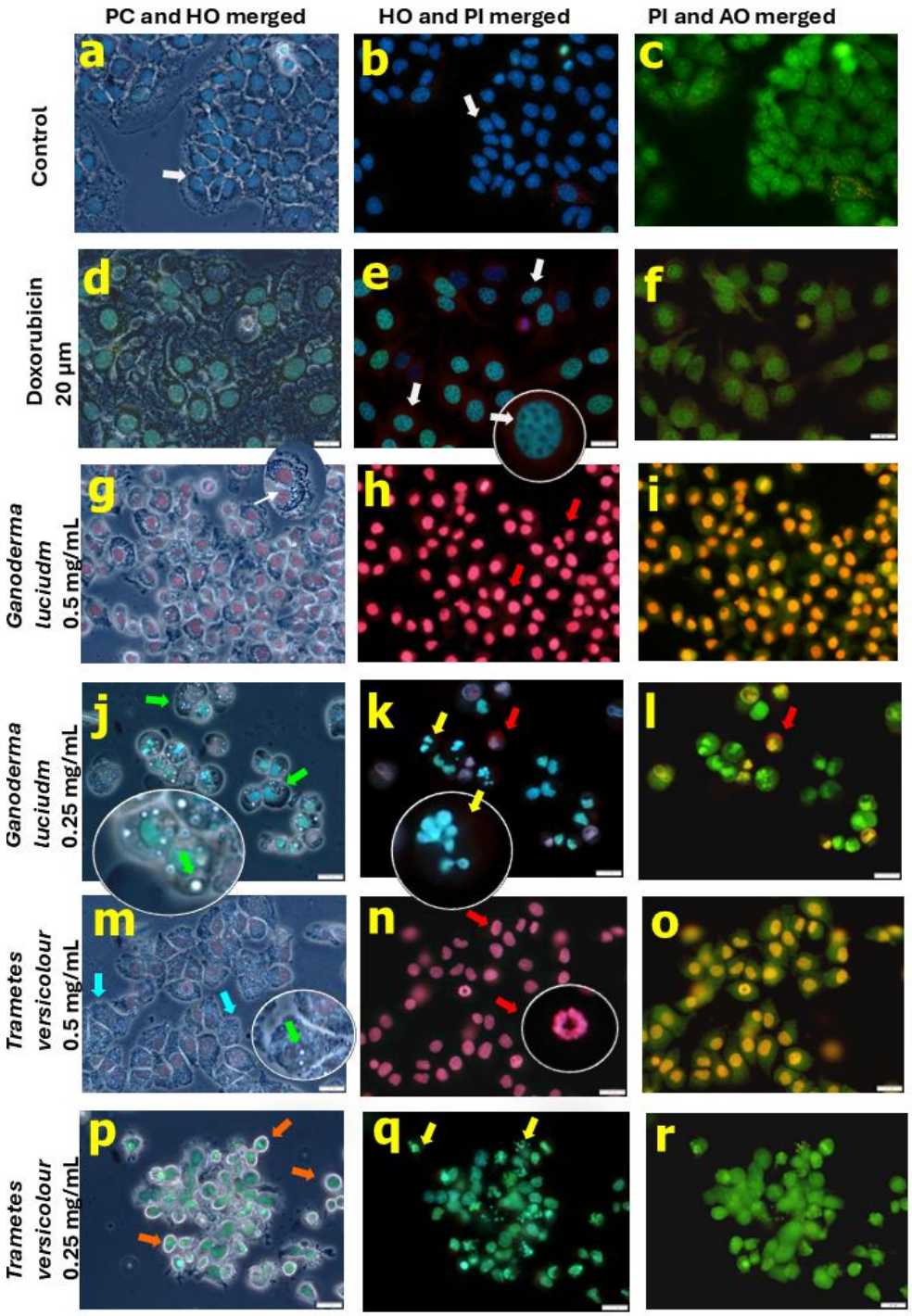


Figure 3.17 Representative photomicrographs showing the morphological changes caused by *Ganoderma lucidum*, *Trametes versicolour* and doxorubicin on A549 cells after a 24 h treatment. Panels a-c shows untreated cells, panels d-f shows the effect of 0.5 mg/mL *Ganoderma lucidum* extract, panels j-l shows the effect of 0.25 mg/mL *Ganoderma lucidum* extract, panels m-o shows the effect of 0.5 mg/mL *Trametes versicolour* extract, and panels p-r shows the effect of 0.25 mg/mL *Trametes versicolour* extract. Cells were viewed with the Olympus BX41 microscope and images were captured with the DP72 digital camera (magnification: 400×, scalebar 20µm). Legend – PC=Phase contrast, HO=Hoechst 33342, PI=Propidium iodide, and AO=Acridine orange. Arrows – white=nucleus, blue=granules, orange=rounded cell, red=necrotic cell, green=vacuoles, yellow=apoptotic cell.

In summary, in A549 cells, doxorubicin-treated cells showed different effects over time, with an 18 h treatment causing granulation. At 24 h, apoptosis was evident, accompanied by cytoplasmic red fluorescence. Cells treated with 0.5 mg/mL *G. lucidum* showed necrosis at both treatment points, with necrosis increasing from 59 ± 6% at 18 h to 100% at 24 h. At 0.25 mg/mL *G. lucidum*, apoptosis was observed at 18 h, while both apoptosis and necrosis were observed at 24 h, with necrosis being more prevalent. *T. versicolour* treatment for 18 h at 0.5 mg/mL caused apoptosis and necrosis at 24 h. At a lower concentration of 0.25 mg/mL, apoptosis was present at both treatment periods.

3.5.2 The cytotoxic effects of *G. lucidum* and *T. versicolour* on HEK293 cell morphology.

Cells were exposed to the compounds for a period of 18 h and 24 h. Cells were then stained using a combination of HO, AO and PI fluorescent dyes to visualise changes in the morphology of cells as described in (Chapter 2, Section 2.6). Results are shown as follows: PC merged with HO images, HO merged with PI, and PI merged with AO. The effects of *G. lucidum* and *T. versicolour* on HEK293 cells is shown in Figure 3.18 (18 h incubation) and 3.19 (24 h incubation).

Panels a-c shows untreated HEK293 cells. The cells were uniform in shape and size and had smooth membranes (Figure 3.18, panel a). Their nuclei were stained uniformly with HO (panel b) and their membranes were intact as indicated by the absence of PI (panel c).

Doxorubicin was used as the positive control (Figure 3.18, panels d-f). Cells treated with doxorubicin for 18 h had extensive perinuclear granulation which showed as dark circles around the nuclei of the cells (Figure 3.18, panel d). Doxorubicin accumulated in the perinuclear region, as indicated by the red fluorescence in the region (Figure 3.18, panel e). Cells show a decrease in blue fluorescence due to doxorubicin competing with HO for the binding to DNA (Figure 3.18, panel e). The red fluorescence from the merged PI and AO image is brighter than the green fluorescence of AO, cells do therefore not appear green (Figure 3.18, panel f).

When treated with *G. lucidum* at 0.5 mg/mL for 18 h, cells appeared vacuolated (Figure 3.18, panel g). Nuclear fragmentation was seen in a few cells, indicating apoptosis (Figure 3.18, panel h). There was no evidence of apoptosis or necrosis in this treatment. Orange specs within green cells were seen (Figure 3.18, panel i). AO staining showed orange specs within green cells (Figure 3.18, panel i). The orange specs were located in the cytoplasm of cells. This indicates the presence of lysosomes, which is a preliminary feature of autophagy.

G. lucidum treatment at 0.25 mg/mL caused cells to detach from the growth surface and assume a rounded morphology (Figure 3.18, panel j). The merged HO and PI image shows uniformly stained nuclei (Figure 3.18, panel k). There was a low percentage of cells (3.0 ± 1.0 %) which had a positive signal for PI. Orange specks within cells were observed in Figure 3.18, panel l. This indicates the presence of lysosomes which is a preliminary feature of autophagy.

Cells treated with *T. versicolour* at a concentration of 0.5 mg/mL appeared non-uniform, with some cells detaching from the growth surface and assuming a round morphology (Figure 3.18, panel m). A low percentage of cells (18.0 ± 4.0 %) were undergoing nuclear fragmentation as indicated by yellow arrows (Figure 3.18, panel n). Red fluorescence was observed in some cells (9.5 ± 0.5 %), indicating the membrane integrity was compromised which is a feature of necrotic cell death (Figure 3.18, panel n). Some cells in the PI and AO merged image appeared orange because of the PI red fluorescence overlayed with the green from the AO (Figure 3.18, panel o). Additionally, lysosomes appeared as small orange specks and indicate preliminary signs of autophagy.

At the lower concentration of *T. versicolour* extract (0.25 mg/mL), cells appeared irregular in shape and size (Figure 3.18, panel p). A low percentage of cells (15.0 ± 2.0 %) had cellular changes consistent with apoptosis, i.e. nuclear fragmentation (Figure 3.18, panel q). While 5.0 ± 2.0 % of cells stained positive for PI which is indicative on a compromised plasma membrane and therefore necrosis (Figure 3.18, panel q). Cells which had a positive signal for PI appeared orange in the merged PI and AO image (Figure 3.18, panel r). Additionally, the smaller specks of orange are lysosomes. Lysosomes are a preliminary feature of autophagy.

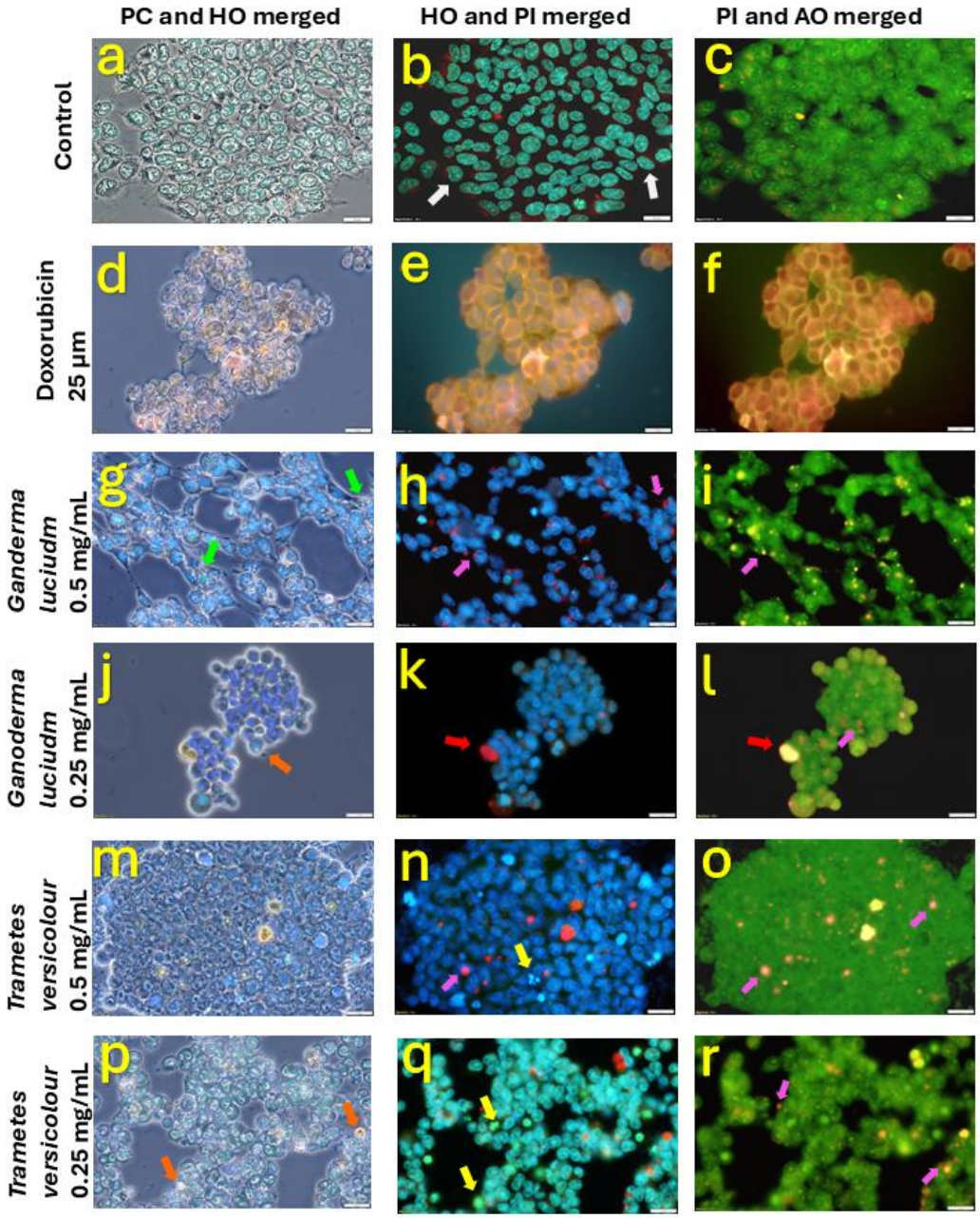


Figure 3.18 Representative photomicrographs showing the morphologic changes caused by *Ganoderma lucidum*, *Trametes versicolour* and doxorubicin on HEK293 cells after a 18 h treatment. Panels a-c shows untreated cells, panels d-f shows the effect of 0.5 mg/mL *Ganoderma lucidum* extract, panels j-l shows the effect of 0.25 mg/mL *Ganoderma lucidum* extract, panels m-o shows the effect of 0.5 mg/mL *Trametes versicolour* extract, and panels p-r shows the effect of 0.25 mg/mL *Trametes versicolour* extract. Cells were viewed with the Olympus BX41 microscope and images were captured with the DP72 digital camera (magnification: 400×, scalebar 20µm). Legend – PC=Phase contrast, HO=Hoechst 33342, PI=Propidium iodide, and AO=Acridine orange. Arrows – white = nucleus, purple = granulated cells, orange = cells shrinking / rounding up, red = necrotic cell, green = vacuoles, yellow = apoptotic nuclei. Arrows – white=nucleus, orange=rounded cell, red=necrotic cell, green=vacuoles, yellow=apoptotic cell, pink=lysosomes.

Untreated cells appeared uniform in shape and size with even cell membranes (Figure 3.19, panel a). Cells were growing elongated, which is normal when there are large spaces between cells. Lysosomes were seen in panel b (Figure 3.19). Lysosomes tend to cluster around the nucleus when cells are deprived of nutrients (Ebner *et al*., 2023). Since there was nothing inhibiting the growth of untreated cells, they were still actively growing and used up most of the nutrients in the culture media, resulting in the lysosomes forming. Cells were stained uniformly with HO (Figure 3.19, panel b).

Doxorubicin was used as the positive control. Cells appeared larger than untreated cells (Figure 3.19, panel d). This is indicative of cytoplasmic swelling. Cells were granular and the plasma membranes appeared uneven (Figure 3.19, panel d). Uneven membranes are an indication of compromised membrane integrity. This means that PI could penetrate the membrane, and the red fluorescence is due to PI (Figure 3.19, panel e). Treatment with doxorubicin for 24 h caused HEK293 cells to undergo necrosis. The green fluorescence from AO is not visible due to the bright red fluorescence in the merged PI and AO image (Figure 3.19, panel f).

Cells treated at 0.5 mg/mL of *G. lucidum* appeared rounded (Figure 3.19, panel g). Cells were positive for PI, indicating compromised plasma membrane integrity and therefore necrosis (Figure 3.19, panel h). The merged PI and AO images shows orange cells because of the combination of the PI and AO signal (Figure 3.19, panel i).

Cells treated with *G. lucidum* at 0.25 mg/mL appeared vacuolated (Figure 3.19, panel j). Panel k shows cells positive for PI (Figure 3.19). This is consistent with necrosis. A small percentage of cells were undergoing nuclear fragmentation, being indicative of apoptosis.

T. versicolour treatment at 0.5 mg/mL caused cells to appear granular with uneven membranes (Figure 3.19, panel m). Uneven membranes indicate compromised membrane integrity which is a feature of necrosis (Figure 3.19, panel m and o).

At 0.25 mg/mL of *T. versicolour*, cells appeared irregular in shape and size (Figure 3.19, panel p). At this concentration, cellular changes consistent with apoptosis were observed such as an increase in HO fluorescence and nuclear fragmentation (Figure 3.19, panel q).

In summary, in HEK293 cells, untreated cells remained uniform in shape with smooth membranes across both exposure periods. Doxorubicin treatment at 18 h led to perinuclear accumulation and signs of autolysis, whereas at 24 h, necrosis was dominant, characterized by rough membranes and PI-positive staining. Treatment with 0.5 mg/mL *G. lucidum* did not

induce significant cell death at 18 h; however, necrosis was predominant at 24 h. At 0.25 mg/mL *G. lucidum*, no apoptosis was observed at 18 h, but both apoptosis and necrosis were present at 24 h. *T. versicolour* at 0.5 mg/mL caused both apoptosis and necrosis at 18 h, with necrosis becoming predominant at 24 h. At 0.25 mg/mL *T. versicolour*, apoptosis was the primary mechanism at 18 h, while both apoptosis and necrosis were observed at 24 h. Overall, prolonged exposure (24 h) generally increased necrosis, particularly at higher extract concentrations, while apoptosis was more prominent at 18 h, especially at lower concentrations.

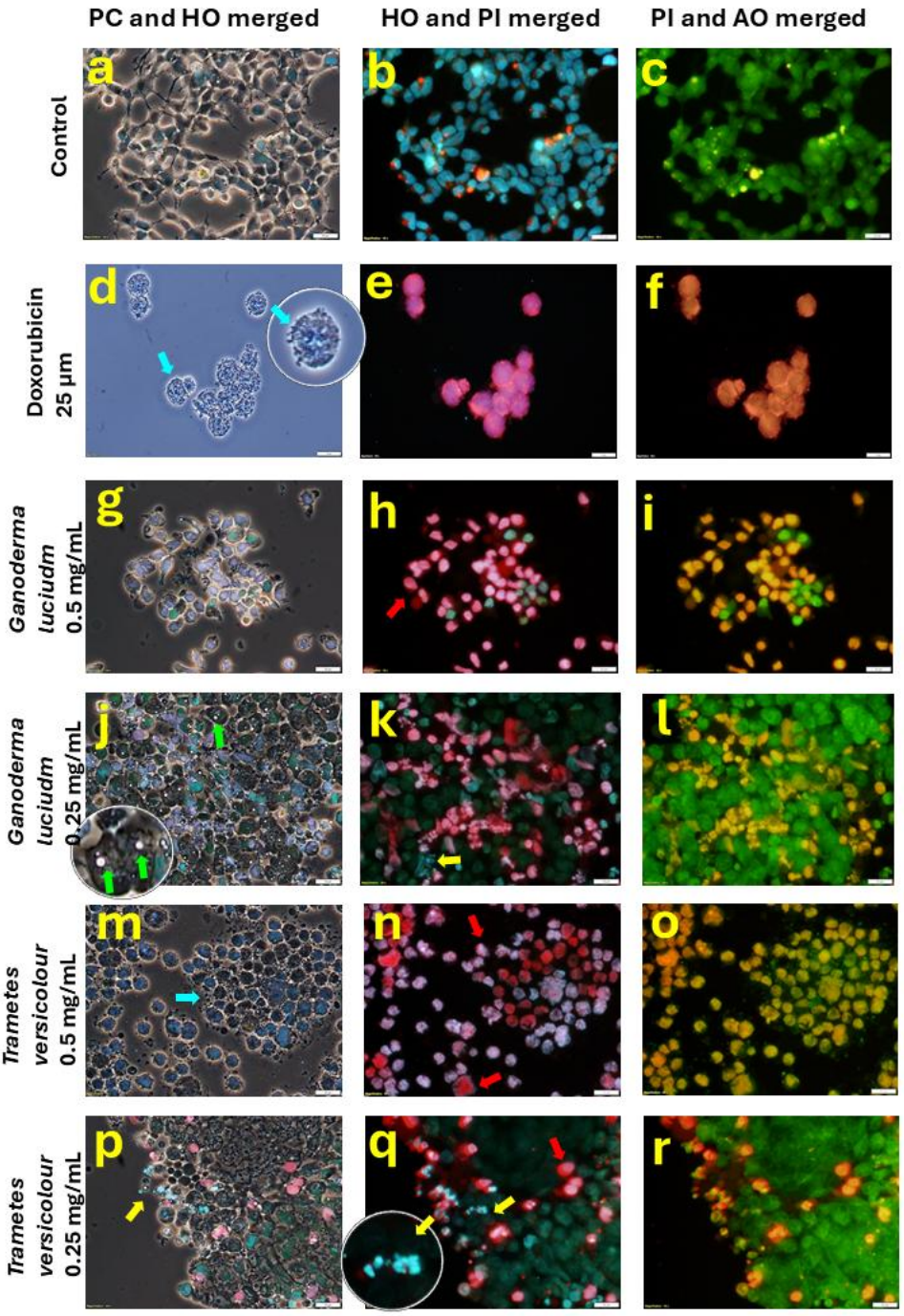


Figure 3.19 Representative photomicrographs showing the morphological changes caused by *Ganoderma lucidum*, *Trametes versicolour* and doxorubicin on HEK293 cells after a 24 h treatment. Panels a-c: untreated cells, panels d-f shows the effect of 0.5 mg/mL *Ganoderma lucidum* extract, panels j-l: 0.25 mg/mL *Ganoderma lucidum* extract, panels m-o: 0.5 mg/mL *Trametes versicolour* extract, and panels p-r: the effect of 0.25 mg/mL *Trametes versicolour* extract. Cells were viewed with the Olympus BX41 microscope and images were captured with the DP72 digital camera (magnification: 400×, scalebar 20µm). Legend – PC=Phase contrast, HO=Hoechst 33342, PI=Propidium iodide, and AO=Acridine orange. Arrows – white=nucleus, blue=granules, orange=rounded cell, red=necrotic cell, green=vacuoles, yellow=apoptotic cell.

Figure 3.20 shows the average percentages of cells undergoing apoptosis and necrosis when treated with *G. lucidum* and *T. versicolour*. A549 cells treated with *G. lucidum* at 0.5 mg/mL for 18 h solely underwent necrosis, with 59.0 ± 6.0 % of cells undergoing necrosis, apoptosis was not induced in this treatment (Figure 3.20, panel A). The lower concentration of *G. lucidum* (0.25 mg/mL) caused apoptosis (31 ± 1.0 %), whereas necrosis did not occur.

T. versicolour extracts caused A549 cells to undergo apoptosis at both 0.5 mg/mL and 0.25 mg/mL with percentages of 38.0 ± 3.0 % and 25.5 ± 0.5 %, respectively (Figure 3.20, Panel A). At 24 h, A549 cells exclusively underwent necrosis (100 ± 0.0 %) when treated with 0.5 mg/mL *G. lucidum* with no apoptosis observed in this treatment (Figure 3.20, Panel B). At 0.25 mg/mL *G. lucidum*, A549 cells underwent both apoptosis (29.5 ± 0.5 %) and necrosis (39.5 ± 5.5 %), with necrosis being predominant. *T. versicolour* at 0.5 mg/mL caused cells to undergo necrosis exclusively (100 ± 0.0 %) (Figure 3.20, Panel B), whereas the 0.25 mg/mL concentration of *T. versicolour* caused cells to undergo apoptosis exclusively (47.0 ± 2.0 %) (Figure 3.20, Panel B).

HEK293 cells treated with *G. lucidum* at both 0.5 mg/mL and 0.25 mg/mL for 18 h did not undergo apoptosis (Figure 3.20, Panel C). In the lower concentration (0.25 mg/mL) 3.0 ± 1.0 % of cells were necrotic. *T. versicolour* at 0.5 mg/mL caused HEK293 cells to undergo apoptosis (18.0 ± 4 %) and necrosis (9.5 ± 0.5 %) (Figure 3.20, Panel C). The lower concentration of *T. versicolour* (0.25 mg/mL) caused 15.0 ± 2.0 % of cells to undergo apoptosis while 3.0 ± 1.0 % were necrotic. At 24 h, 0.5 mg/mL *G. lucidum* caused cells to undergo necrosis primarily (71.0 ± 7.0 %) (Figure 3.20, Panel D). Both apoptosis (48.0 ± 7.0) and necrosis (73.5 ± 4.5) were observed in the 0.25 mg/mL treatment, necrosis being predominant (Figure 3.20, Panel D). *T. versicolour* treated cells underwent both apoptosis (2.0 ± 2.0 %) and necrosis (34.5 ± 8.5 %) when treated at 0.5 mg/mL. Again, at 0.25 mg/mL *T. versicolour*, both apoptosis (18.0 ± 5.0 %) and necrosis (17.0 ± 1.0 %) were observed (Figure 3.20, Panel D).

In summary, *G. lucidum* and *T. versicolour* show a concentration dependent effect on cell death mechanisms in both A549 and HEK293 cell lines. In A549 cells, high concentrations of *G. lucidum* primarily induce necrosis at both 18 h and 24 h. Apoptosis dominates at 18 h for 0.25 mg/mL *G. lucidum* and *T. versicolour* at both concentrations. Low concentrations of *G. lucidum* (0.25 mg/mL) result in predominantly necrosis. The same was true for *T. versicolour* at high concentrations (0.5 mg/mL), whereas at low concentrations apoptosis was favoured. In HEK293 cells, *G. lucidum* does not induce cell death at 18 h. At 24 h, high concentrations of

G. lucidum result in necrosis, whereas lower concentrations prompt both apoptosis and necrosis. At 18 h, *T. versicolour* induces apoptosis primarily. When exposed for longer (24 h), necrosis is the predominant cell death mechanism at high concentrations (0.5 mg/mL). Low concentrations of *T. versicolour* (0.25 mg/mL) caused both apoptosis and necrosis.

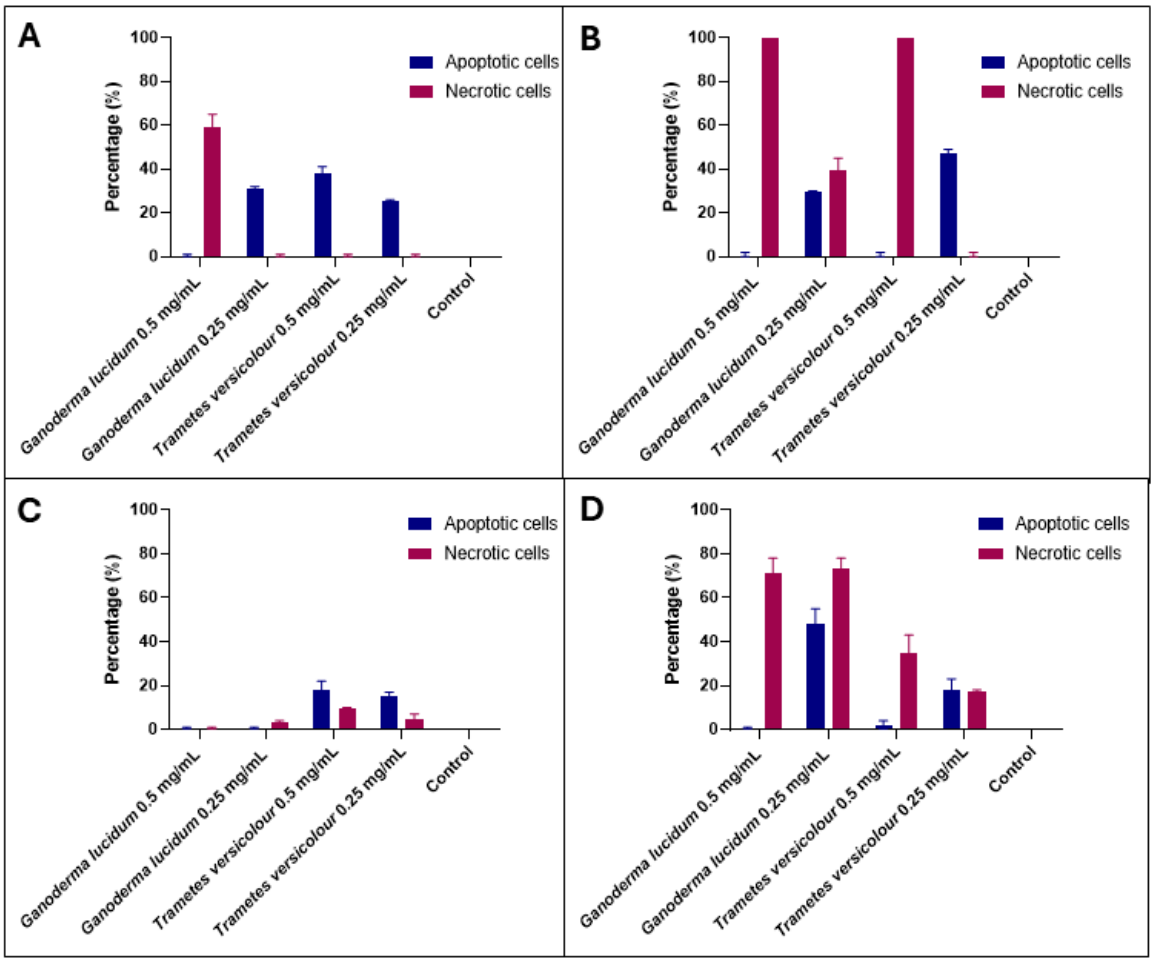


Figure 3.20 Average percentage of cells that underwent apoptosis or necrosis when treated with *Ganoderma lucidum* and *Trametes versicolour*. A549 and HEK293 cells were treated with 0.5 mg/mL and 0.25 mg/mL of mushroom extract (*Ganoderma lucidum* and *Trametes versicolour*) for 18 h and 24 h. Panel A represents A549 cells for 18 h, (B) A549 cells for 24 h, (C) HEK293 cells for 18 h and (D) HEK293 cells for 24 h. Each bar represents the mean and error bars represent the SEM. Results were obtained from three independent experiments.

3.6 The effect of the mushroom extracts and doxorubicin on Annexin-V binding to phosphatidylserine.

The translocation of phosphatidylserine, an early indicator for apoptosis, was evaluated after cells were treated with 0.25 and 0.5 mg/mL *G. lucidum* and *T. versicolour* extract for 24 h. Cells were treated with doxorubicin at a concentration equivalent to the IC_{80} value (Chapter 2, Section 2.5). Following the treatment, the Invitrogen annexin V Alexa Fluor™ 488 conjugate

(Thermo-Fisher Scientific, A13201) was used to detect the translocated phosphatidylserine as described in Chapter 2, Section 2.7. Cells were viewed using the Olympus BX41 microscope and images were captured using the Olympus DP72 camera. Representative photomicrographs from three independent experiments are shown in Figure 3.21 and Figure 3.22 for A549 and HEK293 cells respectively.

3.6.1 Annexin-V binding to phosphatidylserine in A549 cells

The untreated cells (Figure 3.21, panel a) show oval nuclei within a healthy cell and the absence of PI and AV binding are observed (Figure 3.21, panel b). Doxorubicin was used as the positive control and is shown in panel c and d (Figure 3.21). All doxorubicin treated cells had red nuclei due to doxorubicin's innate red fluorescence. The fluorescence from doxorubicin and PI are indistinguishable. A549 cells were treated with doxorubicin at 20 µM. Cells were granulated (Figure 3.21, panel c) with some cells assuming a round morphology because they have detached from the growth surface. Panel d shows the presence of acidic granules (Figure 3.21). Dark perinuclear circles are visible in doxorubicin treated cells (Figure 3.21, panel c). This is a morphological feature of autosis. Autosis is a type of autophagic cell death which is Na^+, K^+ -ATPase-regulated (Liu *et al*., 2013). Morphological features include increase autophagosomes at early stages, while late-stage morphology includes focal swelling of the perinuclear space (Liu *et al*., 2013). Cellular nuclei are stained red as a result of the innate fluorescence of doxorubicin (Figure 3.21, panel d).

G. lucidum at a concentration of 0.5 mg/mL caused cells to detach from the growth surface, assume a round morphology, and clump together (Figure 3.21, panel e). Panel f shows binding for both the annexin-V conjugate and PI occurred, being indicative of a late stage of apoptosis or secondary necrosis (Figure 3.21, panel f). Secondary necrosis occurs when apoptotic cells are not cleared. Apoptosis then progresses to secondary necrosis and cells lose their membrane integrity (Sachet *et al*., 2017). Annexin-V binding appears granular, spread over the entire cell. This is typical for the late stage of apoptosis because of the membrane dysregulation. Cells treated with a lower concentration of *G. lucidum* (0.25 mg/mL) were vacuolated and rounded (Figure 3.21, panel g). Panel h shows annexin-V binding with fewer cells indicating PI binding than in the 0.5 mg/mL treatment (Figure 3.21, panel h). Annexin-V binding appeared granular in late apoptotic cells while the binding appeared smooth in early apoptotic cells.

A concentration of 0.5 mg/mL *T. versicolour* extract appeared to be smaller and had a more rounded appearance with prominent nuclei (Figure 3.21, panel i). Cells showed binding for the

annexin-V conjugate. Some cells were undergoing secondary necrosis based on the positive PI signal. Annexin-V binding appeared uniform and covered the entire cell (Figure 3.21, panel j). This is indicative of early apoptosis because phosphatidylserine is externalized to the outer leaflet.

A lower concentration of *T. versicolour* (0.25 mg/mL) showed some cells resembling the untreated cells while other cells were detaching from the growth surface and appeared rounder and smaller (Figure 3.21, panel k). Cells in this treatment showed a positive signal for the annexin-V conjugate and no signal for PI (Figure 3.21, panel l). Annexin-V binding appeared granular, scatter across entire cells. Punctate fluorescence occurs due to membrane disintegration.

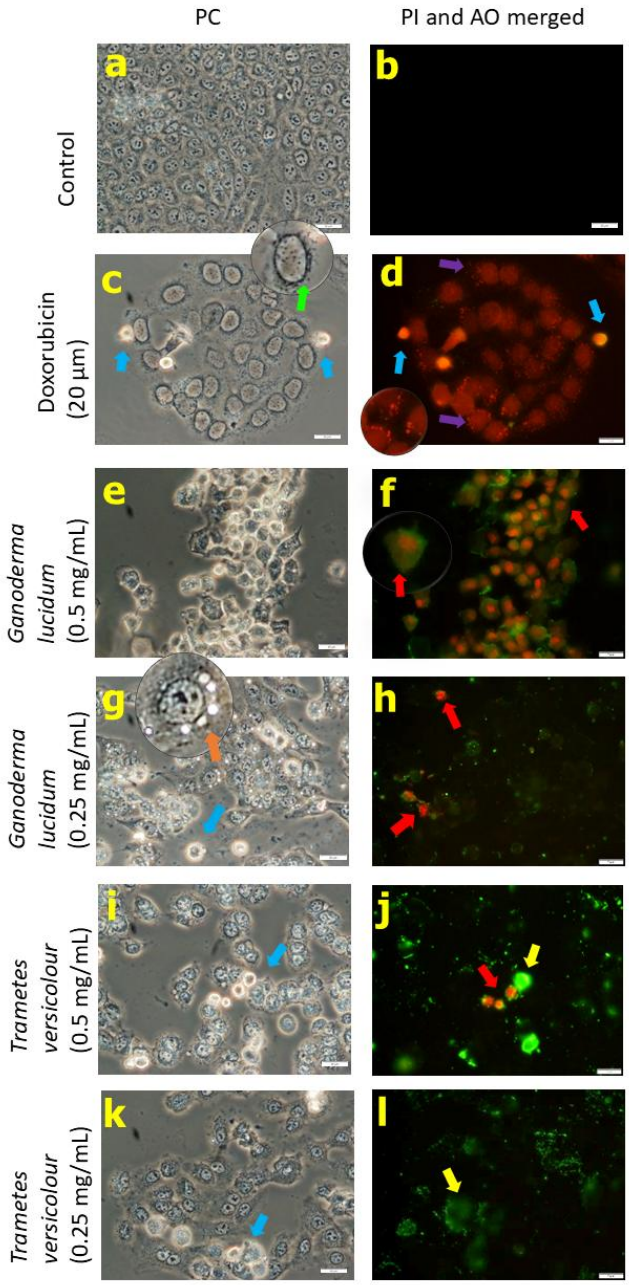


Figure 3.21 Representative photomicrographs showing binding of annexin-V to phosphatidylserine in A549 cells when treated with doxorubicin, *Ganoderma lucidum* and *Trametes versicolour*. A549 cells were treated with doxorubicin at 20 µM and *Trametes versicolour* and *Ganoderma lucidum* extracts at concentrations of 0.25 mg/mL and 0.5 mg/mL for 24 h. Panels a and b show untreated cells, panel c and d show the effect of doxorubicin, panels e and f show the effect of *Ganoderma lucidum* at 0.5 mg/mL, panels g and h show the effect of *Ganoderma lucidum* at 0.25 mg/mL, panels i an j show the effect of *Trametes versicolour* at 0.5 mg/mL, and panels k and l show the effect of *Trametes versicolour* at 0.25 mg/mL. An Olympus BX41 microscope was used to observe cells and the Olympus DP72 camera was used to capture images (Magnification: 400x; scalebar: 20µm). LEGEND: PC= phase contrast, PI= propidium iodide. The experiment was repeated three times (n=3). Arrows: green = granules, blue = rounded cell, purple = acidic granules, red = late apoptosis/necrosis, yellow = apoptotic cell, and orange = vacuoles.

3.6.2 Annexin-V binding to phosphatidylserine in HEK293 cells

Untreated HEK293 cells are shown in panel a and b (Figure 3.22). Cells appeared uniform in shape and size (Figure 3.22, panel a) and showed a negative signal for both the annexin-V conjugate and PI, indicating intact plasma membranes (Figure 3.22, panel b). Doxorubicin was used as the positive control (Figure 3.22, panel c and d). Cells treated with doxorubicin appeared granular and larger than untreated cells (Figure 3.22, panel c). All doxorubicin treated cells appeared red because of the innate fluorescence of doxorubicin (Figure 3.22, panel d). Doxorubicin fluorescence was indistinguishable from that of PI.

At 0.5 mg/mL of *G. lucidum* cells appeared granulated, smaller, and rounder than untreated cells (Figure 3.22, panel e). This is indicative of cellular stress. A positive signal for both annexin-V and PI was observed, this is indicative of late apoptosis or secondary necrosis (Figure 3.22, panel f). When apoptotic cells are not engulfed by cells of the immune system, they progress to secondary necrosis where cells lose their membrane integrity (Sachet *et al*., 2017). Annexin-V binding appeared granular, due to the membrane disintegration. At a lower concentration of *G. lucidum* (0.25 mg/mL) cells appeared rounded (Figure 3.22, panel g). A signal for both annexin-V and PI were observed, indicating the plasma membrane is compromised (Figure 3.22, panel g and h). In some cells within this treatment, Annexin-V binding occurred uniformly, indicating cells are in an early stage of apoptosis.

T. versicolour at a concentration of 0.5 mg/mL appeared larger and more granulated than untreated cells (Figure 3.22, panel i). Cells were positive for annexin-V binding. Annexin-V binding appears around the nucleus, this is indicative of an early stage of apoptosis. A minority of cells were positive for PI and annexin-V (Figure 3.22, panel i and j). This is indicative of secondary necrosis. At the lower concentration of *T. versicolour* (0.25 mg/mL) treatment, cells appeared rounded and clumped together (Figure 3.22, panel k). These cells showed binding to phosphatidylserine, but no PI crossed the membranes. Annexin-V binding occurred around the nucleus, indicating early apoptosis.

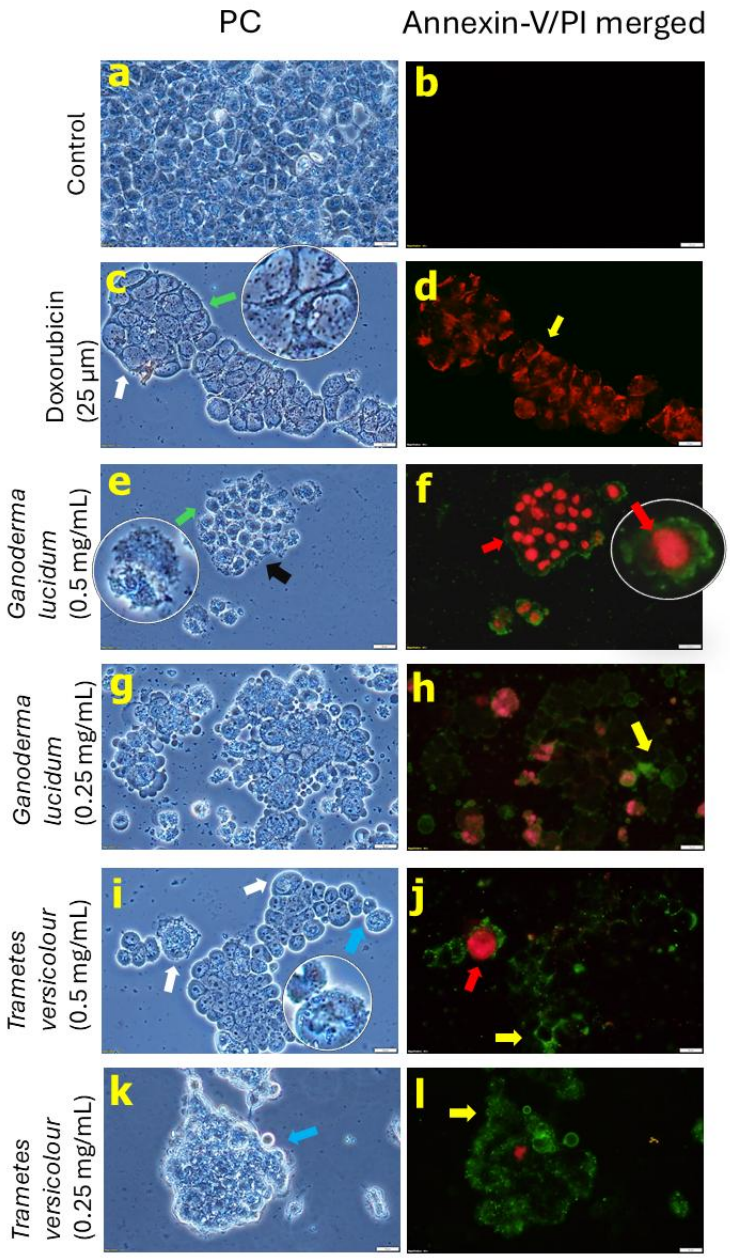


Figure 3.22 Representative photomicrographs showing binding of annexin-V to phosphatidylserine in HEK293 cells when treated with doxorubicin, *Ganoderma lucidum* and *Trametes versicolour*. HEK293 cells were treated with doxorubicin at 25 µM and *Trametes versicolour* and *Ganoderma lucidum* extracts at concentrations of 0.25 mg/mL and 0.5 mg/mL for 24 h. Panels a and b show untreated cells, panel c and d show the effect of doxorubicin, panels e and f show the effect of *Ganoderma lucidum* at 0.5 mg/mL, panels g and h show the effect of *Ganoderma lucidum* at 0.25 mg/mL, panels i an j show the effect of *Trametes versicolour* at 0.5 mg/mL, and panels k and l show the effect of *Trametes versicolour* at 0.25 mg/mL. An Olympus BX41 microscope was used to observe cells and the Olympus DP72 camera was used to capture images (Magnification: 400x; scalebar: 20µm). LEGEND: PC= phase contrast, PI= propidium iodide. Arrows: green = granules, white = enlarged cell, blue = rounded cell, red = late apoptosis/necrosis, yellow = apoptotic cell, and black = cellular shrinkage. Results were obtained from three independent experiments (n=3).

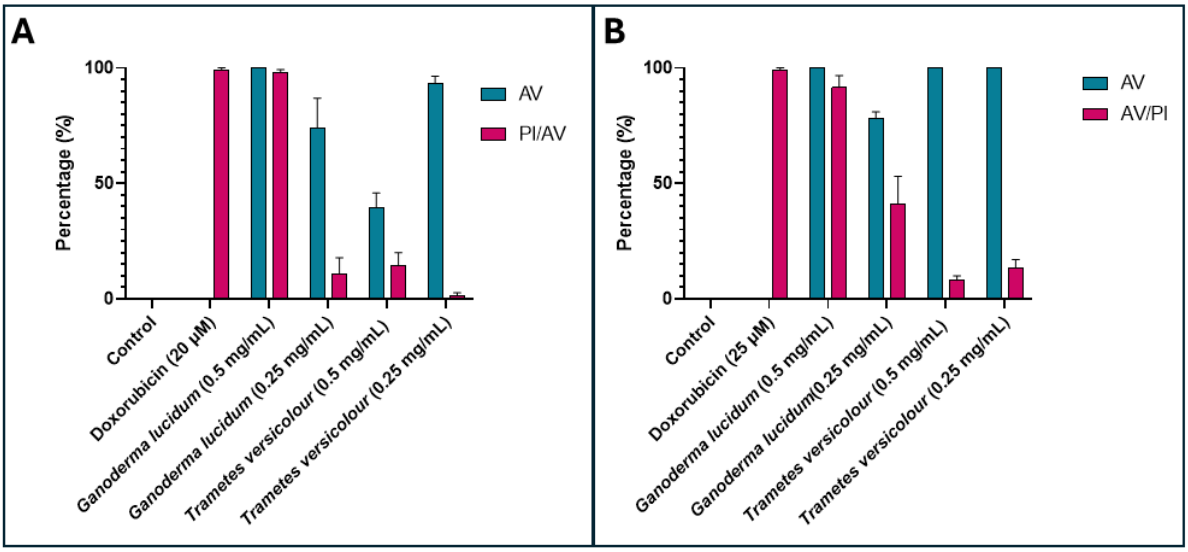


Figure 3.23 Average percentage of (A) A549 and (B) HEK293 cells positive for Annexin-V and PI after 24 h exposure to doxorubicin, *Ganoderma lucidum* and *Trametes versicolour*. Cells were treated with 0.5 mg/mL and 0.25 mg/mL of *Ganoderma lucidum* and *Trametes versicolour* and doxorubicin at a concentration equivalent to the IC_{80} value (20 µM in A549 cells and 25 µM in HEK293 cells). Each bar represents the mean and error bars represent the SEM. Results were obtained from three independent experiments.

The effects of *G. lucidum* and *T. versicolour* on phosphatidylserine translocation and membrane integrity varied between A549 and HEK293 cells (Figure 3.23). Untreated A549 and HEK293 cells showed no detectable AV or PI fluorescence, confirming the absence of apoptosis or membrane disintegration. Doxorubicin-treated cells showed no annexin-V binding, indicating a lack of phosphatidylserine externalization and the absence of apoptosis. All doxorubicin-treated cells appeared uniformly red. The fluorescence of PI could not be distinguished from the intrinsic fluorescence of doxorubicin, making it difficult to assess membrane integrity using PI staining alone.

At the highest concentration (0.5 mg/mL), *G. lucidum* induced near-complete phosphatidylserine externalization in both cell lines, with 100 ± 0% of cells positive for annexin-V. However, most A549 cells (97.99 ± 1.26%) were also PI-positive, indicating membrane disintegration and late apoptosis or secondary necrosis, compared to HEK293 cells (91.50 ± 5.27%), which retained membrane integrity (Figure 3.23 A, 3.25).

At the lower concentration (0.25 mg/mL), *G. lucidum* still caused significant phosphatidylserine translocation in both cell lines, with 74.03 ± 12.92% of A549 cells and 78.00 ± 3.00% of HEK293 cells being annexin-V-positive. However, the extent of membrane

permeabilization differed notably. In A549 cells, only 11.03 ± 6.81% were PI-positive, suggesting that a majority of cells were apoptotic. Conversely, 41.00 ± 12.00% of HEK293 cells were PI-positive, indicating a higher proportion undergoing late apoptosis or secondary necrosis at this concentration. Suggesting that while *G. lucidum* effectively induced phosphatidylserine externalization in both cell lines, its impact on membrane integrity was concentration- and cell type-dependent. At 0.25 mg/mL, A549 cells primarily underwent apoptosis without extensive membrane disruption, whereas HEK293 cells showed a higher proportion of membrane-compromised cells, indicative of late apoptosis or secondary necrosis. This suggests that HEK293 cells may be more susceptible to membrane permeabilization at lower concentrations of *G. lucidum*, potentially due to intrinsic differences in membrane stability or apoptotic regulation between the two cell lines.

Treatment with *T. versicolour* (0.5 mg/mL) had a differential effect between the two cell lines. In A549 cells, only 39.45 ± 6.44% stained positive for annexin-V, with 14.37 ± 5.67% PI-positive, indicating a more limited induction of apoptosis at 24 h. In contrast, all HEK293 cells (100 ± 0%) showed phosphatidylserine externalization, but with minimal membrane disintegration, as only 8.00 ± 2.00% were PI-positive. This suggests that while *T. versicolour* induced early apoptosis in HEK293 cells, it was poorly effective in promoting apoptosis in A549 cells (Figure 3.23).

At the lower concentration (0.25 mg/mL), *T. versicolour* induced high levels of phosphatidylserine translocation in both cell lines with 93.18 ± 3.28% of A549 cells and 100 ± 0% of HEK293 cells showing annexin-V binding. However, membrane integrity was intact, as indicated by the low percentage of PI-positive cells (1.56 ± 1.26% in A549 and 13.5 ± 3.5% in HEK293). This suggests that *T. versicolour* at lower concentrations predominantly induces early apoptosis rather than late apoptosis or necrosis in both cell lines at 24 h.

Overall, *G. lucidum* induced higher levels of membrane disintegration in A549 cells, whereas HEK293 cells appeared more sensitive to phosphatidylserine externalization, particularly in response to *T. versicolour*.

3.7 The activation of caspase-3/7 in cells treated with *G. lucidum* and *T. versicolour*

The CellEvent™ Caspase-3/7 Green Detection Reagent (Thermo-Fisher Scientific) was used in alive-cell assay to determine if caspase-3/7 was activated by doxorubicin, *G. lucidum* and *T. versicolour*. Cells were treated with doxorubicin at 20µM and *G. lucidum* and *T. versicolour* at 0.5 mg/mL and 0.25 mg/mL for 24 h (Chapter 2, Section 2.8). The effect of the treatments

on the expression of caspase-3/7 is presented below in Figure 3.24 (A549) and Figure 3.25 (HEK293). Phase-contrast images are indicated to determine the percentage of cells with active caspase-3/7.

3.7.1 The activation of caspase 3/7 in A549 cells after treatment with *G. lucidum* and *T. versicolour.*

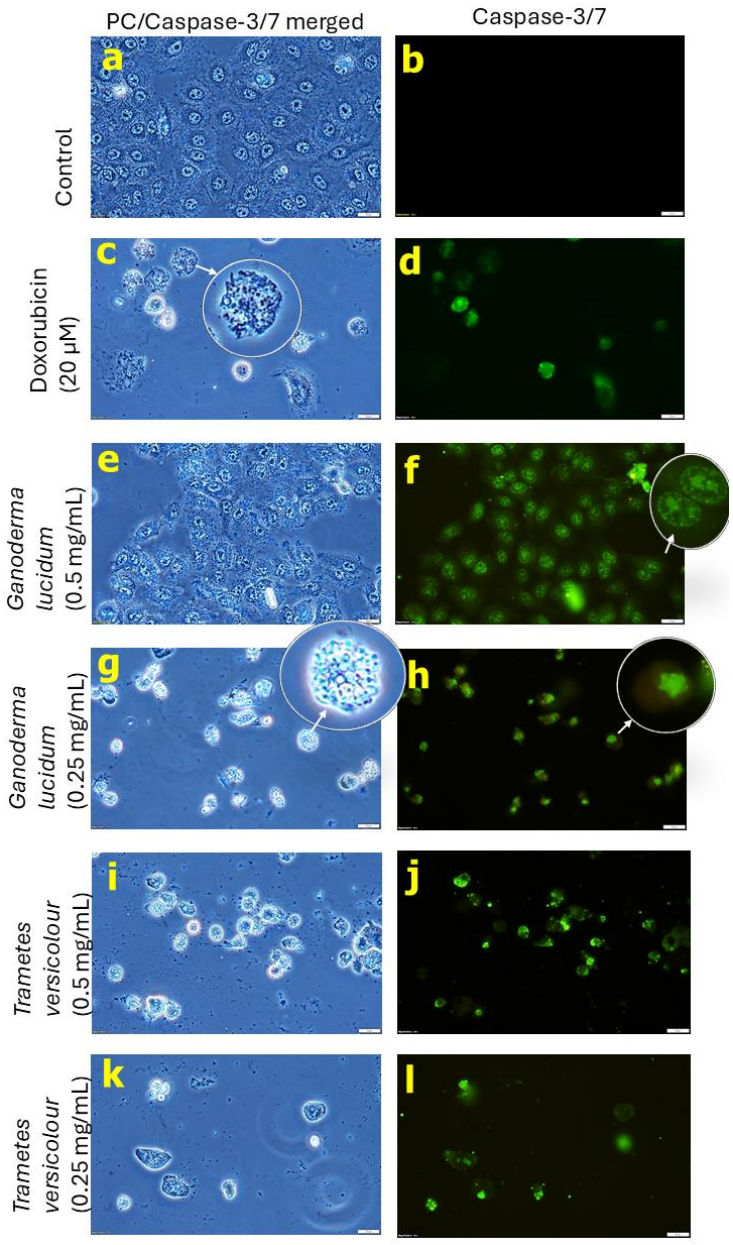


Figure 3.24 Representative photomicrographs showing the expression of Caspase-3/7 in A549 cells when treated with mushroom extracts and doxorubicin. A549 cells were treated with doxorubicin at concentrations equivalent to the IC_{80} values (20 µM) and *Ganoderma lucidum* and *Trametes versicolour* at concentrations of both 0.5 and 0.25 mg/mL. Cells were viewed with the Olympus BX41 microscope and images were captured with the DP72 digital camera (magnification: 400×, scalebar 20µm). Each experiment was done in triplicate.

Control cells appeared uniform in shape and size (Figure 3.24, panel a and b) with no fluorescence present. Doxorubicin treated cells appeared granulated, rounded with uneven membranes (Figure 3.24, panel c). Some cells in this treatment appeared smaller than the untreated cells (Figure 3.24, panel c). Doxorubicin treated cells had an increase in fluorescence compared to the untreated cell (Figure 3.24, panel d).

G. lucidum (0.5 mg/mL) treated A549 cells, had a significant increase in the number of cells with a fluorescence signal (100%) compared to the untreated cells (Figure 3.24, panel e-f). The lower concentration of *G. lucidum* (0.25 mg/mL) showed an increased fluorescence, compared to untreated cells, suggesting apoptosis (Figure 3.24, panel g-h). At both concentrations of *G. lucidum*, cells appeared granular. At the lower concentration (0.25 mg/mL), cells appeared vacuolated (Figure 3.24, panel g). Again, the fluorescence was located in the nucleus indicating apoptosis has occurred (Figure 3.24, panel h).

When A549 cells were treated with *T. versicolour* at 0.5 mg/mL, A549 appeared rounded and vacuolated (Figure 3.24, panel i). This treatment showed an increased number of fluorescent cells (100%) (Figure 3.24, panel i-j). When treated at 0.25 mg/mL of *T. versicolour,* there was an increase in fluorescence which is indicative of apoptosis (Figure 3.24, panel k – l). Cells appeared irregular in shape and size with some cells larger than the untreated cells while others were smaller (Figure 3.24, panel k).

Untreated cells showed the absence of caspase-3/7 activation in A549 cells. Doxorubicin treatment induced activation in 41 ± 1% of A549 cells (Figure 3.25). Treatment with *G. lucidum* at 0.5 mg/mL and 0.25 mg/mL, *and T. versicolour* at 0.5 mg/mL resulted in activation in 99.0 ± 1.0 % of cells, while *T. versicolour* at 0.25 mg/mL induced activation in 93.0 ± 7.0 %. Doxorubicin treatment resulted in the lowest percentage of caspase-3/7 activation, while *G. lucidum* induced the highest (Figure 3.25).

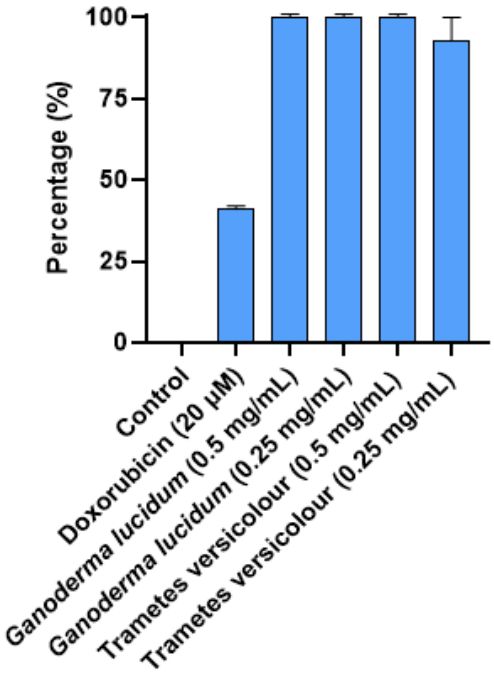


Figure 3.25 The average percentages of A549 cells with caspase-3/7 activity. A549 cells were treated with doxorubicin (20 µM), and *Ganoderma lucidum* and *Trametes versicolour* at both 0.5 mg/mL and 0.25 mg/mL. Error bars represent the SEM and was calculated from three independent experiments.

3.7.2 The activation of caspase-3/7 in HEK293 cells treated with *G. lucidum* and *T. versicolour*.

Phase contrast images showed that untreated cells were granular, which is normal for HEK293 cells (Figure 3.26, panel a). Fluorescence was not detected which indicates the absence of caspase-3/7 activity (Figure 3.26, panel b). Doxorubicin was used as the positive control at a concentration of 20 µM (Figure 3.26, panel c-d). Cells appeared larger than untreated cells as observed by phase contrast (Figure 3.26, panel c) and the green, fluorescent signal indicates cells with active caspase-3/7 (Figure 3.26, panel d). An increase (100%) in cells with fluorescent activity was present, indicating increased caspase-3/7 activity (Figure 3.26, panel d).

G. lucidum treated HEK293 cells appeared rounded and smaller than untreated cells at both concentrations (0.5 mg/mL and 0.25 mg/mL) with an increase of cells with a green, fluorescent signal (Figure 3.26, panel e and f). The fluorescent intensity appeared to be more intense in the 0.5 mg/mL *G. lucidum* treatment compared to the 0.25 mg/mL *G. lucidum* treatment (Figure 3.26, panel f and h).

T. versicolour at a concentration of 0.5 mg/mL caused HEK293 cells to appear vacuolated (Figure 3.26, panel i). There was no fluorescence detected after treatment with *T. versicolour* at 0.5 mg/mL and 0.25 mg/mL. This indicates the absence of caspase-3/7 activity. Doxorubicin and *G. lucidum* caused caspase activation in HEK293 cells, whereas *T. versicolour* did not.

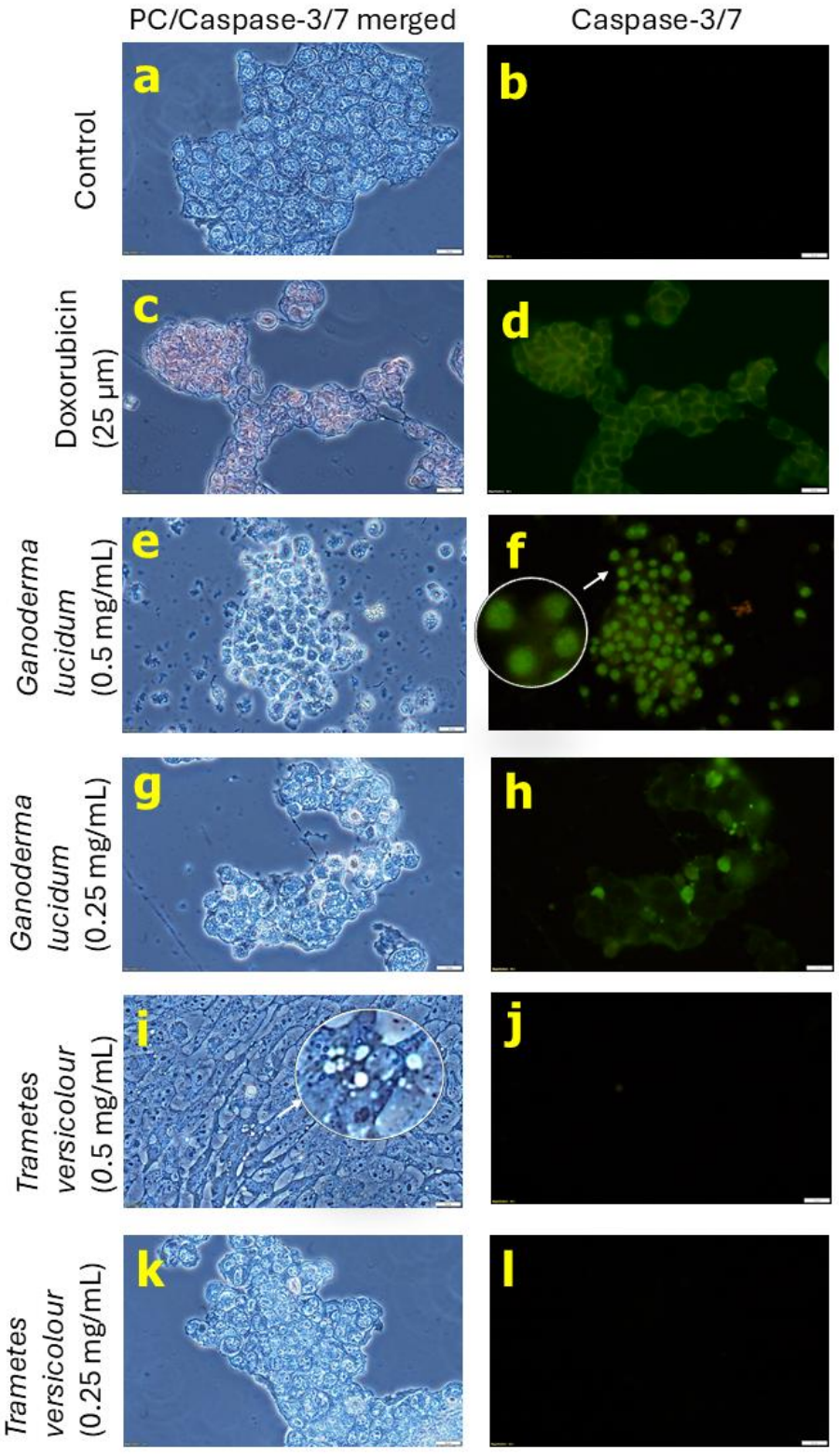


Figure 3.26 Representative photomicrographs showing the expression of Caspase-3/7 on HEK293 cells when treated with mushroom extracts and doxorubicin. HEK293 cells were treated with doxorubicin at concentrations equivalent to the IC_{80} values (25 µM) and *Ganoderma lucidum* and *Trametes versicolour* at concentrations of 0.5 and 0.25 mg/mL. Cells were viewed with the Olympus BX41 microscope and images were captured with the DP72 digital camera (magnification: 400×, scalebar 20µm).

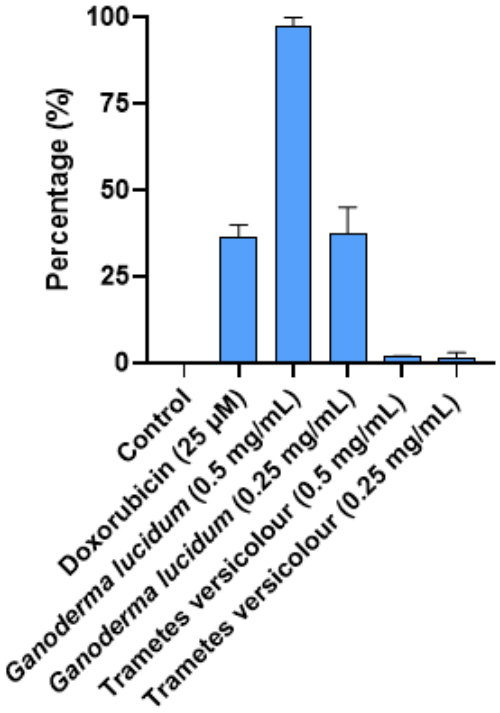


Figure 3.27 The average percentages of HEK293 cells with caspase-3/7 activity. HEK293 cells were treated with doxorubicin (25 µM), and *Ganoderma lucidum* and *Trametes versicolour* at both 0.5 mg/mL and 0.25 mg/mL. Error bars represent the SEM and was calculated from three independent experiments.

In HEK293 cells, untreated controls had no caspase-3/7 activity. Doxorubicin treatment led to activation in 36.5 ± 3.5 % of cells. *G. lucidum* at 0.5 mg/mL induced the highest caspase activation (97.5 ± 2.5 %), while 0.25 mg/mL *G. lucidum* treatment caused activation in 37.5 ± 7.5 % of cells. *T. versicolour* induced the lowest levels of caspase activation, with 1.9 ± 0.1 % and 1.5 ± 1.5 % of cells at 0.5 mg/mL and 0.25 mg/mL, respectively (Figure 3.27).

3.8 Determination of the effect of reactive oxygen species level caused by *G. lucidum* and *T. versicolour* treatment

A549 and HEK293 cells were treated with doxorubicin at concentrations equivalent to their IC_{80} values and *G. lucidum* and *T. versicolour* at both 0.5 mg/mL and 0.25 mg/mL for 4 h as described in Chapter 2, Section 2.10. The CellROX™ Deep Red Reagent (ThermoFisher Scientific, Invitrogen), is non-fluorescent in the reduced state and upon oxidation by ROS,

becomes fluorescent with an absorption/emission maximum of ~644/665 nm. The detection of ROS is shown in Section 3.8.1 (A549 cells) and 3.8.2 (HEK293 cells).

3.8.1 Reactive oxygen species levels in A549 cells treated with *G. lucidum* and *T. versicolour*

Figure 3.28 shows the presence of reactive oxygen species in A549 cells when treated with doxorubicin, *G. lucidum* and *T. versicolour*. Doxorubicin was used as the positive control. Cells were treated with doxorubicin at concentrations equivalent to the IC_{80} values (20 μM). *G. lucidum* and *T. versicolour* were used to treat cells at two concentrations, i.e. 0.5 mg/mL and 0.25 mg/mL. Control cells appeared uniform in shape and size (Figure 3.28, panel a). There was no fluorescent signal present, suggesting the absence of basal ROS levels under unstressed conditions (Figure 3.28, panel b). When treated with doxorubicin, A549 cells appeared granular and irregular in shape and size (Figure 3.28, panel c). Red, bright fluorescence was observed in the cytoplasm of cells, as granules (Figure 3.28, panel d). Doxorubicin has an innate red fluorescence, but the granular appearance of the red fluorescence indicates increased ROS formation.

G. lucidum (0.5 mg/mL) caused cells to appear irregular in shape and size (Figure 3.28, panel e). Red fluorescence was detected in *G. lucidum* (0.5 mg/mL) treated cells (Figure 3.28, panel f). At the lower concentration of *G. lucidum* (0.25 mg/mL), cells appeared granular (Figure 3.28, panel g). Increased ROS levels were detected at both concentrations of *G. lucidum* (Figure 3.28, panel f and h). *T. versicolour* treated cells, at both 0.5 mg/mL and 0.25 mg/mL, appeared granular and showed an increase in the fluorescent signal, indicating elevated ROS levels (Figure 3.28, panel j and l).

T. versicolour had an increased formation of ROS compared to *G. lucidum*. ROS fluorescence was primarily located in the cytoplasm. Some nuclear staining was observed. This is consistent the cellular response for oxidative stress. The granular appearance of the fluorescent signal suggests localized ROS formation within cellular organelles, such as mitochondria, lysosomes, or the endoplasmic reticulum, which are primary sites of ROS generation and oxidative damage.

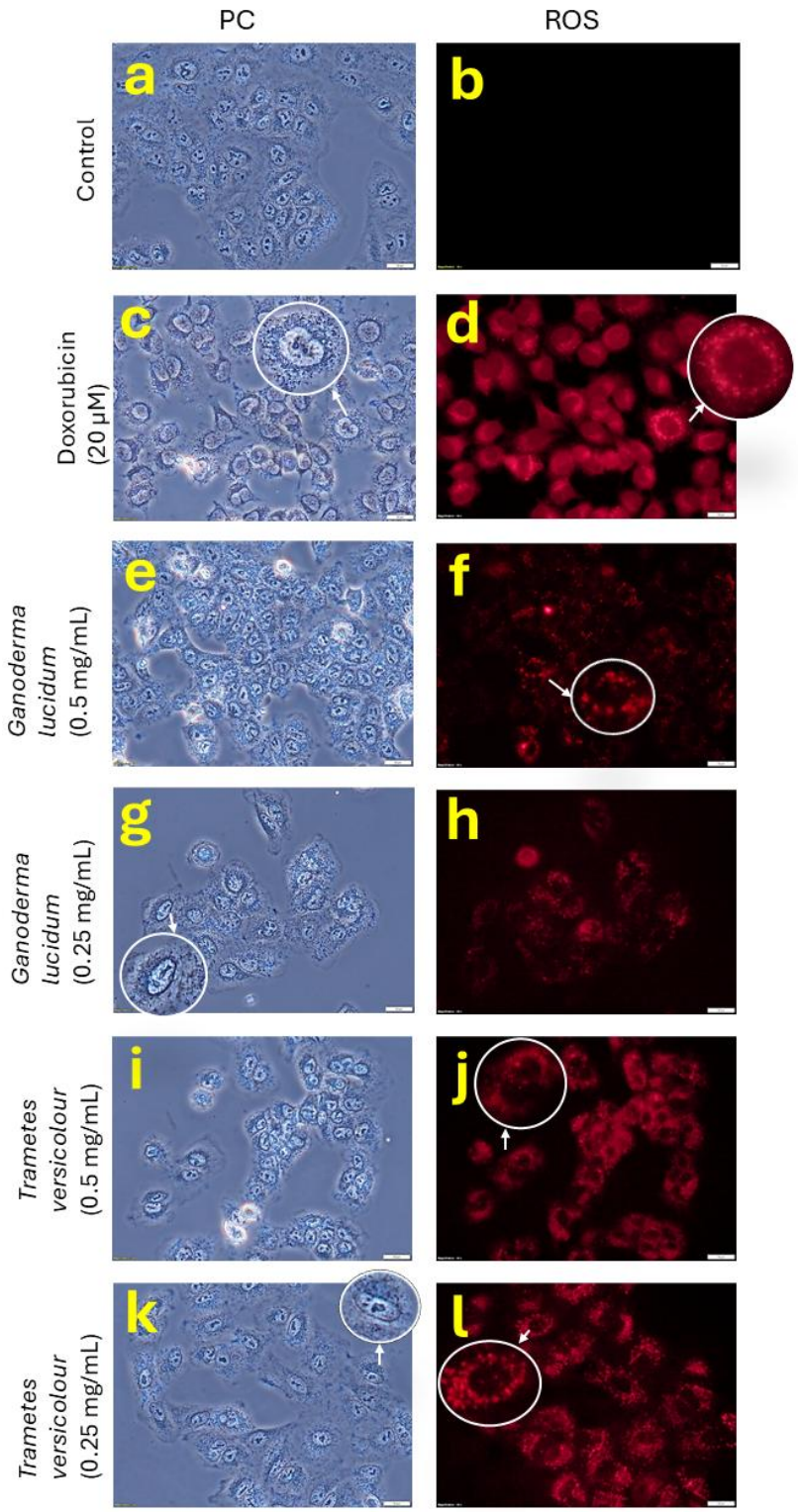


Figure 3.28 Photomicrographs showing the detection of reactive oxygen species in A549 cells when treated with doxorubicin, *Trametes versicolour* and *Ganoderma lucidum* for 4 h. Doxorubicin was used as the positive control. A549 cells were treated at a concentration of 20 µM. *Trametes versicolour* and *Ganoderma lucidum* were treated at both 0.5 mg/mL and 0.25 mg/mL for 4 h.

3.8.2 Reactive oxygen species levels in HEK293 cells treated with *G. lucidum* and *T. versicolour*.

Figure 3.29 shows the representative photomicrographs showing the presence or absence of ROS in HEK293 cells when treated with doxorubicin, *G. lucidum* and *T. versicolour* at 0.5 mg/mL. Untreated cells are shown in panel a (Figure 3.29). These cells appear uniform in shape and size (Figure 3.29, panel a). There was no fluorescent signal detected, indicating no basal ROS level under unstressed condition in HEK293 cells (Figure 3.29, panel b).

Doxorubicin was used the positive control. HEK293 cells were treated with doxorubicin at concentrations equivalent to the IC_{80} values (25 µM). Doxorubicin treated cells appeared rounded and smaller than untreated cells (Figure 3.29, panel c). There was an increase ROS formation as seen by the increase in fluorescence, indicating elevated ROS levels (Figure 3.29, panel d). The granular appearance of the fluorescence signal indicates organelle-specific ROS formation, particularly in mitochondria, lysosomes, and the endoplasmic reticulum, which are crucial sites of oxidative stress.

G. lucidum (0.5 mg/mL) treated HEK293 cells appeared rounded and irregular in comparison to untreated cells (Figure 3.29, panel e). An increased fluorescent signal indicative of increased ROS was observed in panel f (Figure 3.29). *G. lucidum* at a concentration of 0.5 mg/mL had an elevated ROS level (Figure 3.29, panel f). At the lower concentration of *G. lucidum* (0.25 mg/mL), cells in panel g (Figure 3.29) showed changes consistent with cellular stress. Cells were rounded and irregular in shape and size. However, no fluorescent signal was present, indicating no increased ROS level (Figure 3.29, panel h). *T. versicolour* at 0.5 mg/mL and 0.25 mg/mL caused cells to lose normal morphology (Figure 3.29, panel i and k) and showed an increased fluorescence and an increase basal ROS level (Figure 3.29, panel j and l).

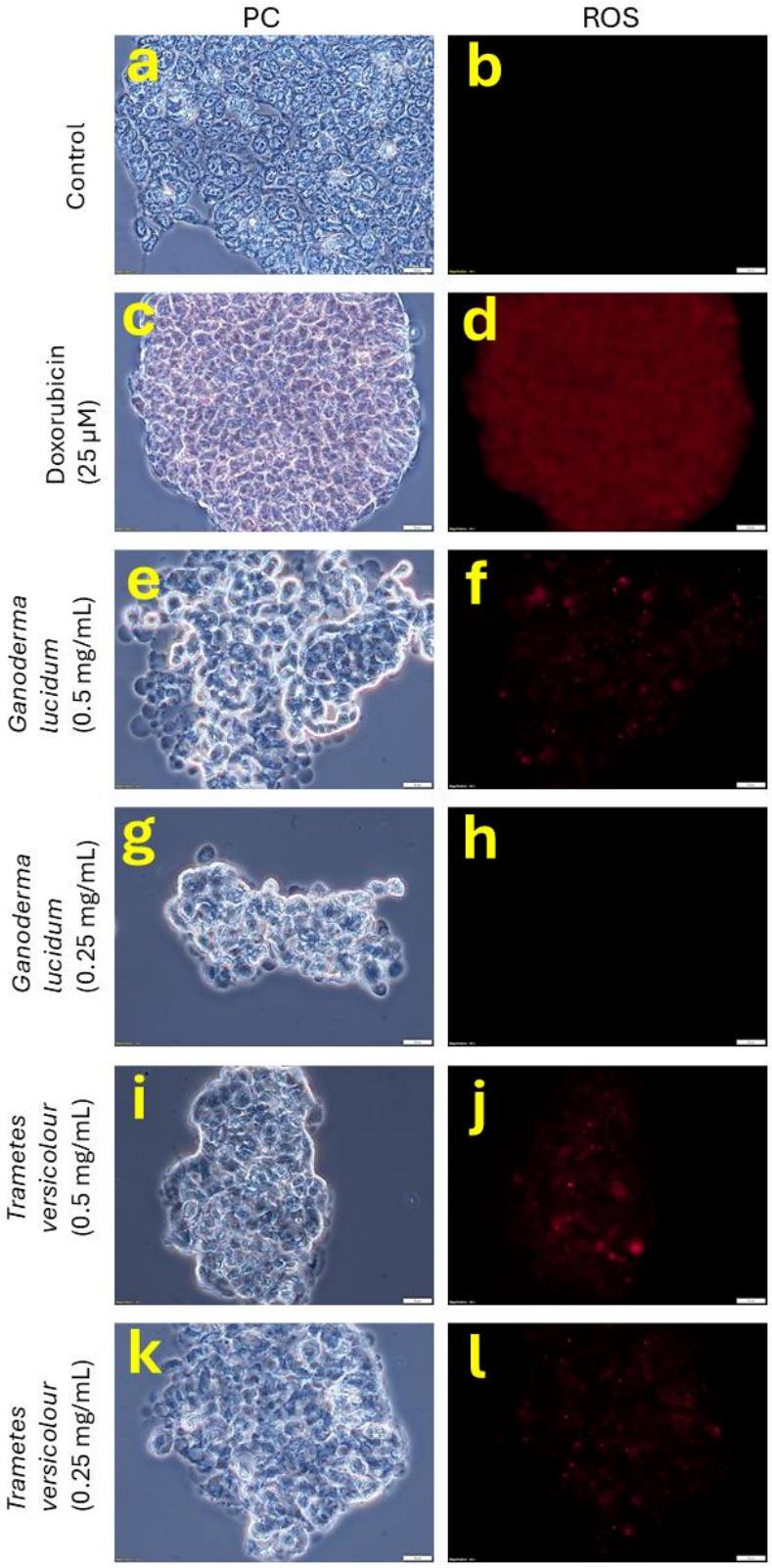


Figure 3.29 Representative photomicrographs showing the detection of reactive oxygen species in HEK293 cells when treated with doxorubicin, *Ganoderma lucidum* and *Trametes versicolour*. Doxorubicin was used as the positive control. HEK293 cells were treated at a concentration of 20 µM. *Ganoderma lucidum* and *Trametes versicolour* were used at both 0.5 mg/mL and 0.25 mg/mL for 4 h.

3.9 The detection of P-glycoprotein levels in A549 and HEK293 cells

The expression of P-glycoprotein in A549 and HEK293 cells following treatment with doxorubicin, *G. lucidum*, and *T. versicolour* was assessed using immunofluorescence, as described in Chapter 2, Section 2.10. Both cell lines were treated with doxorubicin at concentrations equivalent to the IC_{80} values, while *G. lucidum* and *T. versicolour* were used at concentrations of 0.5 mg/mL for 12 h.

The effect of doxorubicin, *G. lucidum* and *T. versicolour* on P-glycoprotein expression in A549 and HEK293 cells showed no green fluorescence signal, indicating the absence of P-glycoprotein expression despite the usual morphological changes seen previously (Appendix B and C).

CHAPTER 4: DISCUSSION

4.1 Assessment of information provided on the labels of commercial preparations of mushrooms

The labelling of commercially available mushroom products has inconsistencies, regulatory gaps, and misleading claims, posing potential risks to consumers (Risoli *et al*., 2023). Labelling transparency is crucial for consumer safety, yet 40% of products fail to disclose their manufacturing origin, complicating traceability and quality assurance. More than half (53.33%) lack dosing instructions, which may result in improper use or ineffective dosing. Ingredient disclosure is incomplete, with only 86.67% listing components, a concern for consumers with allergies or dietary restrictions. A study by Cohen *et al*. (2023) tested 57 performance-enhancing botanical ingredients and found that 89% of them did not accurately list the ingredients and 12% contained at least one ingredient which is prohibited by the FDA (Cohen *et al*., 2023). Additionally, 53.33% of products do not display expiration dates, increasing the risk of degraded or ineffective products. The absence of batch numbers on 46.67% of labels further hampers quality control and recall efforts. Risolli *et al*. (2023) found that 68% of analysed mushroom supplements had DNA sequences mismatched to the species listen on the labels. Many supplements labelled as *G. lucidum* contained Ganoderma *resinaceum* or *Ganoderma sichuanense*.

Only 33.33% of products include warning statements, and just 6.67% specify contraindications, raising concerns about consumer awareness of potential health risks. The generic warning "Use with caution during pregnancy and lactation" (33.33%) lacks specificity and fails to reflect current scientific evidence on potential drug interactions. Without explicit contraindications, consumers with pre-existing conditions or those on medications may unknowingly expose themselves to adverse effects.

While 53.33% of products include disclaimers stating they are not evaluated by health authorities, these same products frequently make unsubstantiated health claims. The statement advising consultation with a "complementary health practitioner" during pregnancy is particularly problematic, as it lacks clarity on professional qualifications and could lead to misleading or unsafe guidance.

Over half (53.33%) of products make unsupported health claims, including "immune support" (26.67%), "antioxidative properties" (26.67%), and "cancer support" (20%), despite insufficient scientific evidence to substantiate these claims. The claim of "cancer support" is

particularly concerning, as it may mislead consumers into believing these products have clinically proven anticancer effects, potentially discouraging them from seeking evidence-based medical treatment. Furthermore, one product included a QR code intended to provide lab results, but scanning the code resulted in an error message, undermining transparency and consumer trust.

To protect consumers, regulatory authorities must enforce stricter labelling standards, requiring clear ingredient lists, dosing instructions, batch numbers, and evidence-based health claims. Disclaimers should be precise and prevent misleading statements, and digital verification tools such as QR codes must be functional to ensure transparency. Without robust regulatory oversight, consumers remain vulnerable to misinformation and potential health risks. Regulators should be held accountable on reported infractions.

4.2 Extract Preparation and Solubility Considerations

The dual extraction method, using a 1:1 methanol and dichloromethane solvent system, caused different residue yields across the examined mushroom species. Notably, *I. obliquus* showed a higher extraction yield (5.4%) compared to *G. lucidum* (1.65%) and *T. versicolour* (4.45%). These variations may be attributed to differences in the composition of bioactive compounds present in each species.

Emerging from this analysis is the concern of solubility of the extracts in different solvents. While *I. obliquus* was insoluble in ethanol and DMSO, *G. lucidum* and *T. versicolour* were insoluble in water. This observation has direct implications for supplement consumption, as most mushroom supplements are ingested with water. Therefore, formulation strategies should consider solubility properties to enhance the absorption and therapeutic potential of these extracts.

The analysis of tincture residues further supported these findings, with *I. obliquus* yielding the highest residue weight (0.06 g per 10 mL), followed by *G. lucidum* (0.05 g) and *T. versicolour* (0.08 g). These residues were dissolved in the same solvents as the dry extracts, ensuring uniform extract concentrations (20 mg/mL). However, the storage stability of these extracts requires further investigation, as variations in temperature and solvent evaporation could impact their long-term potency.

4.3 Consistency of Mushroom Tincture across 3 batches

The FTIR analysis of three batches of *G. lucidum* and *T. versicolour* tinctures from the same manufacturer showed no significant differences in their chemical compositions. The spectra for *G. lucidum* tinctures showed minimal variation, with only small peak shifts observed in the 2000–3000 cm^{-1} region and fingerprint region (<1500 cm^{-1}). Statistical analysis using one-way ANOVA confirmed that these differences were not statistically significant, indicating a high level of batch-to-batch consistency.

In contrast, the FTIR spectra of *T. versicolour* tinctures showed larger peak shifts and less spectral overlap, indicating greater variability in chemical composition between batches. However, statistical analysis still found no significant differences in wavenumber values or percentage transmittance. These findings indicate that *G. lucidum* and *T. versicolour* tinctures maintain a uniform chemical profile.

4.4 Extract stability under different storage conditions

The stability of *T. versicolour* and *G. lucidum* extracts under different storage conditions (room temperature, -18°C, and 4°C) was evaluated over a period of five weeks using FTIR spectroscopy. The spectral changes observed provide insight into the molecular stability and potential degradation pathways of these extracts.

At room temperature, both *T. versicolour* and *G. lucidum* extracts showed notable changes in their FTIR spectra, particularly in the fingerprint region (650–1500 cm^{-1}). For *T. versicolour*, the emergence of peaks at week 5 indicates chemical modifications, such as a reduction in C-Cl bonds and increases in aromatic ether and amine groups. The increased %T at key wavenumbers (e.g., 1174 cm^{-1}, 1240 cm^{-1}, and 1722 cm^{-1}) implies the degradation of corresponding functional groups, i.e. cyanate, aromatic ethers and carboxylic acids (Nandiyando *et al*., 2019).

For *G. lucidum*, the upward spectral shift observed at week 5 is indicative of significant instability, corroborated by the visual and olfactory signs of fermentation. The broad changes in the fingerprint region and high %T values for certain wavenumbers indicate the loss of molecular integrity and the formation of volatile degradation products.

Storage at -18°C resulted in relatively better preservation of the extracts, as evidenced by fewer changes in the spectra during weeks 1–4. However, by week 5, both *T. versicolour* and *G. lucidum* showed spectral alterations indicative of degradation.

For *T. versicolour*, increased %T in the fingerprint region and the emergence of new peaks indicate bond cleavage and the loss of certain molecular structures, such as carboxylic acids and sulfonates. In *G. lucidum*, the week 5 spectrum showed an upward shift, reduced intensity in zone IV (single bonds), and high %T values for most wavenumbers. The observed instability may be attributed to incomplete freezing or structural changes due to the crystallization of water and other components in the extract.

At 4℃, the FTIR profiles of both *T. versicolour* and *G. lucidum* extracts showed the least variation over the 5-week period. This indicates that refrigeration is the most effective storage condition for preserving the molecular integrity of the extracts. The overlapping spectra from weeks 1–5 with week 0 indicates minimal chemical changes. The stability at this temperature may be due to slowed chemical reaction rates and reduced microbial activity, which are sufficient to maintain the functional groups present in the extracts.

4.4.1 Summary

The comparative analysis of storage conditions highlights the critical role of temperature in preserving the stability of bioactive compounds in mushroom extracts. The instability observed at room temperature and -18℃ indicates that extreme conditions, either too warm or too cold, promote degradation through different mechanisms, such as oxidation, hydrolysis, or crystallization. Refrigeration at 4℃ appears to offer the optimal balance, minimizing molecular and functional group changes over time.

This study emphasizes the need for careful storage considerations when handling mushroom extracts, particularly for pharmaceutical or nutraceutical applications. The findings also underscore the utility of FTIR spectroscopy as a rapid and non-destructive tool for monitoring extract stability and molecular changes over time.

4.5 The cytotoxic effects of chemotherapeutic drugs and mushroom extracts towards the A549 and HEK293 cell lines.

Three anticancer drugs were selected as potential positive controls for this study. Those drugs were doxorubicin, camptothecin and irinotecan. Additionally, three mushroom species were screened. These were *G. lucidum*, *T. versicolour* and *I. obliquus*. The results highlight differences in drug efficacy, selectivity, and time-dependent responses.

4.5.1 Doxorubicin

Doxorubicin was the most active chemotherapeutic drug and was selected as the positive control for this study. Doxorubicin is an antibiotic derived from *Streptomyces peucetius* bacterium. Doxorubicin has a wide range of indications and has been used as a chemotherapeutic agent since the 1960's (Johnson-Arbor and Dubey, 2023). It is commonly used in solid tumours in both adult and paediatric patients (Johnson-Arbor and Dubey, 2023). The mechanism of action of doxorubicin is the intercalation of doxorubicin with DNA base pairs, the intercalation causes DNA stands to break which leads to the inhibition of DNA and RNA synthesis. Further, doxorubicin inhibits topoisomerase II which induces DNA damage and apoptosis (Johnson-Arbor and Dubey, 2023).

Doxorubicin was active in A549 cells and had an IC_{50} value of 9.85 ± 1.56 µM at 24 h and 5.51 ± 0.93 µM at 48 h. Gordon *et al*. (2022) found the IC_{50} value to be 7.12 ± 0.34 µM at 48 h using an MTT assay. For comparison with the IC_{50} values of the mushroom extracts, the IC_{50} value of doxorubicin is also given in units of mg/mL. At 24 h it was 0.005 ± 0.001 mg/mL and 0.003 ± 0.001 mg/mL at 48 h.

HEK293 cells showed higher resistance at 24 h (IC_{50}: 18.62 ± 1.84 µM) but became more sensitive by 48 h (IC_{50}: 4.79 ± 0.51 µM). The difference at 24 h indicates a greater initial tolerance in non-cancerous cells, though sensitivity converged over time. Literature reports a substantially lower IC_{50} in HEK293 cells (0.24 ± 0.12 µM at 48 h; Lima *et al*., 2023). The substantial discrepancy between these values may be attributed to differences in experimental conditions, assay methodologies, cell confluency, and media composition (Muelas *et al*., 2018; Selenius *et al*., 2019). Additionally, variations in cell passage number and genetic drift between HEK293 cell lines could influence drug sensitivity (Riss *et al*., 2021).

4.5.2 *G. lucidum*

G. lucidum, a member of the Ganodermataceae family within the Basidiomycetes, is an edible mushroom that has been widely used in traditional Eastern medicine for its purported medicinal properties (Jin *et al*., 2016). Its bioactive compounds primarily include polysaccharides, such as β-glucans, and triterpenoids, which are believed to contribute to its immunomodulatory and anticancer effects (Jin *et al*., 2016).

In this study, *G. lucidum* showed cytotoxic activity against A549 cells, with IC_{50} values of 0.255 ± 0.022 mg/mL at 24 h and 0.246 ± 0.049 mg/mL at 48 h. The stability of these IC_{50} values over time indicates a sustained cytotoxic effect. Previous studies have reported varying IC_{50} values for *G. lucidum* extracts, likely due to differences in extraction methods and

compound composition. For instance, triterpene-rich extracts, through a supercritical CO_2 fluid extraction method, of *G. lucidum* showed an IC_{50} of 24.63 µg/mL (Feng *et al*., 2013), while a lanostane triterpenoid methanolic isolated from *G. lucidum* showed an IC_{50} of 15.6 µg/mL (Min *et al*., 2000). These discrepancies highlight not only the influence of extraction technique, but also the broader issue of phytomedicine variability i.e. the lack of quality control and variability of source material. The biological activity of fungal extracts can be significantly affected by factors such as the source of the material (wild vs. cultivated), quality and age of the fruiting bodies, and seasonal or environmental conditions during growth and harvesting (Gilbert and Favre-Godal, 2017; Sakurai *et al*., 2011). These variables impact the concentration and diversity of bioactive compounds in the final extract, making reproducibility and standardization in natural product research particularly challenging. As such, variations in IC_{50} values between studies are expected and emphasize the need for better quality control and transparency in phytochemical sourcing and preparation (World Health Organization, 2007).

In HEK293 cells, at 24 h, the IC_{50} value of *G. lucidum* was 0.591 ± 0.101 mg/mL, decreasing to 0.151 ± 0.008 mg/mL at 48 h. The higher IC_{50} at 24 h in HEK293 cells shows selective activity against cancerous cells. However, the increased cytotoxicity at 48 h in HEK293 cells may indicate a delayed metabolic response or compound accumulation. There is limited data on the cytotoxic effects of *G. lucidum* in HEK293 cells, making direct comparisons with other studies challenging. Research on normal human dermal fibroblast cells has shown that *G. lucidum* extracts generally had low toxicity, further supporting the idea of preferential activity against malignant cells (Lin *et al.*, 2003). However, without more studies specifically evaluating *G. lucidum* in HEK293 cells, definitive conclusions regarding its selectivity and mechanism of action remain uncertain.

4.5.3 *T. versicolour*

T. versicolour, a member of the *Polyporaceae* family, contains several bioactive polysaccharides, including β-glucans, polysaccharide krestin, and polysaccharide peptin, which are believed to contribute to its therapeutic properties (Friedman, 2016).

In A549 cells, the IC_{50} value of *T. versicolour* was 0.304 ± 0.007 mg/mL at 24 h and 0.613 ± 0.040 mg/mL at 48 h. The increase in IC_{50} at 48 h shows a time-dependent reduction in cytotoxic potency, potentially due to cellular adaptation, detoxification mechanisms, or extract instability. Previous studies have reported varying IC_{50} values for *T. versicolour*, likely due to differences in extraction techniques and experimental conditions (Muelas *et al*., 2018; Selenius

et al., 2019). The anticancer activity of *T. versicolour* has been observed at concentrations below 1 mg/mL (Pawlikowska *et al.*, 2020). However, Jędrzejewski *et al.* (2025) reported an IC_{50} value exceeding 250 µg/mL in A549 cells, indicating lower cytotoxicity. Their study also found *T. versicolour* to be more effective in HeLa and MCF-7 cells, showing that its cytotoxic effects may be cell line-dependent (Jędrzejewski *et al.*, 2025). Both studies (i.e. Pawlikowska *et al*. and Jedrzejewski *et al*.) obtained extracts from an outside company and did not provide details of the extraction methods. These variations underscore the need for standardized methodologies to accurately assess the cytotoxic potential of *T. versicolour* across different cellular models.

T. versicolour showed a time-dependent cytotoxic response similar to *G. lucidum*, with lower IC_{50} values in HEK293 cells at 24 h (0.880 ± 0.380 mg/mL) and increased IC_{50} values at 48 h (0.282 ± 0.052 mg/mL). The delayed increase in cytotoxicity at 48 h may be attributed to the accumulation of bioactive compounds, prolonged cellular stress, or metabolic activation within HEK293 cells.

4.5.4 *I. obliquus*

I. obliquus is a parasitic fungus that colonizes trees and is recognized for its diverse bioactive constituents, including polysaccharides, polyphenols, triterpenoids, β-glucans, and melanin (Arata *et al*., 2016; Lu *et al*., 2021). These compounds have been associated with various therapeutic properties, including potential anticancer effects. *I. obliquus* had minimal cytotoxicity in both cell lines, with A549 cell viability remaining high at 82% (0.5 mg/mL) and 98% (0.25 mg/mL) at 24 h. In HEK293 cells, cytotoxic effects were similarly weak. Previous studies have reported IC_{50} values between 1.27 and 1.80 mg/mL, with some aqueous extracts showing greater potency with an IC_{50} value of 0.02 mg/mL at 48 h (Zhong *et al*., 2009). The substantial variation in reported values highlights the impact of extraction methods on bioactivity.

4.5.5 Summary

Doxorubicin showed the highest cytotoxicity in both cell lines, with delayed effects in HEK293 cells at 24 h but comparable sensitivity at 48 h. The fungal extracts were generally more cytotoxic in A549 cells than in HEK293 cells at 24 h, indicating some selectivity towards cancer cells. However, cytotoxicity increased in HEK293 cells at 48 h treatments, indicating a delayed response. This may be attributed to slower uptake, processing or cellular responses to the fungal extracts.

Among the fungal extracts, *G. lucidum* maintained consistent cytotoxicity over time, whereas *T. versicolour* showed reduced potency in A549 cells but increased cytotoxicity in HEK293 cells at 48 h. *I. obliquus* had the weakest cytotoxic effects overall. These findings highlight the importance of time-dependent responses and selectivity in evaluating potential therapeutic agents.

4.6 The effect of mushroom extracts on doxorubicin efficacy in A549 and HEK293 cells.

The integration of conventional cancer therapies with natural complementary medicine has gained increasing attention due to the potential for enhanced therapeutic efficacy and reduced side effects. CAMs, including dietary supplements such as herbal extracts, has been widely used alongside chemotherapy, yet the interactions between these natural products and conventional drugs remain largely unexplored (Ventola, 2010). One of the main concerns with combining CAM with standard treatments is the lack of evidence-based data on potential drug interactions, which could lead to altered drug efficacy or unexpected toxicity (Ventola, 2010).

This study investigates the impact of mushroom extracts on the efficacy of doxorubicin in A549 cancer cells, while also assessing its effects on HEK293 cells as a non-cancerous control. By examining these interactions, the research aims to provide critical insights into the safety and efficacy of combining conventional chemotherapeutic agents with natural compounds. Understanding these interactions is crucial for developing more effective and safer treatment strategies, ensuring that complementary therapies do not inadvertently compromise standard treatments (Jiang *et al*., 2010).

4.6.1 *G. lucidum*

At 24 h, *G. lucidum* did not significantly alter doxorubicin's cytotoxic effects in A549 cells. However, after 48 h, doxorubicin was less effective in A549 cells. In contrast, HEK293 cells showed increased sensitivity to doxorubicin in the presence of *G. lucidum* at both time points, with a nearly 10-fold increase in potency at 24 h and a 1.7-fold increase at 48 h.

The literature on *G. lucidum*'s effects in cancer models is limited, with Yue *et al*. (2008) reporting that *G. lucidum* triterpenes enhanced doxorubicin-induced oxidative stress and apoptosis in HeLa cells. If similar mechanisms are at play, the increased potency observed in HEK293 cells may result from enhanced oxidative stress or disrupted repair pathways. This indicates a potential risk of increased toxicity, reduced therapeutic benefit or increased adverse

effects underscoring the necessity of systematically evaluating these combinations in both cancerous and non-cancerous cell models (Fan *et al*., 1998).

Conversely, the reduction in doxorubicin efficacy in A549 cells indicates that *G. lucidum* may interfere with doxorubicin's cytotoxic action, potentially through interfering with uptake, antioxidant activity or modulation of apoptosis pathways. These differing effects emphasize the need for further investigation into the molecular mechanisms underlying these interactions.

In summary, the effects of *G. lucidum* are cell line specific. In HEK293 cells, *G. lucidum* enhanced doxorubicin potency whereas it reduced doxorubicin potency in the A549 cell line.

4.6.2 *T. versicolour*

T. versicolour had no significant effect on doxorubicin's potency in A549 or HEK293 cells at 24 h. However, after 48 h, doxorubicin was less effective in A549 cells, while its potency increased 1.9-fold in HEK293 cells. The reduction in A549 cells may be linked to the ability of *T. versicolour* extracts to alter DNA conformation as shown by Hsieh *et al*. (2019). While the relaxation of supercoiled DNA by *T. versicolour* extracts may resemble doxorubicin's own DNA-interacting properties, it could also competitively alter DNA conformation in a way that reduces the ability of doxorubicin to induce cytotoxic damage in cancer cells.

T. versicolour polysaccharides, including PSK and PSP, have been studied for their immunomodulatory and anti-tumour properties (Habtemariam, 2020). However, their role in chemotherapy interactions is less understood. The observed increase in doxorubicin potency in HEK293 cells indicates a potential pro-oxidative or immune-modulating effect, which may enhance doxorubicin's cytotoxicity in normal tissues. This raises concerns about possible off-target toxicity and the need for further research to determine the safety of combining *T. versicolour* with chemotherapy.

These findings highlight the importance of further investigating the molecular interactions between *T. versicolour* and chemotherapeutic agents like doxorubicin. Given the widespread use of *T. versicolour*-derived products in complementary medicine, understanding whether such interactions compromise or enhance drug efficacy is critical.

4.6.3 Summary

These findings highlight the complexity of supplement-drug interactions. The reduction in doxorubicin efficacy in A549 cells at 48 h indicates a potential risk of decreased therapeutic

effectiveness when combined with *G. lucidum* or *T. versicolour*. Conversely, the increased sensitivity of HEK293 cells to doxorubicin in the presence of these extracts raises concerns about heightened toxicity in normal tissues. The differing effects observed in cancerous and non-cancerous cells emphasize the importance of understanding the molecular mechanisms driving these interactions. Further research is needed to clarify these effects and assess the safety of integrating mushroom extracts with chemotherapy. Clinicians and patients should approach complementary therapies with caution to avoid unintended consequences in cancer treatment.

4.7 Cytotoxic effects of *G. lucidum*, *T. versicolour* and doxorubicin on A549 and HEK293 cells

Fluorescence staining revealed features of apoptosis, and necrosis in treated A549 and HEK293 cells. Apoptosis is a caspase-dependent, regulated form of cell death, while necrosis is typically unregulated and results in membrane rupture and inflammation (Elmore, 2007; Zong & Thompson, 2006). In vitro, apoptosis often progresses to secondary necrosis due to the absence of phagocytes to clear apoptotic bodies (Khalid & Azimpouran, 2023). The presence of multiple death modalities suggests that *G. lucidum*, T. *versicolour*, and doxorubicin exert their cytotoxic effects through overlapping or sequential death pathways, which may impact both efficacy and safety.

4.7.1 Doxorubicin

In A549 cells, perinuclear accumulation was observed at 18 h without nuclear accumulation evident by the lack of nuclear staining, indicating cytoplasmic localization. By 24 h, nuclear deformation and fragmentation became prominent, indicating apoptosis. The absence of PI-positive staining, as indicated by smooth intact cellular membranes, at earlier time points ruled out necrosis.

In HEK293 cells, doxorubicin showed a different pattern. At 18 h, perinuclear accumulation was observed, but by 24 h, necrosis became the dominant mode of cell death, indicated by roughened membranes and red-stained nuclei. This indicates that while apoptosis was prevalent in A549 cells, HEK293 cells had necrotic damage with prolonged exposure.

Nephrotoxicity is a well-documented side effect of doxorubicin, primarily attributed to oxidative stress, inflammation, and mitochondrial dysfunction. Previous research has shown that doxorubicin induces renal injury by reducing antioxidant enzyme activity (superoxide

dismutase, Glutathione Peroxidase), increasing apoptosis-related proteins (Bax/Bcl-2 ratio, caspase-3 activation), and triggering inflammatory pathways involving NF-κB and ERK1/2 signalling (Su *et al*., 2015). Additionally, doxorubicin-mediated nitric oxide production plays a role in renal damage by forming peroxynitrite, a cytotoxic molecule that contributes to membrane lipid peroxidation. Further studies using proximal tubule HK-2 cells have shown that doxorubicin-induced nephrotoxicity can be mitigated by antioxidant and anti-inflammatory agents such as madecassoside (Su *et al*., 2015). These findings highlight the potential mechanisms by which doxorubicin affects non-cancerous cells, particularly in the kidney.

4.7.2 *G. lucidum*

At 0.5 mg/mL, *G. lucidum* induced necrosis in A549 cells at both time points, with increasing PI-positive staining and loss of cell integrity. At 0.25 mg/mL, apoptosis was dominant at 18 h, but necrosis became evident by 24 h. Similarly, Vetchinkina *et al*. (2016) reported that *G. lucidum* induced necrosis and late apoptosis in A549 cells at concentrations above 20 mg/mL after 24 h of incubation. At 15 mg/mL or lower, apoptosis was the primary mode of cell death, with cells having nuclear fragmentation, apoptotic granules, and reduced cell size. This further confirms that *G. lucidum* has a concentration dependent effect on A549 cells, causing necrosis at high concentrations and apoptosis at low concentrations.

In HEK293 cells, *G. lucidum* induced vacuolation at 18 h with minimal signs of apoptosis or necrosis. However, by 24 h, necrosis became prevalent, characterized by membrane rupture and PI staining. This delayed cytotoxic effect indicates that HEK293 cells initially resist *G. lucidum*-induced damage but eventually undergo necrosis. The time-dependent increase in necrosis raises concerns about potential toxicity in non-cancerous cells with prolonged exposure. Mousavi *et al*. (2023) reported that methanolic extracts of *G. lucidum* were less toxic to HEK293 cells than to cancer cell lines (MCF-7 and K-562). At the highest tested concentration (3000 µg/mL), HEK293 cell viability remained at 43.63% (Mousavi *et al*., 2023). However, this study used a shorter incubation time (12 h). The increased cytotoxicity observed between 18 and 24 h shows that longer exposure enhances the toxic effects of *G. lucidum* on HEK293 cells. The delayed onset of necrosis seen in this study emphasizes the need for caution, as prolonged exposure could pose significant risks to non-cancerous cells.

4.7.3 *T. versicolour*

T. versicolour induced apoptosis in A549 cells at 18 h, as indicated by nuclear fragmentation without PI staining. By 24 h, necrosis became more prominent, particularly at 0.5 mg/mL, showing a biphasic response where apoptosis transitions into necrosis over time (secondary necrosis). Prior research has linked *T. versicolour* cytotoxicity to cell cycle arrest and DNA interaction, which may contribute to these effects. Stošić-Grujičić *et al*. (2011) reported that *T. versicolour* extracts inhibit proliferation in A549 cells. The cytotoxicity of *T. versicolour* is associated with cell cycle arrest (G0/G1 phase) which leads to apoptosis (Stošić-Grujičić *et al*., 2011). Hsieh *et al*. (2019) reported that aqueous extracts of *T. versicolour* significantly inhibited A549 cell proliferation, while ethanolic extracts had a minimal effect on proliferation. Both the aqueous and ethanolic extracts of *T. versicolour* interacted with supercoiled plasmid DNA, leading to DNA relaxation in a time- and concentration-dependent manner. This indicates that *T. versicolour* may exert its anticancer effects by altering DNA structure and function (Hsieh *et al*., 2019).

4.7.4 Summary

Both fungal extracts had dose- and time-dependent cytotoxicity in A549 and HEK293 cells, with differing mechanisms. In A549 cells, *G. lucidum* and *T. versicolour* initially induced apoptosis, with necrosis becoming more prevalent at higher concentrations and longer exposures. In HEK293 cells, cytotoxic effects were delayed, with minimal apoptosis at 18 h but substantial necrosis by 24 h.

Doxorubicin primarily induced apoptosis in A549 cells but caused necrosis in HEK293 cells, likely due to its nephrotoxic effects. *G. lucidum* and *T. versicolour* showed selective cytotoxicity toward A549 cells initially but also compromised HEK293 cell viability over time, raising concerns about potential off-target effects in non-cancerous tissues. The transition to necrosis in HEK293 cells shows that prolonged exposure could lead to unintended toxicity in healthy cells. Further investigation into their bioactive components and molecular targets is necessary to evaluate their safety profile.

4.8 The effect of *G. lucidum* and *T. versicolour* extracts on phosphatidylserine translocation

The translocation of phosphatidylserine is a marker for apoptosis. The distribution of phospholipids between the two layers of the phospholipid bilayer is asymmetrical in viable cells. The outer leaflet consists of phosphatidylcholine and sphingomyelin while the inner leaflet contains phosphatidylethanolamine and phosphatidylserine. The maintenance of the

asymmetry is an ATP-dependant process, indicating it is essential for normal cell function (Balasubramanian and Schroit, 2003). The exposure of phosphatidylserine, and the loss of asymmetry, is a universal process which is independent of apoptosis inducer, cell type or species and occurs early on during apoptosis. Annexin-V specifically binds to phosphatidylserine in the presence of calcium (Van Engeland *et al*., 1998). It cannot permeate the cell membrane and so will not bind to viable cells. PI is used to differentiate between apoptotic and necrotic/dead cells (Van Engeland *et al*., 1998).

In this study, the effect of doxorubicin, *G. lucidum* extracts and *T. versicolour* extracts on phosphatidylserine translocation was evaluated in two different cell lines, A549 and HEK293. The results show that both extracts induce phosphatidylserine externalization, although the extent of this effect and the resulting cell death mechanisms varied between the cell lines.

4.8.1 Doxorubicin

Doxorubicin treatment induced distinct cytotoxic effects in A549 and HEK293 cells. In A549 cells, roughened membranes and PI uptake indicated necrosis rather than apoptosis. No phosphatidylserine translocation was observed, indicating the absence of apoptosis. Previous studies reported phosphatidylserine translocation in A549 cells treated with doxorubicin, but this was accompanied by high necrotic levels, mitotic catastrophe, and polyploidization (Litwiniec *et al*., 2010). Additionally, cells appeared enlarged and flattened, which are morphological hallmarks of senescence (Litwiniec *et al*., 2010).

In contrast, HEK293 cells retained membrane integrity with perinuclear accumulation of doxorubicin, indicating a different mechanism of toxicity. The absence of phosphatidylserine translocation and PI staining indicates that doxorubicin did not induce apoptosis in these cells. These findings shows that doxorubicin triggers necrosis in A549 cells but exerts a different, possibly delayed, effect in HEK293 cells.

4.8.2 *G. lucidum*

G. lucidum induced phosphatidylserine translocation in both cell lines in a concentration-dependent manner. In A549 cells, 0.5 mg/mL *G. lucidum* led to significant PI uptake, indicating late apoptosis or secondary necrosis, while 0.25 mg/mL primarily induced early apoptosis. HEK293 cells followed a similar pattern, but more cells remained in early apoptosis even at the higher concentration, indicating a slower apoptotic progression.

While no studies specifically assess *G. lucidum*-induced phosphatidylserine translocation in A549 or HEK293 cells, research in other cancer cell lines links *G. lucidum* to apoptosis via mitochondrial dysfunction, oxidative stress, and caspase activation (Gao and Homayoonfal, 2023). The stronger apoptotic response in A549 cells indicates that *G. lucidum* may preferentially target cancerous cells, but its induction of late apoptosis and secondary necrosis in HEK293 cells raises concerns about toxicity in non-cancerous tissues.

4.8.3 *T. versicolour*

T. versicolour induced phosphatidylserine translocation in both A549 and HEK293 cells but at a slower rate than *G. lucidum*. In A549 cells, 0.5 mg/mL resulted in early apoptosis with minimal PI uptake, while 0.25 mg/mL induced phosphatidylserine translocation without significant membrane permeabilization. A similar trend was observed in HEK293 cells, where apoptosis remained at an early stage even at higher concentrations.

Limited literature exists on *T. versicolour*-induced phosphatidylserine translocation in these cell lines, but its known immunomodulatory effects suggest apoptotic induction without excessive necrosis. The slower apoptotic progression in both A549 and HEK293 cells indicates that *T. versicolour* may have a more selective and regulated cytotoxic effect.

4.8.4 Summary

Doxorubicin primarily induced necrosis in A549 cells, whereas HEK293 cells retained membrane integrity without phosphatidylserine translocation, indicating different cytotoxic mechanisms. *G. lucidum* and *T. versicolour* both induced apoptosis, but *G. lucidum* promoted a more rapid transition to late apoptosis and secondary necrosis, while *T. versicolour* maintained membrane integrity for longer. In HEK293 cells, *G. lucidum* induced a stronger apoptotic response at higher concentrations, whereas *T. versicolour* predominantly caused early apoptosis with minimal membrane disruption.

While *G. lucidum* and *T. versicolour* show promising apoptotic effects in A549 cells, their impact on HEK293 cells indicates potential toxicity to non-cancerous cells. The induction of secondary necrosis in HEK293 cells, particularly by *G. lucidum*, raises concerns about non-selective cytotoxicity. Further studies should focus on optimizing treatment concentrations to maximize cancer cell apoptosis while minimizing toxicity to healthy cells. Investigating apoptotic pathways such as mitochondrial integrity, caspase activation, and oxidative stress responses will be essential for refining their therapeutic potential.

4.9 The effect of *G. lucidum*, *T. versicolour* and doxorubicin on caspase-3/7 activity

Caspase-3 and caspase-7 are key executioner caspases in the apoptotic pathway, playing a crucial role in programmed cell death by cleaving a range of intracellular substrates to facilitate cellular disassembly. Upon activation by initiator caspases, these proteases catalyse the cleavage of proteins essential for maintaining cellular integrity, leading to DNA fragmentation, cytoskeletal breakdown, and membrane blebbing (Eskandari and Eaves, 2022; Kamada *et al*., 2005).

Caspase-3, in particular, is recognized as a central mediator of apoptosis, responsible for the proteolytic inactivation of DNA fragmentation factor-45 (DFF45/ICAD), which subsequently triggers the activation of caspase-activated DNase and the hallmark fragmentation of nuclear DNA (Wolf *et al*., 1999). Additionally, studies indicate that nuclear translocation of active caspase-3 is a tightly regulated process, dependent on its proteolytic activation and interaction with substrate-like proteins (Kamada *et al*., 2005).

In this study, a caspase-3/7 activity assay was utilized to evaluate the apoptotic response of treated cells, providing insights into the mechanisms underlying cell death.

4.9.1 Doxorubicin

Doxorubicin treatment induced moderate caspase-3/7 activation in A549 cells, indicating apoptosis. However, the extent of the activation was limited, which can be explained by findings by Sato *et al*. (2022), where doxorubicin causes phosphorylation of ERK, which inhibits caspase activity. The study further showed that ERK inhibition amplified doxorubicin-induced apoptosis in A549 cells via caspase-3 activation (Sato *et al*., 2022).

In this study, doxorubicin triggered substantial caspase-3/7 activation in HEK293 cells. This was supported by a study by Houshdarpour *et al*. (2021) which found that doxorubicin causes concentration dependent caspase-3 activation, with higher doses resulting in a more significant increase in caspase-3 activation in HEK293 cells. Apoptosis is then induced through DNA damage, cytoskeletal degradation, membrane blebbing and phosphatidylserine externalization.

4.9.2 *G. lucidum*

G. lucidum induced near-complete caspase-3/7 activation in A549 cells at both tested concentrations (0.5 mg/mL and 0.25 mg/mL). The observed fluorescence and apoptotic morphology indicate activation of apoptosis, potentially linked to ERK inhibition (Qiu *et al*.,

2023) and Fas-mediated caspase-8 activation (Gao and Homayoonfal, 2023). Unlike doxorubicin, which promotes ERK phosphorylation, *G. lucidum* may enhance apoptosis by suppressing this pro-survival pathway. *G. lucidum* engages both extrinsic (Fas-mediated) and intrinsic (mitochondrial) pathways, enhances apoptotic signalling (Gao and Homayoonfal, 2023).

In HEK293 cells, *G. lucidum* also induced caspase-3/7 activation, particularly at 0.5 mg/mL, indicating concentration dependent cytotoxicity. While the response was similar to A549 cells, its impact on non-cancerous cells raises concerns about its selectivity. The observed toxicity indicates that further studies are needed to assess its potential off-target effects and therapeutic safety.

Future studies should explore whether co-treatment with *G. lucidum* and doxorubicin could achieve greater apoptosis induction by effectively suppressing ERK-mediated survival pathways and recruiting Fas-associated death domain which activates caspase-8 and subsequently, caspase-3.

4.9.3 *T. versicolour*

T. versicolour treatment led to moderate caspase-3/7 activation in A549 cells. Increased fluorescence and apoptotic morphology were evident at higher concentrations. While there are no studies directly assessing the effect of *T. versicolour* extracts on caspase-3/7 activity in A549 cells, Jiménez-Medina *et al*. (2008) found that PSK, a polysaccharide component of *T. versicolour*, significantly increased caspase-3 expression in A549 cells, from 4.20% in untreated cells to 31.15% when treated with 100 µg/mL of PSK. Additionally, PSK induced caspase-3 activation in various other cancer cell lines, including HL-60, WiDr, HT29, SW480, KATOIII, AGS, U937 (Hirahara *et al*., 2011; Hirahara *et al*., 2012; Hirahara *et al*., 2013; Wang *et al*., 2012; Yang *et al*., 2005; Jiménez-Medina *et al*., 2008).

In contrast, *T. versicolour* had minimal effects on HEK293 cells, with no significant caspase-3/7 activation observed. This indicates a degree of selectivity, as it induced apoptosis in cancer cells while sparing non-cancerous cells. Compared to *G. lucidum* and doxorubicin, *T. versicolour* appears to have a safer profile with lower toxicity toward HEK293 cells.

4.9.4 Summary

Doxorubicin, *G. lucidum*, and *T. versicolour* increased caspase-3/7 activation in A549 cells, with *G. lucidum* showing the strongest apoptotic effect. Doxorubicin induced apoptosis but to

a lesser extent, potentially due to ERK-mediated survival mechanisms. In HEK293 cells, doxorubicin caused substantial apoptosis, while *G. lucidum* also activated caspase-3/7, raising concerns about its non-selective toxicity. *T. versicolour* had limited effects in HEK293 cells, indicating a safer profile. These findings highlight the need for further studies on selective toxicity and the mechanisms underlying apoptosis induction in cancer and non-cancerous cells.

4.10 The effect of *G. lucidum* and *T. versicolour* in A549 and HEK293 Cells on ROS levels

This study investigated the ROS formation induced by *G. lucidum*, *T. versicolour* and doxorubicin treatments in two different cell lines, A549 and HEK293. The primary aim was to compare the ROS-generating effects of these treatments at two different concentrations (0.5 mg/mL and 0.25 mg/mL). The presence of ROS was detected using a fluorescence-based assay, where increased fluorescence signals were indicative of ROS formation.

ROS play a critical role in cancer biology, acting as a double-edged sword in tumour development and treatment (Nakamura and Takada, 2021). As natural byproducts of cellular metabolism, ROS regulate key signalling pathways involved in cell proliferation, differentiation, and survival (Nakamura and Takada, 2021). While moderate ROS levels promote cancer progression by enhancing proliferation, migration, and drug resistance, excessive ROS formation induces oxidative stress, leading to DNA damage, apoptosis, and cell death (Cui *et al*., 2018). Cancer cells often had elevated basal ROS levels due to increased metabolic activity and oncogenic signalling, necessitating robust antioxidant systems to maintain redox balance and prevent lethal oxidative stress. This redox adaptability is a major factor in therapy resistance, as cancer cells exploit antioxidant pathways to evade ROS-induced cell death. Consequently, targeting ROS homeostasis, either by increasing oxidative stress to induce apoptosis or by inhibiting antioxidant defences, has emerged as a promising strategy for cancer treatment (Cui *et al*., 2018).

Building on this understanding of ROS in cancer biology, this study aimed to assess how *G. lucidum*, *T. versicolour*, and doxorubicin influence ROS formation in A549 and HEK293 cells. By evaluating fluorescence-based ROS detection, the results provide insight into the extent to which these treatments induce oxidative stress in different cellular environments. The following sections will discuss the observed ROS formation patterns in each treatment group, comparing these findings to existing literature to better understand the implications for cancer therapy and cellular redox regulation.

4.10.1 Doxorubicin

Doxorubicin induced significant morphological changes and fluorescence in A549 cells, indicating ROS formation. The fluorescence appeared granular and localized within organelles such as mitochondria, lysosomes, or the endoplasmic reticulum. This aligns with previous studies showing doxorubicin generates ROS through mitochondrial dysfunction, cytochrome c release, and oxidative stress pathways (Upadhayay *et al*., 2020). The fluorescence pattern indicates ROS generation within oxidative stress-related organelles, supporting findings that anthracyclines induce high ROS levels in cancer cells (Mizutani *et al*., 2005).

In HEK293 cells, fluorescence was uniformly distributed across the nucleus and cytoplasm without bright speckled regions, indicating minimal ROS formation. This contrasts with Mehdizadeh *et al*. (2020), who reported significant ROS accumulation in HEK293 cells treated with 5 µM doxorubicin for 30 h. The difference may stem from experimental conditions, such as drug concentration, exposure time, or metabolic state.

4.10.2 *G. lucidum*

A549 cells treated with 0.5 mg/mL *G. lucidum* showed fluorescence localized in the cytoplasm, while at 0.25 mg/mL, fluorescence appeared as specks, indicating ROS formation within organelles. Literature indicates that *G. lucidum* polysaccharides increase ROS in A549 cells, leading to apoptosis via mitochondrial and EGFR-related pathways (Gao and Homayoonfal, 2023). The observed fluorescence patterns in this study are consistent with these mechanisms.

In HEK293 cells, 0.5 mg/mL *G. lucidum* induced fluorescence, while 0.25 mg/mL did not, indicating a concentration-dependent effect. Literature suggests *G. lucidum* has antioxidant properties under hypoxic stress (Mishra *et al*., 2018), contrasting with the ROS formation observed here. Mishra *et al*. (2018) showed that only specific solvent fractions, particularly ethyl acetate and diethyl ether extracts, demonstrated strong antioxidant properties, attributed to high flavonoid and phenolic content. This indicates that its effects may be solvent dependent.

4.10.3 *T. versicolour*

T. versicolour induced ROS formation in both A549 and HEK293 cells, with fluorescence appearing as specks in the cytoplasm. While direct studies on *T. versicolour* in A549 cells are lacking, related polysaccharides have been shown to enhance ROS generation and apoptosis in cancer models (Jedrzejewski *et al*., 2019). In leukaemia cells, PSK enhances the cytotoxicity of chemotherapeutic agents (doxorubicin and etoposide) through increased ROS production and apoptosis. The effectiveness of PSK against Walker 256 fibrosarcoma tumour cells was

linked to the ability to increase superoxide dismutase activity and ROS levels. Further, animal studies have shown that *T. versicolour* polysaccharides increase ROS production in rats (Jedrzejewski *et al*., 2019).

In HEK293 cells, *T. versicolour* caused fluorescence at both concentrations, indicating an increase in ROS formation. The absence of literature on *T. versicolour* in HEK293 cells limits comparisons, but the observed fluorescence indicates direct ROS formation or secondary stress responses.

4.10.4 Summary and comparison

The fluorescence intensity was consistently higher in A549 cells across all treatments, indicating greater susceptibility to ROS formation. This aligns with studies showing cancer cells, including A549, are more prone to oxidative stress due to altered metabolism and genetic instability (Yilmazer, 2018; Perillo *et al*., 2020). Yilmazer (2018) used hydrogen peroxide (H_2O_2) treatments to induce oxidative stress in cancer cell lines, including A549, G361 (melanoma), and MCF-7 (breast cancer) cells. The study found that cancer cells form ROS more readily than normal human primary melanocytes and underwent apoptosis at lower ROS thresholds (Yilmazer, 2018). Yilmazer used fluorescence microscopy using CellROX Deep Red to confirm that ROS levels increased in a concentration-dependent manner following H_2O_2 treatment, leading to significant reductions in cell viability. The lower ROS response in HEK293 cells indicates more efficient antioxidant defences or different metabolic pathways. Further research is needed to clarify the molecular mechanisms underlying these differences, particularly in non-cancerous cells.

4.11 The effect of doxorubicin, *G. lucidum* and *T. versicolour* on P-glycoprotein expression in A549 and HEK293 cells

P-Glycoprotein a member of the ABC transporter family, is a well-established mediator of multidrug resistance (MDR) in cancer cells. Acting as an efflux pump, P-glycoprotein actively transports a wide range of chemotherapeutic agents out of cells, thereby reducing intracellular drug accumulation and diminishing therapeutic efficacy (Housman *et al*., 2014). Overexpression of P-glycoprotein has been linked to resistance against a variety of anticancer drugs, including doxorubicin, paclitaxel, and vinblastine, among others, which significantly hampers the effectiveness of chemotherapy (Bukowski *et al*., 2020).

The aim of this experiment was to investigate the expression of P-glycoprotein in A549 and HEK293 cells following treatment with doxorubicin, *G. lucidum*, and *T. versicolour* using immunofluorescence techniques. This approach allowed for the visualization of P-glycoprotein localization and expression levels within these cell lines.

In both A549 and HEK293 cells, doxorubicin treatment there was in an increase in green fluorescence. However, while fluorescence was detectable, it was not particularly intense, indicating that this was a non-specific signal and not an increase in P-glycoprotein expression. A study by Kibria *et al*. (2014) found that A549 cells inherently had low or undetectable levels of P-glycoprotein. The same study reported that A549 cells retain high levels of intracellular doxorubicin, likely due to the absence of active drug efflux mechanisms like P-glycoprotein. This aligns with our findings, as doxorubicin was frequently observed accumulating in the perinuclear region of A549 cells following treatment. Research indicates that HEK293 cells do not constitutively express high levels of P-glycoprotein, but they can be genetically engineered or induced to overexpress it under certain conditions (Chen *et al*., 2024).

The results for *G. lucidum* and *T. versicolour* differed significantly from those observed with doxorubicin. Neither *G. lucidum* nor *T. versicolour* in A549 and HEK293 cells caused any observable green, fluorescent signal, indicating that these natural extracts did not upregulate P-glycoprotein at the tested concentration (0.5 mg/mL) and exposure time (12 h).

Since P-glycoprotein is a key mediator of multidrug resistance by actively effusing chemotherapeutic agents from cells (Housman *et al*., 2014), its absence indicates that these extracts would remain inside the cells, potentially enhancing their cytotoxic effects. This outcome is particularly favourable in A549 lung cancer cells, where intracellular accumulation could improve anti-cancer efficacy. However, in non-cancerous HEK293 cells, this raises safety concerns, as it may lead to unintended cytotoxicity in normal tissues.

4.12 Integrated discussion

The combined results from the ROS, caspase-3/7, and Annexin-V assays provided sufficient evidence that in A549 cells, the mushroom extracts induced apoptosis. However, the presence of necrotic cell death is present as well.

Elevated levels of reactive oxygen species (ROS) suggest that the extracts initiate oxidative stress, which may activate the intrinsic apoptotic pathway. ROS-induced damage to mitochondria and DNA is known to activate caspase-9, which subsequently leads to the

activation of executioner caspases such as caspase-3 and -7. The increased activity of caspase-3/7 observed in treated A549 cells supports this mechanism, indicating that the apoptotic program had progressed to its execution phase. Annexin-V staining further confirmed apoptosis by detecting the externalization of phosphatidylserine, a hallmark of early apoptosis, on the outer leaflet of the cell membrane. Some cells were positive for both Annexin-V and propidium iodide (PI) staining indicating late-stage apoptosis or secondary necrosis. Taken together, the activation of oxidative stress, caspase-3/7 activation, and membrane alterations strongly suggest that *G. lucidum* and *T. versicolour* extracts induce apoptosis in lung cancer cells through a ROS-mediated, caspase-dependent pathway.

In the HEK293 non-cancerous cell line, Annexin-V staining revealed high levels of phosphatidylserine externalization, and caspase-3/7 activity was detected in *G. lucidum*, but not in *T. versicolour*-treated cells. Cell morphology assessment together with Annexin-V staining indicated that HEK293 cells were undergoing apoptosis; however, the absence of caspase-3/7 activation in the *T. versicolour* group may be attributed to the experimental timeframe.

CHAPTER 5: CONCLUSION

This study evaluated the effects of *G. lucidum*, *T. versicolour*, and *I. obliquus* on A549 lung cancer and HEK293 non-cancerous cells. While *G. lucidum* and *T. versicolour* extracts were cytotoxic to A549 cells, their impact on HEK293 cells raises significant safety concerns. These findings underscore the importance of carefully evaluating natural products marketed as health supplements, as their potential toxicity in normal cells is often overlooked. Although these extracts had anticancer properties, their cytotoxicity in HEK293 cells suggests a lack of selectivity, highlighting the need for further investigation into their mechanisms of action and long-term effects on healthy tissues.

G. lucidum and *T. versicolour* extracts had dose- and time-dependent cytotoxicity, initially showing stronger effects on A549 cells than on HEK293 cells. At lower concentrations, the extracts induced apoptosis in A549 cells, a controlled form of cell death desired in cancer treatment. However, at higher concentrations, the mode of cell death shifted toward necrosis. Necrosis is particularly concerning because, unlike apoptosis, it results in the uncontrolled release of intracellular components into the surrounding environment, triggering inflammation, immune activation, and potential damage to neighbouring tissues. In a clinical context, this inflammatory response could contribute to adverse effects such as increased toxicity, damage to non-cancerous tissues, and the potential promotion of tumour growth through the recruitment of inflammatory mediators that support cancer progression. The transition from apoptosis to necrosis in non-cancerous cells further emphasizes the potential for unwanted toxicity. These findings raise concerns about the widespread, unregulated use of such products, as consumers may unknowingly be exposed to harmful compounds at certain doses or with prolonged use.

Doxorubicin, the positive control, showed the expected potent anticancer activity while also inducing toxicity in HEK293 cells, reinforcing its known adverse effects on non-cancerous tissues. Notably, the fungal extracts reduced doxorubicin's efficacy in A549 cells while increasing its toxicity in HEK293 cells, raising concerns about potential adverse effects. This dual effect suggests that these extracts could not only compromise doxorubicin's ability to kill cancer cells but also exacerbate its toxicity, potentially leading to more severe adverse effects.

The interaction between *T. versicolour* and doxorubicin further highlights the complexity of combining natural extracts with chemotherapy. While *T. versicolour* is known for its immunomodulatory and anti-tumour properties, its influence on chemotherapy outcomes remains poorly understood. Although it initially had no effect on doxorubicin's potency,

prolonged exposure appeared to reduce the drug's cytotoxicity in A549 cells while increasing its toxicity in HEK293 cells. This effect may be linked to *T. versicolour*'s ability to alter DNA conformation, potentially interfering with doxorubicin's mechanism of action and limiting its capacity to induce cytotoxic damage in cancer cells. Given that many cancer patients use natural remedies alongside conventional therapy, these findings highlight the urgent need for stricter regulatory oversight of dietary supplements claiming anticancer benefits.

Beyond their cytotoxic effects, the ability of *G. lucidum* and *T. versicolour* to induce ROS production raises concerns about oxidative stress-related DNA damage. While moderate ROS levels can promote apoptosis in cancer cells, excessive oxidative stress may contribute to genomic instability, lipid peroxidation, and mitochondrial dysfunction, which could paradoxically enhance cancer progression rather than suppression. This is particularly relevant in the context of normal cells, as uncontrolled ROS production can trigger inflammation and cell senescence, leading to tissue damage and an increased risk of secondary malignancies. Given the widespread use of fungal extracts in dietary supplements, further investigations into their pro-oxidative and antioxidant balance are necessary to ensure their safe use.

The lack of P-glycoprotein upregulation in both A549 and HEK293 cells following treatment with *G. lucidum* and *T. versicolour* indicates that these extracts are not actively expelled from cells via efflux mechanisms. As a key efflux transporter, P-glycoprotein plays a central role in multidrug resistance by actively removing chemotherapeutic agents from cancer cells, thereby reducing intracellular drug accumulation and decreasing treatment efficacy. The absence of P-glycoprotein upregulation suggests that these fungal extracts are not actively expelled from cells. In normal cells, the active principles may be that the accumulation over time may contribute to off-target toxicity and adverse effects. Additionally, the lack of P-glycoprotein-mediated drug efflux raises concerns about the potential for these extracts to interact with other chemotherapeutic agents, potentially altering their intracellular concentrations and therapeutic outcomes. Future studies should explore whether prolonged exposure to these extracts influences other drug transporters or cellular detoxification pathways.

The interrelationship between the ROS, caspase-3/7, and Annexin-V assays further elucidates the mode of cell death induced by the fungal extracts and highlights the complexity of their biological activity. In A549 cells, elevated ROS levels preceded caspase-3/7 activation, suggesting oxidative stress as an upstream trigger of apoptosis. This was followed by phosphatidylserine externalization detected via Annexin-V staining, confirming the

progression toward apoptotic cell death. In HEK293 cells, caspase-3/7 activation was observed in *G. lucidum*-treated cells but not in those treated with *T. versicolour*, where the absence of activation may be attributable to the experimental timeframe. Importantly, in both A549 and HEK293 cells, *G. lucidum* and *T. versicolour* occasionally induced necrosis rather than apoptosis. This is of particular concern in HEK293 cells, as it indicates a lack of selectivity and raises the potential for unintended cytotoxic effects in normal tissues. Collectively, these findings highlight the dual apoptotic and necrotic potential of the extracts, reinforcing the need for cautious and well-regulated use of such bioactive compounds.

Regulatory bodies must enforce stricter quality control measures to ensure commercially available fungal extracts are standardized and free from misleading health claims. Given the widespread use of natural supplements, it is crucial to prevent the distribution of products with unverified and potentially harmful effects. This study underscores the need for continued monitoring of supplement safety, particularly for products marketed with unverified anticancer claims.

Ultimately, while *G. lucidum* and *T. versicolour* have some anticancer activity, their lack of selectivity and potential toxicity in non-cancerous cells make them unsuitable for therapeutic use without significant refinement. Future research should prioritize identifying active compounds and their structures. Until such data is available, caution should be exercised in their use, and regulatory agencies must ensure consumers are protected from the risks associated with unregulated natural products.

5.1 Limitations

This study was conducted on A549 and HEK293 cell lines, in two dimensional cultures, which do not fully capture the complexity of the *in vivo* tumour environments or normal tissues. Key physiological factors, such as immune interactions, extracellular matrix dynamics, and systemic metabolism, are absent *in vitro*. Additionally, the study does not address the pharmacokinetics of these fungal extracts, including absorption, distribution, metabolism, and excretion, limiting the ability to predict their *in vivo* effects. The compositional variability of natural product extracts, influenced by extraction methods, fungal strain, and environmental conditions, may affect reproducibility and hinder cross-study comparisons.

5.2 Future studies

Advanced analytical techniques, such as mass spectrometry, HPLC, or NMR spectroscopy, should be used to characterize the chemical composition of fungal extracts and identify key bioactive compounds. Pharmacokinetic studies in animal models are essential to determine absorption, distribution, metabolism, and excretion profiles and identify active metabolites with potential therapeutic or toxic effects. Standardized extraction and purification protocols must be developed to ensure reproducibility across studies.

Future studies should incorporate 3D cultures or organoid models to better mimic tumour architecture and drug penetration, followed by animal studies in nude mice. Investigating interactions between fungal extracts and extracellular matrix components may provide insights into their effects on tumour progression and metastasis. Co-culture systems with immune cells (e.g., macrophages, T cells) should be used to assess immunomodulatory properties, including potential immunosuppressive or immunostimulatory effects.

To assess selectivity and toxicity, future research should evaluate the effects of fungal extracts on normal human primary cells (e.g., fibroblasts, endothelial cells, and organ-specific cells) and compare responses across multiple non-cancerous cell lines.

References

1. Al-Tuwaijri, M., Basal, W., Sabry, N., Moussa, T., Das, B., & Eid, J. (2021). *Inonotus obliquus* polysaccharides inhibited cellular growth of NCI-H23 and A549 lung cancer cells through G0/G1 cell cycle arrest and ROS mediated cell death. *Egyptian Academic Journal of Biological Sciences. C, Physiology and Molecular Biology, 13*(1), 27–40. https://doi.org/10.21608/eajbsc.2021.144738
2. Arata, S., Watanabe, J., Maeda, M., Yamamoto, M., Matsuhashi, H., Mochizuki, M., Kagami, N., Honda, K., & Inagaki, M. (2016). Continuous intake of the Chaga mushroom (*Inonotus obliquus*) aqueous extract suppresses cancer progression and maintains body temperature in mice. *Heliyon, 2*(5), e00111. https://doi.org/10.1016/j.heliyon.2016.e00111
3. Araujo, L. H., Horn, L., Merritt, R. E., Shilo, K., Xu-Welliver, M., & Carbone, D. P. (2020). Cancer of the lung: Non-small cell lung cancer and small cell lung cancer. In J. E. Niederhuber, J. O. Armitage, J. H. Doroshow, M. B. Kastan, & J. E. Tepper (Eds.), *Abeloff's clinical oncology* (6th ed.). Elsevier.
4. Asai, H., Iijima, H., Matsunaga, K., Oguchi, Y., Katsuno, H., & Maeda, K. (2008). Protein-bound polysaccharide K augments IL-2 production from murine mesenteric lymph node CD4+ T cells by modulating T cell receptor signalling. *Journal of Immunology Research.*
5. Atale, N., Gupta, S., Yadav, U. C. S., & Rani, V. (2014). Cell-death assessment by fluorescent and nonfluorescent cytosolic and nuclear staining techniques. *Journal of Microscopy, 255*(1), 7–19. https://doi.org/10.1111/jmi.12133
6. Balasubramanian, K., & Schroit, A. J. (2003). Aminophospholipid asymmetry: A matter of life and death. *Annual Review of Physiology, 65*(1), 701–734. https://doi.org/10.1146/annurev.physiol.65.092101.142459
7. Biomons. Colorful flat tube Trametes versicolor: mushroom of vitality. Biomons. https://biomons.com/en/colorful-flat-tube-trametes-versicolor-mushroom-of-vitality/. Accessed July 15, 2025.
8. Brunton, L. L., Knollmann, B. C., & Goodman, L. S. (2023). *Goodman & Gilman's: The pharmacological basis of therapeutics* (14th ed.). McGraw-Hill Education. https://accessmedicine.mhmedical.com/content.aspx?bookid=3191&sectionid=269714761

9. Bukowski, K., Kciuk, M., & Kontek, R. (2020). Mechanisms of multidrug resistance in cancer chemotherapy. *International Journal of Molecular Sciences, 21*(9), 3233. https://doi.org/10.3390/ijms21093233
10. Camargo, M. R., & Kaneno, R. (2011). Antitumor properties of *Ganoderma lucidum* polysaccharides and terpenoids. *Cancer Research Journal.*
11. Cequier-Sánchez, E., Rodríguez, C., Ravelo, Á. G., & Zárate, R. (2008). Dichloromethane as a solvent for lipid extraction and assessment of lipid classes and fatty acids from samples of different natures. *Journal of Agricultural and Food Chemistry, 56*(12), 4297–4303. https://doi.org/10.1021/jf073471e
12. Chen, X.-Y., Wu, Z.-X., Wang, J.-Q., Teng, Q.-X., Tang, H., Liu, Q., Chen, Z.-S., & Chen, W. (2024). Multidrug resistance transporters P-gp and BCRP limit the efficacy of ATR inhibitor ceralasertib in cancer cells. *Frontiers in Pharmacology, 15*, 1400699. https://doi.org/10.3389/fphar.2024.1400699
13. Chiang, A., Detterbeck, F. C., Stewart, T., Decker, R. H., & Tanoue, L. (2019). Non-small cell lung cancer. In V. T. DeVita, T. S. Lawrence, & S. A. Rosenberg (Eds.), *DeVita, Hellman, and Rosenberg's cancer: Principles and practice of oncology* (11th ed.). Lippincott Williams & Wilkins.
14. Cohen, P. A., Avula, B., Katragunta, K., Travis, J. C., & Khan, I. (2023). Presence and quantity of botanical ingredients with purported performance-enhancing properties in sports supplements. *JAMA Network Open, 6*(7), e2323879. https://doi.org/10.1001/jamanetworkopen.2023.23879
15. Crowley, L. C., Marfell, B. J., & Waterhouse, N. J. (2016). Analyzing cell death by nuclear staining with Hoechst 33342. *Cold Spring Harbor Protocols, 2016*(9), 778–781. https://doi.org/10.1101/pdb.prot087205
16. Cui, Q., Wang, J.-Q., Assaraf, Y. G., Ren, L., Gupta, P., Wei, L., Ashby, C. R., Yang, D.-H., & Chen, Z.-S. (2018). Modulating ROS to overcome multidrug resistance in cancer. *Drug Resistance Updates, 41*, 1–25. https://doi.org/10.1016/j.drup.2018.11.001
17. Degterev, A., Hitomi, J., Germscheid, M., Ch'en, I. L., Korkina, O., Teng, X., Abbott, D., Cuny, G. D., Yuan, C., Wagner, G., Hedrick, S. M., Gerber, S. A., Lugovskoy, A., & Yuan, J. (2008). Identification of RIP1 kinase as a specific cellular target of necrostatins. *Nature Chemical Biology, 4*(5), 313–321. https://doi.org/10.1038/nchembio.83

18. Demchenko, A. P. (2013). Beyond annexin V: Fluorescence response of cellular membranes to apoptosis. *Cytotechnology, 65*(2), 157–172. https://doi.org/10.1007/s10616-012-9481-y
19. Du, B., Meenu, M., Liu, H., & Xu, B. (2019). A concise review on the molecular structure and function relationship of β-glucan. *International Journal of Molecular Sciences, 20*(16), 4032. https://doi.org/10.3390/ijms20164032
20. Du, X., Shao, Y., Qin, H. F., Tai, Y. H., & Gao, H. J. (2018). ALK-rearrangement in non-small-cell lung cancer (NSCLC). *Thoracic Cancer, 9*(4), 423–430. https://doi.org/10.1111/1759-7714.12613.
21. Duke, E. S., Stapleford, L., Drezner, N., Amatya, A. K., Mishra-Kalyani, P. S., Shen, Y. L., et al. (2023). FDA Approval Summary: Mobocertinib for Metastatic Non–Small Cell Lung Cancer with EGFR Exon 20 Insertion Mutations. *Clinical Cancer Research, 29*(3), 508–512. https://doi.org/10.1158/1078-0432.CCR-22-2072.
22. Dunn, J.D., Cannon, H.E., Lewis, T., & Shane-McWhorter, L. (2005). Development of a Complementary and Alternative Medicine (CAM) Pharmacy and Therapeutics (P&T) Subcommittee and CAM Guide for Providers.
23. Ebner, M., Puchkov, D., López-Ortega, O., Muthukottiappan, P., Su, Y., Schmied, C., Zillmann, S., Nikonenko, I., Koddebusch, J., Dornan, G. L., Lucht, M. T., Koka, V., Jang, W., Koch, P. A., Wallroth, A., Lehmann, M., Brügger, B., Pende, M., Winter, D., & Haucke, V. (2023). Nutrient-regulated control of lysosome function by signaling lipid conversion. *Cell, 186*(24), 5328–5346.e26. https://doi.org/10.1016/j.cell.2023.09.027
24. Elgart, V., Lin, J.-R., & Loscalzo, J. (2018). Determinants of drug-target interactions at the single cell level. *PLOS Computational Biology, 14*(12), e1006601. https://doi.org/10.1371/journal.pcbi.1006601
25. Elmore, S. (2007). Apoptosis: A Review of Programmed Cell Death. *Toxicologic Pathology, 35*(4), 495–516. https://doi.org/10.1080/01926230701320337
26. Engel, A. L., Sun, G. C., Gad, E., Rastetter, L. R., Strobe, K., Yang, Y., Dang, Y., Disis, M. L., & Lu, H. (2013). Protein-bound polysaccharide activates dendritic cells and enhances OVA-specific T cell response as vaccine adjuvant. *Immunobiology, 218*(12), 1468–1476. https://doi.org/10.1016/j.imbio.2013.05.001
27. Eskandari, E., & Eaves, C. J. (2022). Paradoxical roles of caspase-3 in regulating cell survival, proliferation, and tumorigenesis. *Journal of Cell Biology, 221*(6), e202201159. https://doi.org/10.1083/jcb.202201159

28. Fan, W., Johnson, K. R., & Miller, M. C. (1998). In vitro evaluation of combination chemotherapy against human tumor cells (Review). *Oncology Reports.* https://doi.org/10.3892/or.5.5.1035
29. Feng, L., Yuan, L., Du, M., Chen, Y., Zhang, M.-H., Gu, J.-F., He, J.-J., Wang, Y., & Cao, W. (2013). Anti-lung cancer activity through enhancement of immunomodulation and induction of cell apoptosis of total triterpenes extracted from *Ganoderma lucidum* (Leyss. Ex Fr.) Karst. *Molecules, 18*(8), 9966–9981. https://doi.org/10.3390/molecules18089966
30. Festjens, N., Van den Berghe, T., & Vandenabeele, P. (2006). Necrosis, a well-orchestrated form of cell demise: Signalling cascades, important mediators and concomitant immune response. *Biochimica et Biophysica Acta - Bioenergetics, 1757*(9–10), 1371–1387. https://doi.org/10.1016/j.bbabio.2006.06.014
31. Foglieni, C., Meoni, C., & Davalli, A. M. (2001). Fluorescent dyes for cell viability: An application on prefixed conditions. *Histochemistry and Cell Biology, 115*(3), 223–229. https://doi.org/10.1007/s004180100249
32. Friedman, M. (2016). Mushroom polysaccharides: Chemistry and antiobesity, antidiabetes, anticancer, and antibiotic properties in cells, rodents, and humans. *Foods, 5*(4), 1–40. https://doi.org/10.3390/foods5040080
33. Gabriels, G., Lambert, M., & Smith, P. (2012). Information on nutritional supplement labels: Time for legislation? *South African Journal of Clinical Nutrition, 25*(1), 22–26. https://doi.org/10.1080/16070658.2012.11734398
34. Gao, X., & Homayoonfal, M. (2023). Exploring the anti-cancer potential of *Ganoderma lucidum* polysaccharides (GLPs) and their versatile role in enhancing drug delivery systems: A multifaceted approach to combat cancer. *Cancer Cell International, 23*(1), 324. https://doi.org/10.1186/s12935-023-03146-8
35. Gilbert, K., & Favre-Godal, Q. (2017). Natural product research: The challenge of consistent sample quality. *Phytochemistry Reviews*, **16**, 405–422. https://doi.org/10.1007/s11101-017-9494-2
36. Glorieux, C., Liu, S., Trachootham, D., & Huang, P. (2024). Targeting ROS in cancer: Rationale and strategies. *Nature Reviews Drug Discovery, 23*(8), 583–606. https://doi.org/10.1038/s41573-024-00979-4
37. Gordon, A. T., Abosede, O. O., Ntsimango, S., Hosten, E. C., Myeza, N., van Eyk, A., Harmse, L., & Ogunlaja, A. S. (2022). Synthesis and anticancer evaluation of

copper(II)- and manganese(II)-theophylline mixed ligand complexes. *Polyhedron, 214*, 115649. https://doi.org/10.1016/j.poly.2022.115649

38. Habtemariam, S. (2020). *Trametes versicolor* (Synn. *Coriolus versicolor*) polysaccharides in cancer therapy: Targets and efficacy. *Biomedicines, 8*(5), 135. https://doi.org/10.3390/biomedicines8050135
39. Heah, K. G., Suhaimi, S. N., Shobri, N. R. B. M., Zhu, H. J., & Froemming, G. (2020). In vitro and in vivo studies of *Ganoderma lucidum* in cancer. *Journal of International Dental and Medical Research, 13*(1), 379–383. ISSN 1309-100X
40. Herbal Reality. (n.d.). *Chaga mushroom (Inonotus obliquus)* [Image]. Herbal Reality. https://www.herbalreality.com/herbalism/western-herbal-medicine/chaga-mushroom-medicinal-properties/
41. Hirahara, N., Edamatsu, T., Fujieda, A., Fujioka, M., Wada, T., & Tajima, Y. (2013). Protein-bound polysaccharide-K induces apoptosis via mitochondria and p38 mitogen-activated protein kinase-dependent pathways in HL-60 promyelomonocytic leukemia cells. *Oncology Reports, 30*(1), 99–104. https://doi.org/10.3892/or.2013.2412
42. Hirahara, N., Edamatsu, T., Fujieda, A., Fujioka, M., Wada, T., & Tajima, Y. (2012). Protein-bound polysaccharide-K (PSK) induces apoptosis via p38 mitogen-activated protein kinase pathway in promyelomonocytic leukemia HL-60 cells. *Anticancer Research*.
43. Hirahara, N., Fujioka, M., Edamatsu, T., Fujieda, A., Sekine, F., Wada, T., & Tanaka, T. (2011). Protein-bound polysaccharide-K (PSK) induces apoptosis and inhibits proliferation of promyelomonocytic leukemia HL-60 cells. *Anticancer Research, 31*(9), 2733–2738.
44. Houshdarpour, R., Ataei, F., & Hosseinkhani, S. (2021). Efficient stable cell line generation of survivin as an in vitro model for specific functional analysis in apoptosis and drug screening. *Molecular Biotechnology, 63*(6), 515–524. https://doi.org/10.1007/s12033-021-00313-y
45. Housman, G., Byler, S., Heerboth, S., Lapinska, K., Longacre, M., Snyder, N., & Sarkar, S. (2014). Drug resistance in cancer: An overview. *Cancers, 6*(3), 1769–1792. https://doi.org/10.3390/cancers6031769
46. Hsieh, T.-C., Chao, H. H., Chu, Y., Doonan, B. B., & Wu, J. M. (2019). Aqueous and ethanolic extracts of medicinal mushroom *Trametes versicolor* interact with DNA: A novel genoactive effect contributing to its antiproliferative activity in cancer cells. In

D. C. Agrawal & M. Dhanasekaran (Eds.), *Medicinal mushrooms* (pp. 207–221). Springer Singapore. https://doi.org/10.1007/978-981-13-6382-5_7

47. Im, K., Mareninov, S., Diaz, M. F. P., & Yong, W. H. (2019). An introduction to performing immunofluorescence staining. In *Methods in Molecular Biology* (Vol. 1897, pp. 299–311). Humana Press Inc. https://doi.org/10.1007/978-1-4939-8935-5_26
48. Inamura, K. (2017). Lung cancer: Understanding its molecular pathology and the 2015 HO classification. *Frontiers in Oncology, 7*(AUG), Article 193. https://doi.org/10.3389/fonc.2017.00193
49. Iyer, R. S., Needham, S. R., Galdadas, I., Davis, B. M., Roberts, S. K., Man, R. C. H., Zanetti-Domingues, L. C., Clarke, D. T., Fruhwirth, G. O., Parker, P. J., Rolfe, D. J., Gervasio, F. L., & Martin-Fernandez, M. L. (2024). Drug-resistant EGFR mutations promote lung cancer by stabilizing interfaces in ligand-free kinase-active EGFR oligomers. *Nature Communications, 15*(1), Article 46284. https://doi.org/10.1038/s41467-024-46284-x
50. Jędrzejewski, T., Sobocińska, J., Maciejewski, B., Slovakova, M., & Wrotek, S. (2025). Enhanced anti-cancer potential: Investigating the combined effects with *Coriolus versicolor* extract and phosphatidylinositol 3-kinase inhibitor (LY294002) in vitro. *International Journal of Molecular Sciences, 26*(4), 1556. https://doi.org/10.3390/ijms26041556
51. Jeitler, M., Michalsen, A., Frings, D., Hübner, M., Fischer, M., Koppold-Liebscher, D. A., Murthy, V., & Kessler, C. S. (2020). Significance of medicinal mushrooms in integrative oncology: A narrative review. In *Frontiers in Pharmacology* (Vol. 11). Frontiers Media S.A. https://doi.org/10.3389/fphar.2020.580656
52. Jiang, Y., Zhang, Y., Luan, J., Duan, H., Zhang, F., Yagasaki, K., & Zhang, G. (2010). Effects of bufalin on the proliferation of human lung cancer cells and its molecular mechanisms of action. *Cytotechnology, 62*(6), 573–583. https://doi.org/10.1007/s10616-010-9310-0
53. Jiménez-Medina, E., Berruguilla, E., Romero, I., Algarra, I., Collado, A., Garrido, F., & Garcia-Lora, A. (2008). The immunomodulator PSK induces in vitro cytotoxic activity in tumour cell lines via arrest of cell cycle and induction of apoptosis. *BMC Cancer, 8*(1), 78. https://doi.org/10.1186/1471-2407-8-78
54. Jin, X., Ruiz Beguerie, J., Sze, D. M. Y., & Chan, G. C. F. (2016). *Ganoderma lucidum* (Reishi mushroom) for cancer treatment. In *Cochrane Database of*

Systematic Reviews (Vol. 2016, Issue 4). John Wiley and Sons Ltd. https://doi.org/10.1002/14651858.CD007731.pub3

55. Johnson, P. D., & Besselsen, D. G. (2002). Practical aspects of experimental design in animal research. *ILAR Journal*, 43(4), 202–208. https://academic.oup.com/ilarjournal/article/43/4/202/981687
56. Johnson-Arbor, K., & Dubey, R. (2023). Doxorubicin. In *StatPearls*. StatPearls Publishing.
57. Jung, S., Jeong, H., & Yu, S. W. (2020). Autophagy as a decisive process for cell death. *Experimental and Molecular Medicine*, 52(6), 921–930. https://doi.org/10.1038/s12276-020-0455-4
58. Kamada, S., Kikkawa, U., Tsujimoto, Y., & Hunter, T. (2005). Nuclear translocation of caspase-3 is dependent on its proteolytic activation and recognition of a substrate-like protein(s). *Journal of Biological Chemistry*, 280(2), 857–860. https://doi.org/10.1074/jbc.C400538200
59. Kerr, J. F. R., Wyllie, A. H., & Currie, A. R. (1972). Apoptosis: A basic biological phenomenon with wide-ranging implications in tissue kinetics. *British Journal of Cancer*, 26(4), 239–257. https://doi.org/10.1038/bjc.1972.33
60. Khalid, N., & Azimpouran, M. (2023, March 6). Necrosis. In *StatPearls* [Internet]. StatPearls Publishing. https://www.ncbi.nlm.nih.gov/books/NBK557627/
61. Kibria, G., Hatakeyama, H., Akiyama, K., Hida, K., & Harashima, H. (2014). Comparative study of the sensitivities of cancer cells to doxorubicin and relationships between the effect of the drug-efflux pump P-gp. *Biological and Pharmaceutical Bulletin*, 37(12), 1926–1935. https://doi.org/10.1248/bpb.b14-00529
62. Kirha, T. J., Newme, T., & Joychan, A. (2023). Types of mushrooms and their bioactive constituents used in the treatment of cancer: A review. *International Journal of Current Research in Biosciences and Plant Biology*, 10(2), 23–32. https://doi.org/10.20546/ijcrbp.2023.1002.003
63. Kroemer, G., Galluzzi, L., Vandenabeele, P., Abrams, J., Alnemri, E. S., Baehrecke, E. H., Blagosklonny, M. V., El-Deiry, W. S., Golstein, P., Green, D. R., Hengartner, M., Knight, R. A., Kumar, S., Lipton, S. A., Malorni, W., Nuñez, G., Peter, M. E., Tschopp, J., Yuan, J., … Melino, G. (2009). Classification of cell death: Recommendations of the Nomenclature Committee on Cell Death 2009. *Cell Death and Differentiation*, 16(1), 3–11. https://doi.org/10.1038/cdd.2008.150

64. Kuete, V. (2010). Potential of Cameroonian Plants and Derived Products against Microbial Infections: A Review. *Planta Medica*, *76*(14), 1479–1491. https://doi.org/10.1055/s-0030-1250027

65. Latt, S. A., Stetten, G., Juergens, L. A., Willard, H. F., & Scher, C. D. (1975). Recent developments in the detection of deoxyribonucleic acid synthesis by 33258 Hoechst fluorescence. *The Journal of Histochemistry and Cytochemistry*, *23*(7), 493-505.

66. Lemjabbar-Alaoui, H., Hassan, O. U. I., Yang, Y. W., & Buchanan, P. (2015). Lung cancer: Biology and treatment options. *Biochimica et Biophysica Acta - Reviews on Cancer*, *1856*(2), 189–210. https://doi.org/10.1016/j.bbcan.2015.08.002

67. Li, C., Wang, H., Jiang, Y., Fu, W., Liu, X., Zhong, R., Cheng, B., Zhu, F., Xiang, Y., He, J., & Liang, W. (2022). Advances in lung cancer screening and early detection. *Cancer Biology & Medicine*, *19*(5), 591–608. https://doi.org/10.20892/j.issn.2095-3941.2021.0690

68. Liang, C., Tian, D., Liu, Y., Li, H., Zhu, J., Li, M., Xin, M., & Xia, J. (2019). Review of the molecular mechanisms of Ganoderma lucidum triterpenoids: Ganoderic acids A, C2, D, F, DM, X, and Y. *European Journal of Medicinal Chemistry*, *174*, 130–141. https://doi.org/10.1016/j.ejmech.2019.04.039

69. Lima, I. B., Alvarenga, B. M., Tótaro, P. I. S. D., Boratto, F., Leite, E. A., & Guimaraes, P. P. G. (2023). Improved antiproliferative activity of doxorubicin-loaded calcium phosphate nanoparticles against melanoma cells. *Brazilian Archives of Biology and Technology*, *66*, e23220572. https://doi.org/10.1590/1678-4324-2023220572

70. Lin, S.-B., Li, C.-H., Lee, S.-S., & Kan, L.-S. (2003). Triterpene-enriched extracts from *Ganoderma lucidum* inhibit growth of hepatoma cells via suppressing protein kinase C, activating mitogen-activated protein kinases, and G2-phase cell cycle arrest. *Life Sciences*, *72*(21), 2381–2390. https://doi.org/10.1016/S0024-3205(03)00124-3

71. Litwiniec, A., Grzanka, A., Helmin-Basa, A., Gackowska, L., & Grzanka, D. (2010). Features of senescence and cell death induced by doxorubicin in A549 cells: Organization and level of selected cytoskeletal proteins. *Journal of Cancer Research and Clinical Oncology*, *136*(5), 717–736. https://doi.org/10.1007/s00432-009-0711-4

72. Liu, J., Shimizu, K., Tanaka, A., Shinobu, W., Ohnuki, K., Nakamura, T., & Kondo, R. (2012). Target proteins of ganoderic acid DM provide clues to various

pharmacological mechanisms. *Scientific Reports, 2*(1), 905. https://doi.org/10.1038/srep00905

73. López-Gil, C. I., Téllez-Jurado, A., Velasco-Velázquez, M. A., & Anducho-Reyes, M. A. (2024). Identification and analysis of anticancer therapeutic targets from the polysaccharide Krestin (PSK) and polysaccharopeptide (PSP) using inverse docking. *Molecules*, *29*(22), 5390. https://doi.org/10.3390/molecules29225390
74. Lu, H., Yang, Y., Gad, E., Inatsuka, C., Wenner, C. A., Disis, M. L., & Standish, L. J. (2011). TLR2 agonist PSK activates human NK cells and enhances the antitumor effect of HER2-targeted monoclonal antibody therapy. *Clinical Cancer Research: An Official Journal of the American Association for Cancer Research, 17*(21), 6742–6753. https://doi.org/10.1158/1078-0432.CCR-11-1142
75. Lu, Y., Jia, Y., Xue, Z., Li, N., Liu, J., & Chen, H. (2021). Recent developments in Inonotus obliquus (Chaga mushroom) polysaccharides: Isolation, structural characteristics, biological activities, and application. *Polymers, 13*(9), 1441. https://doi.org/10.3390/polym13091441
76. Mansoori, B., Mohammadi, A., Davudian, S., Shirjang, S., & Baradaran, B. (2017). The different mechanisms of cancer drug resistance: A brief review. *Advanced Pharmaceutical Bulletin, 7*(3), 339–348. https://doi.org/10.15171/apb.2017.041
77. Mehdizadeh, K., Ataei, F., & Hosseinkhani, S. (2020). Effects of doxorubicin and docetaxel on susceptibility to apoptosis in high expression level of survivin in HEK and HEK-S cell lines as in vitro models. *Biochemical and Biophysical Research Communications, 532*(1), 139–144. https://doi.org/10.1016/j.bbrc.2020.08.028
78. Meyer, M.-L., Peters, S., Mok, T. S., Lam, S., Yang, P.-C., Aggarwal, C., Brahmer, J., Dziadziuszko, R., Felip, E., Ferris, A., Forde, P. M., Gray, J., Gros, L., Halmos, B., Herbst, R., Jänne, P. A., Johnson, B. E., Kelly, K., Leighl, N. B., & Hirsch, F. R. (2024). Lung cancer research and treatment: Global perspectives and strategic calls to action. *Annals of Oncology, 35*(12), 1088–1104. https://doi.org/10.1016/j.annonc.2024.10.006
79. Min, B. S., Gao, J. J., Nakamura, N., & Hattori, M. (2000). Triterpenes from the spores of Ganoderma lucidum and their cytotoxicity against meth-A and LLC tumor cells. *Chemical & Pharmaceutical Bulletin, 48*(7), 1026–1033. https://doi.org/10.1248/cpb.48.1026
80. Mishra, J., Joshi, A., Rajput, R., Singh, K., Bansal, A., & Misra, K. (2018). Phenolic rich fractions from mycelium and fruiting body of Ganoderma lucidum inhibit

bacterial pathogens mediated by generation of reactive oxygen species and protein leakage and modulate hypoxic stress in HEK 293 cell line. *Advances in Pharmacological Sciences, 2018*, 1–10. https://doi.org/10.1155/2018/6285615

81. Mizutani, H., Tada-Oikawa, S., Hiraku, Y., Kojima, M., & Kawanishi, S. (2005). Mechanism of apoptosis induced by doxorubicin through the generation of hydrogen peroxide. *Life Sciences, 76*(13), 1439–1453. https://doi.org/10.1016/j.lfs.2004.05.040
82. Modhia, H. (2022). A study on the impacts of hypertension and its treatment in South Africa. *Journal of Cardiovascular Health, 17*(3), 45-56. Retrieved from [URL or DOI]
83. Mosmann, T. (1983). Rapid colorimetric assay for cellular growth and survival: Application to proliferation and cytotoxicity assays. *Journal of Immunological Methods, 65*.
84. Mousavi, S. M., Hashemi, S. A., Gholami, A., Omidifar, N., Chiang, W.-H., Neralla, V. R., Yousefi, K., & Shokripour, M. (2023). Ganoderma lucidum methanolic extract as a potent phytoconstituent: Characterization, in-vitro antimicrobial and cytotoxic activity. *Scientific Reports, 13*(1), 17326. https://doi.org/10.1038/s41598-023-44135-1
85. Muelas, M.W, Ortega, F., Breitling, R., Bendtsen, C., & Westerhoff, H. V. (2018). Rational cell culture optimization enhances experimental reproducibility in cancer cells. *Scientific Reports, 8*(1), 3029. https://doi.org/10.1038/s41598-018-21050-4
86. Myers, D. J., & Wallen, J. M. (2023). Lung adenocarcinoma. [Updated 2023 Jun 12]. In *StatPearls* [Internet]. Treasure Island (FL): StatPearls Publishing; 2024 Jan-. Available from: https://www.ncbi.nlm.nih.gov/books/NBK519578/
87. Nakamura, H., & Takada, K. (2021). Reactive oxygen species in cancer: Current findings and future directions. *Cancer Science, 112*(10), 3945–3952. https://doi.org/10.1111/cas.15068
88. Nandiyanto, A. B. D., Oktiani, R., & Ragadhita, R. (2019). How to read and interpret FTIR spectroscope of organic material. *Indonesian Journal of Science and Technology, 4*(1), 97. https://doi.org/10.17509/ijost.v4i1.15806
89. Nandiyanto, A. B. D., Ragadhita, R., & Fiandini, M. (2022). Interpretation of Fourier transform infrared spectra (FTIR): A practical approach in the polymer/plastic thermal decomposition. *Indonesian Journal of Science and Technology, 8*(1), 113–126. https://doi.org/10.17509/ijost.v8i1.53297
90. National Cancer Institute. (2024). Physician Data Query (PDQ). Patient version. Non-small cell lung cancer treatment. Accessed at

https://www.cancer.gov/types/lung/patient/non-small-cell-lung-treatment-pdq on February 23, 2025.

91. National Center for Biotechnology Information (2025). PubChem Compound Summary for CID 5460033, Cisplatin. Retrieved July 14, 2025 from https://pubchem.ncbi.nlm.nih.gov/compound/5460033.
92. National Center for Biotechnology Information (2025). PubChem Compound Summary for CID 426756, Paraplatin. Retrieved July 14, 2025 from https://pubchem.ncbi.nlm.nih.gov/compound/carboplatin.
93. National Center for Biotechnology Information (2025). PubChem Compound Summary for CID 426756, Paraplatin. Retrieved July 14, 2025 from https://pubchem.ncbi.nlm.nih.gov/compound/carboplatin.
94. National Center for Biotechnology Information (2025). PubChem Compound Summary for CID 148124, Docetaxel. Retrieved July 14, 2025 from https://pubchem.ncbi.nlm.nih.gov/compound/Docetaxel.
95. National Center for Biotechnology Information (2025). PubChem Compound Summary for CID 60750, Gemcitabine. Retrieved July 14, 2025 from https://pubchem.ncbi.nlm.nih.gov/compound/Gemcitabine.
96. National Center for Biotechnology Information (2025). PubChem Compound Summary for CID 5311497, Vinorelbine. Retrieved July 14, 2025 from https://pubchem.ncbi.nlm.nih.gov/compound/Vinorelbine.
97. National Center for Biotechnology Information (2025). PubChem Compound Summary for CID 36462, Etoposide. Retrieved July 14, 2025 from https://pubchem.ncbi.nlm.nih.gov/compound/Etoposide.
98. National Center for Biotechnology Information (2025). PubChem Compound Summary for CID 135410875, Pemetrexed. Retrieved July 14, 2025 from https://pubchem.ncbi.nlm.nih.gov/compound/Pemetrexed.
99. National Center for Biotechnology Information. (2025). PubChem substance record for SID 489167564, Asp-Cys-Pro-Pro-Cys-Glu, source: NIAID ChemDB. Retrieved March 12, 2025, from https://pubchem.ncbi.nlm.nih.gov/substance/489167564
100. National Comprehensive Cancer Network. (2024). *NCCN clinical practice guidelines in oncology: Non-small cell lung cancer* (V.1.2024). Accessed at https://www.nccn.org/professionals/physician_gls/pdf/nscl.pdf on February 23, 2025.
101. Pasquier, J., Rioult, D., Abu-Kaoud, N., Marie, S., Rafii, A., Guerrouahen, B. S., & Le Foll, F. (2013). P-glycoprotein-activity measurements in multidrug resistant

cell lines: Single-cell versus single-well population fluorescence methods. *BioMed Research International, 2013*, 676845. https://doi.org/10.1155/2013/676845

102. Pawlikowska, M., Jadrzejewski, T., Broayna, A. A., & Wrotek, S. (2020). Protein-bound polysaccharides from *Coriolus versicolor* induce RIPK1/RIPK3/MLKL-mediated necroptosis in ER-positive breast cancer and amelanotic melanoma cells. *Cellular Physiology and Biochemistry, 54*(4), 591–604. https://doi.org/10.33594/000000242

103. Perillo, B., Di Donato, M., Pezone, A., Di Zazzo, E., Giovannelli, P., Galasso, G., Castoria, G., & Migliaccio, A. (2020). ROS in cancer therapy: The bright side of the moon. *Experimental & Molecular Medicine, 52*(2), 192–203. https://doi.org/10.1038/s12276-020-0384-2

104. Pfeffer, C., & Singh, A. (2018). Apoptosis: A target for anticancer therapy. *International Journal of Molecular Sciences, 19*(2), 448. https://doi.org/10.3390/ijms19020448

105. Piccinini, F., Tesei, A., Arienti, C., & Bevilacqua, A. (2017). Cell counting and viability assessment of 2D and 3D cell cultures: Expected reliability of the trypan blue assay. *Biological Procedures Online, 19*(1). https://doi.org/10.1186/s12575-017-0056-3

106. Provencio, M., Isla, D., Sánchez, A., & Cantos, B. (2011). Inoperable stage III non-small cell lung cancer: Current treatment and role of vinorelbine. *Journal of Thoracic Disease, 3*(3), 197–204. https://doi.org/10.3978/j.issn.2072-1439.2011.01.02

107. Qiu, W. L., Lo, H. C., Lu, M. K., & Lin, T. Y. (2023). Significance of culture period on the physiochemistry and anti-cancer potentials of polysaccharides from mycelia of *Ganoderma lucidum*. *International Journal of Biological Macromolecules, 242*, 125181. https://doi.org/10.1016/j.ijbiomac.2023.125181

108. Risoli, S., Nali, C., Sarrocco, S., Cicero, A. F. G., Colletti, A., Bosco, F., Venturella, G., Gadaleta, A., Gargano, M. L., & Marcotuli, I. (2023). Mushroom-based supplements in Italy: Let's open Pandora's box. *Nutrients, 15*(3), 776. https://doi.org/10.3390/nu15030776

109. Riss, T. L., Moravec, R. A., Duellman, S. J., & Niles, A. L. (2021). Treating cells as reagents to design reproducible assays. *SLAS Discovery, 26*(10), 1256–1267. https://doi.org/10.1177/24725552211039754

110. Roca-Lema, D., Martinez-Iglesias, O., de Ana Portela, C. F., Rodríguez-Blanco, A., Valladares-Ayerbes, M., Díaz-Díaz, A., Casas-Pais, A., Prego, C., &

Figueroa, A. (2019). In vitro anti-proliferative and anti-invasive effect of polysaccharide-rich extracts from *Trametes versicolor* and *Grifola frondosa* in colon cancer cells. *International Journal of Medical Sciences, 16*(2), 231–240. https://doi.org/10.7150/ijms.28811

111. Rodriguez-Canales, J., Parra-Cuentas, E., & Wistuba, I. I. (2016). Diagnosis and molecular classification of lung cancer. In *Cancer Treatment and Research* (Vol. 170, pp. 25–46). Kluwer Academic Publishers. https://doi.org/10.1007/978-3-319-40389-2_2

112. Sabbula, B. R., Gasalberti, D. P., Mukkamalla, S. K. R., et al. (2024). Squamous cell lung cancer. In *StatPearls* [Internet]. Treasure Island (FL): StatPearls Publishing. Available from https://www.ncbi.nlm.nih.gov/books/NBK564510/

113. Sachet, M., Liang, Y. Y., & Oehler, R. (2017). The immune response to secondary necrotic cells. *Apoptosis: An International Journal on Programmed Cell Death, 22*(10), 1189–1204. https://doi.org/10.1007/s10495-017-1413-z

114. Sakamoto, J., Morita, S., Oba, K., Matsui, T., Kobayashi, M., Nakazato, H., & Ohashi, Y. (2006). Efficacy of adjuvant immunochemotherapy with polysaccharide K for patients with curatively resected colorectal cancer: A meta-analysis of centrally randomized controlled clinical trials. *Cancer Immunology, Immunotherapy, 55*(4), 404–411. https://doi.org/10.1007/s00262-005-0054-1

115. Sakurai, A., Suzuki, Y., & Shimizu, H. (2011). Environmental factors affecting the production of secondary metabolites in fungi. *Bioscience, Biotechnology, and Biochemistry*, **75**(4), 877–882. https://doi.org/10.1271/bbb.100826

116. Saritha, K. V., Prakash, B., Khilare, V. C., Khedkar, G. D., Reddy, Y. M., & Khedkar, C. D. (2016). Mushrooms and truffles: Role in the diet. *Encyclopedia of Food and Health*, 1–8.

117. Sato, K., Ota, N., Endo, S., Nakata, A., Yamashita, H., & Tatsunami, R. (2022). Effect of chloroquine on doxorubicin-induced apoptosis in A549 cells. *Anticancer Research, 42*(8), 4025–4035. https://doi.org/10.21873/anticanres.15899

118. Selenius, L.A, Lundgren, M.W, Jawad, R., Danielsson, O., & Björnstedt, M. (2019). The cell culture medium affects growth, phenotype expression and the response to selenium cytotoxicity in A549 and HepG2 cells. *Antioxidants, 8*(5), 130. https://doi.org/10.3390/antiox8050130

119. Sharma, G., Ojha, R., Noguera-Ortega, E., Rebecca, V. W., Attanasio, J., Liu, S., Piao, S., Lee, J. J., Nicastri, M. C., Harper, S. L., Ronghe, A., Jain, V., Winkler, J.

D., Speicher, D. W., Mastio, J., Gimotty, P. A., Xu, X., Wherry, E. J., Gabrilovich, D. I., & Amaravadi, R. K. (2022). PPT1 inhibition enhances the antitumor activity of anti-PD-1 antibody in melanoma. *JCI Insight, 7*(20), e165688. https://doi.org/10.1172/jci.insight.165688

120. Shimizu, S., Yoshida, T., Tsujioka, M., & Arakawa, S. (2014). Autophagic cell death and cancer. In *International Journal of Molecular Sciences* (Vol. 15, Issue 2, pp. 3145–3153). Molecular Diversity Preservation International. https://doi.org/10.3390/ijms15023145

121. Silva, M. T. (2010). Secondary necrosis: The natural outcome of the complete apoptotic program. *FEBS Letters, 584*(22), 4491–4499. https://doi.org/10.1016/j.febslet.2010.10.046

122. South African Health Products Regulatory Authority (SAHPRA). (2020). Regulatory overview on medication approvals in South Africa. SAHPRA. Retrieved from https://pmg.org.za/committee-meeting/32599/

123. Standish, L. J., Wenner, C. A., Sweet, E. S., Bridge, C., Nelson, A., Martzen, M., Novack, J., & Torkelson, C. (2008). Trametes versicolor mushroom immune therapy in breast cancer. *Journal of the Society for Integrative Oncology, 6*(3), 122–128.

124. Starr, R. R. (2015). Too little, too late: Ineffective regulation of dietary supplements in the United States. *Public Health Ethics*.

125. Statista. (2023). Revenue of antihypertensive drugs worldwide from 2015 to 2023 (in billion U.S. dollars). *Statista*. Retrieved from https://www.statista.com/outlook/hmo/pharmaceuticals/anti-hypertensive-drugs/worldwide

126. Stošić-Grujičić, S., Mijatović, S., & Maksimović-Ivanić, D. (2011). An evidence-based perspective of *Coriolus versicolor* (multicolored polypore mushroom) for cancer patients. In W. C. S. Cho (Ed.), *Evidence-based Anticancer Materia Medica* (pp. 265–302). Springer Netherlands. https://doi.org/10.1007/978-94-007-0526-5_13

127. Strasser, A., & Vaux, D. L. (2020). Cell death in the origin and treatment of cancer. *Molecular Cell, 78*(6), 1045–1054. https://doi.org/10.1016/j.molcel.2020.05.014

128. Su, Z., Ye, J., Qin, Z., & Ding, X. (2015). Protective effects of madecassoside against doxorubicin-induced nephrotoxicity in vivo and in vitro. *Scientific Reports, 5*(1), 18314. https://doi.org/10.1038/srep18314

129. Sugimachi, K., Ide, H., Okamura, T., Matsuura, H., Endo, M., & Inokuchi, K. (1984). Cytophotometric DNA analysis of mucosal and submucosal carcinoma of the esophagus. *Cancer, 53*.

130. Sung, H., Ferlay, J., Siegel, R. L., Laversanne, M., Soerjomataram, I., Jemal, A., & Bray, F. (2021). Global cancer statistics 2020: GLOBOCAN estimates of incidence and mortality worldwide for 36 cancers in 185 countries. *CA: A Cancer Journal for Clinicians, 71*(3), 209–249. https://doi.org/10.3322/caac.21660

131. Upadhayay, S., Sharma, N., Mantha, A. K., & Dhiman, M. (2020). Anti-cancer drug doxorubicin induced cardiotoxicity: Understanding the mechanisms involved in ROS generation resulting in mitochondrial dysfunction. *Rasayan Journal of Chemistry, 13*(2), 1042–1053. https://doi.org/10.31788/RJC.2020.1325603

132. Van Engeland, M., Nieland, L. J. W., Ramaekers, F. C. S., Schutte, B., & Reutelingsperger, C. P. M. (1998). Annexin V-affinity assay: A review on an apoptosis detection system based on phosphatidylserine exposure. *Cytometry, 31*(1), 1–9. https://doi.org/10.1002/(SICI)1097-0320(19980101)31:1<1::AID-CYTO1>3.0.CO;2-R

133. Ventola, C. L. (2010). Current issues regarding complementary and alternative medicine (CAM) in the United States. *Complementary and Alternative Medicine*.

134. Vetchinkina, E., Shirokov, A., Bucharskaya, A., Navolokin, N., Prilepskii, A., Burov, A., Maslyakova, G., & Nikitina, V. E. (2016). Antitumor activity of extracts from medicinal basidiomycetes mushrooms. *International Journal of Medicinal Mushrooms, 18*(11), 955–964. https://doi.org/10.1615/IntJMedMushrooms.v18.i11.10

135. Villalobos, P., & Wistuba, I. I. (2017). Lung cancer biomarkers. *Hematology/Oncology Clinics of North America, 31*(1), 13–29. https://doi.org/10.1016/j.hoc.2016.08.006

136. Wang, D. F., Lou, N., & Li, X. D. (2012). Effect of Coriolus versicolor polysaccharide-B on the biological characteristics of human esophageal carcinoma cell line ECA109. *Cancer Biology & Medicine, 9*(3), 164–167. https://doi.org/10.7497/j.issn.2095-3941.2012.03.002

137. Watanabe, T., Miura, T., Degawa, Y., Fujita, Y., Inoue, M., Kawaguchi, M., & Furihata, C. (2010). Comparison of lung cancer cell lines representing four

histopathological subtypes with gene expression profiling using quantitative real-time PCR. *Cancer Cell International, 10*. https://doi.org/10.1186/1475-2867-10-2

138. Whaley, D., Damyar, K., Witek, R. P., Mendoza, A., Alexander, M., & Lakey, J. R. T. (2021). Cryopreservation: An overview of principles and cell-specific considerations. In *Cell Transplantation* (Vol. 30). SAGE Publications Ltd. https://doi.org/10.1177/0963689721999617

139. Winder, M., Bulska-Będkowska, W., & Chudek, J. (2021). The use of Hericium erinaceus and Trametes versicolor extracts in supportive treatment in oncology. *Acta Pharmaceutica, 71*(1), 1–16. https://doi.org/10.2478/acph-2021-0007

140. Wolf, B. B., Schuler, M., Echeverri, F., & Green, D. R. (1999). Caspase-3 is the primary activator of apoptotic DNA fragmentation via DNA fragmentation factor-45/inhibitor of caspase-activated DNase inactivation. *Journal of Biological Chemistry, 274*(43), 30651–30656. https://doi.org/10.1074/jbc.274.43.30651

141. World Health Organization. (2007). *Guidelines for assessing quality of herbal medicines with reference to contaminants and residues*. Geneva: WHO. Available online

142. Xu, Z., Chen, X., Zhong, Z., & Chen, L. (2011). Ganoderma lucidum polysaccharides: Immunomodulation and potential anti-tumor activities. *39*(1), 15–27.

143. Yang, X., Sit, W., Chan, D. K., & Wan, J. M. (2005). The cell death process of the anticancer agent polysaccharide-peptide (PSP) in human promyelocytic leukemic HL-60 cells. *Oncology Reports, 13*, 1201–1210. https://doi.org/10.3892/or.13.6.1201

144. Yilmazer, A. (2018). Cancer cell lines involving cancer stem cell populations respond to oxidative stress. *Biotechnology Reports, 17*, 24–30. https://doi.org/10.1016/j.btre.2017.11.004

145. Yue, Q., Xie, F., Guan, S., Ma, C., Yang, M., Jiang, B., Liu, X., & Guo, D. (2008). Interaction of Ganoderma triterpenes with doxorubicin and proteomic characterization of the possible molecular targets of Ganoderma triterpenes. *Cancer Science, 99*(7), 1461–1470. https://doi.org/10.1111/j.1349-7006.2008.00824.x

146. Zeng, P., Chen, Y., Zhang, L., & Xing, M. (2019). Ganoderma lucidum polysaccharide used for treating physical frailty in China. In L. Zhang (Ed.), *Progress in molecular biology and translational science* (Vol. 163, pp. 179–219). Academic Press. https://doi.org/10.1016/bs.pmbts.2019.02.009

147. Zhang, T., Wan, B., Zhao, Y., Li, C., Liu, H., Lv, T., Zhan, P., & Song, Y. (2019). Treatment of uncommon EGFR mutations in non-small cell lung cancer: New

evidence and treatment. *Translational Lung Cancer Research, 8*(3), 302–316. https://doi.org/10.21037/tlcr.2019.04.12

148. Zhong, X., Ren, K., Lu, S., Yang, S., & Sun, D. (2009). Progress of research on *Inonotus obliquus*. *Chinese Journal of Integrative Medicine, 15*(2), 156–160. https://doi.org/10.1007/s11655-009-0156-2

149. Zion Market Research. (2021). Global antihypertensive drugs market report: Industry analysis, market size, share, growth, trends, and forecast 2020-2027. Retrieved from https://www.zionmarketresearch.com/report/antihypertensives-market

150. Zong, W.-X., & Thompson, C. B. (2006). Necrotic death as a cell fate. *Genes & Development, 20*(1), 1–15. https://doi.org/10.1101/gad.1376506

Appendix A: Research Ethics Approval

UNIVERSITY OF THE WITWATERSRAND, JOHANNESBURG	HUMAN RESEARCH ETHICS COMMITTEE (MEDICAL)

Office of the Deputy Vice-Chancellor (Research & Innovation)

31/08/2022

Ref: W-CBP-220831-01

TO WHOM IT MAY CONCERN

Waiver: This certifies that the following research does not require clearance from the Human Research Ethics Committee (Medical)

Investigator: Ms Y Patel
Student No. (if appropriate): 1605976
Staff No. (if appropriate):

Supervisor: Dr L Harmse

School: Therapeutic Sciences
Department: Pharmacy and Pharmacology
Pharmacology
Medical School
University

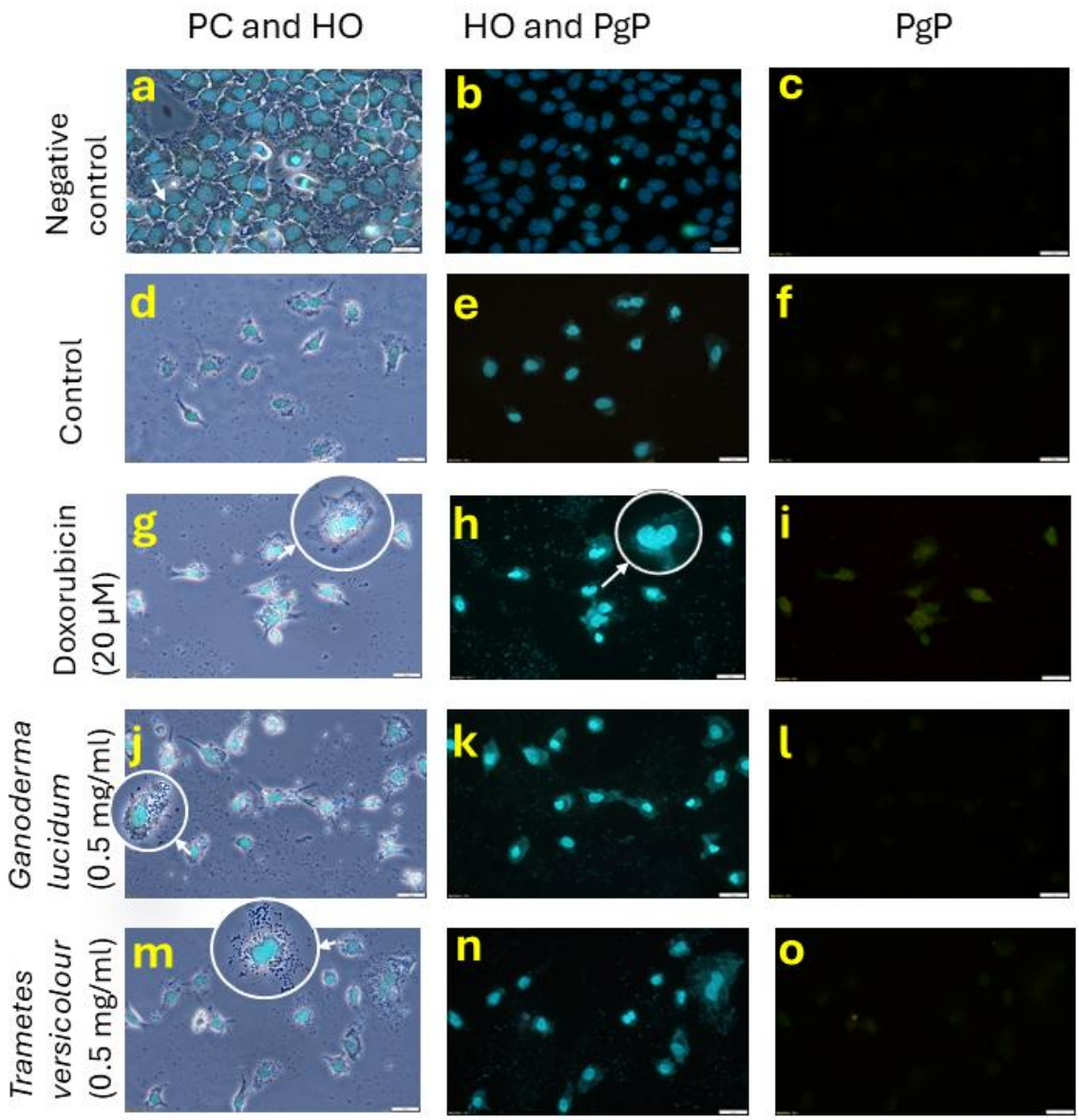
Project title: *The effect of selected mushrooms on the efficacy of cancer chemotherapeutic agents in A549 lung cancer cells*

Reason: In vitro laboratory study
No human participants will be involved in the study

Dr CB Penny
Chairperson: Human Research Ethics Committee (Medical)

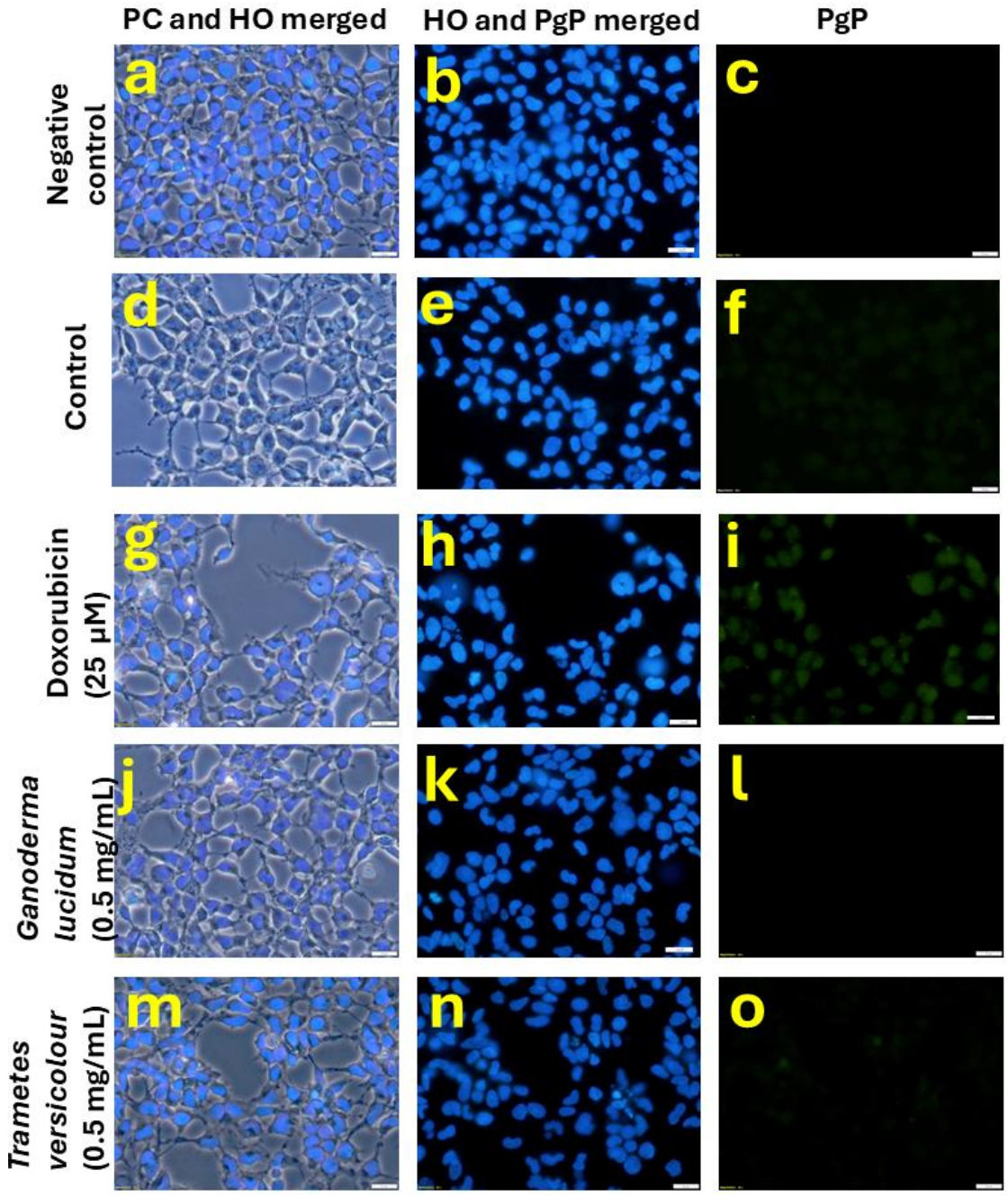
Research Office Secretariat:
Third Floor, Phillip Tobias Building, corner of St Andrews and York Roads, Parktown, Johannesburg 2193
Postal address: Private Bag 3, Wits 2050
Tel Nos: +27 (0)11 717 1234/1252/2656/2700
Office E-mail: HREC-Medical.ResearchOffice@wits.ac.za
Website:
https://www.wits.ac.za/research/researcher-support/research-ethics/ethics-committees/

Appendix B: The detection of P-glycoprotein levels in A549 cells



Representative photomicrographs showing the effect of doxorubicin, *Ganoderma lucidum* and *Trametes versicolour* on P-glycoprotein expression and localization. A549 cells were treated with doxorubicin at 20 µM and *Ganoderma lucidum* and *Trametes versicolour* at 0.5 mg/mL. Alexa Fluor 488 was used for PGP detection. The Olympus BX41 microscope was used to view cells and the DP72 digital camera was used to capture images (Magnification: 400x; scalebar: 20 µm).

Appendix C: The detection of P-glycoprotein levels in HEK293 cells.



Representative photomicrographs showing the effect of doxorubicin, *Ganoderma lucidum* and *Trametes versicolour* on P-glycoprotein expression and localization. HEK293 cells were treated with doxorubicin at concentrations equivalent to the IC_{80} values and *Ganoderma lucidum* and *Trametes versicolour* at 0.5 mg/mL. Alexa Fluor 488 was used for PGP detection. The Olympus BX41 microscope was used to view cells and the DP72 digital camera was used to capture images (Magnification: 400x; scalebar: 20 µm).

Appendix D: Turnitin Report

MSc dissertation draft 1 for turnitin (no references)-1.docx

ORIGINALITY REPORT

15%	11%	14%	%
SIMILARITY INDEX	INTERNET SOURCES	PUBLICATIONS	STUDENT PAPERS

PRIMARY SOURCES

1	wiredspace.wits.ac.za Internet Source	2%
2	Gangat, Nadia. "The Effect of Copper-Imidazo[1,2-a]Pyridine Complexes on HT-29 and DLD-1 Colorectal Cancer Cells", University of the Witwatersrand, Johannesburg (South Africa), 2025 Publication	1%
3	www.mdpi.com Internet Source	1%
4	www.frontiersin.org Internet Source	1%
5	Green, Blake Delroy. "Evaluation of the Effect of Selected Complementary and Alternative Medicines on the Efficacy of Cancer Chemotherapeutic Agents", University of the Witwatersrand, Johannesburg (South Africa), 2025 Publication	1%
6	www.biorxiv.org Internet Source	<1%
7	www.thno.org Internet Source	<1%
8	eprints.whiterose.ac.uk Internet Source	<1%
9	hdl.handle.net Internet Source	<1%